

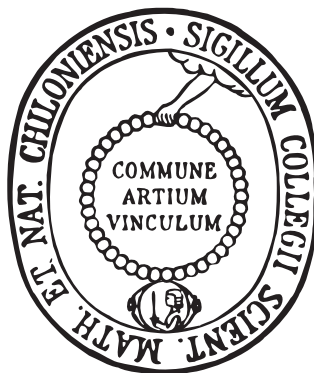
Christian-Albrechts-Universität zu Kiel
Institut für Theoretische Physik und Astrophysik


DISSERTATION
ZUR ERLANGUNG DES AKADEMISCHEN GRADES
DOCTOR RERUM NATURALIUM
DER MATHEMATISCH-NATURWISSENSCHAFTLICHEN FAKULTÄT
DER CHRISTIAN-ALBRECHTS-UNIVERSITÄT ZU KIEL

GROUND STATE AND EXCITATION PROPERTIES OF YUKAWA BALLS

VORGELEGT VON
CHRISTIAN HENNING
GEB. AM 02.08.1979 IN POTSDAM
AUS KIEL

KIEL, MAI 2009



This work was typeset in \LaTeX . Figures were created using  *Asymptote*.

Referent: Prof. Dr. Michael Bonitz

Korreferent/in: _____

Tag der mündlichen Prüfung: _____

Zum Druck genehmigt: Kiel, _____

Der Dekan

For my beloved family.

Abstract

The present thesis is concerned with the theoretical investigation of essential ground state and excitation properties of Yukawa balls – spherical crystalline clusters composed of microparticles embedded into a plasma environment.

The ground state of a Yukawa ball is characterized by a particle distribution consisting of nested spherical shells. This distribution strongly depends on the screening effect of the surrounding plasma. The theoretical analysis of this dependence is a major concern of this work. To this end, a statistical theory is introduced, which allows for the analytical determination of ground state density profiles within two essential approximations – the mean-field and the local density approximation. By means of these approximations, analytical results for the density profiles are derived, which quantitatively explain the remarkable influence of the plasma screening on the average particle distribution. An alternative approach towards this ground state particle distribution is given by shell models, in which a shell-like structure is included a priori. While previous shell models, however, are only appropriate for the description of the Yukawa balls within a small range of the physical parameters, within the thesis at hand a Yukawa shell model is derived, which is not subject to these restrictions.

The theoretical investigation of excitation properties of Yukawa balls is feasible by normal mode analyses, which allow for a spectral analysis of excited motions. One of the most important normal modes is the breathing mode. The detailed investigation of its existence conditions is the second central topic of this thesis. Previously assumed to exist for Yukawa balls and other spherical clusters, this breathing mode is shown to be present only in a small class of systems, to which Yukawa balls and many other clusters do not generally belong to. These findings implicate that the response of such a system to radial excitations characteristically depends on intrinsic system properties and may serve as a sensitive experimental diagnostics.

Zusammenfassung

Die vorliegende Doktorarbeit widmet sich der theoretischen Untersuchung fundamentaler Grundzustands- und Anregungseigenschaften von Yukawa-Balls – kugelförmige, kristalline Cluster bestehend aus in ein Plasma eingebetteten Mikroteilchen.

Der Grundzustand eines Yukawa-Balls zeichnet sich durch eine Teilchenverteilung aus, die durch ineinander geschachtelte, sphärische Schalen beschrieben werden kann. Diese Verteilung hängt maßgeblich von der Abschirmungswirkung des umgebenden Plasmas ab. Die theoretische Untersuchung dieser Abhängigkeit ist ein zentrales Anliegen dieser Arbeit. Zu diesem Zweck wird eine statistische Theorie eingesetzt, die die analytische Berechnung des Dichteprofiles im Grundzustand in zwei wesentlichen Näherungen ermöglicht – in der Mean-Field-Näherung und in der Lokale-Dichte-Näherung. Unter Verwendung dieser Approximationen werden analytische Resultate für die Dichteprofile hergeleitet, die den auffallenden Effekt der Plasmaabschirmung auf die mittlere Teilchenverteilung quantitativ erklären. Einen alternativen Zugang zur Teilchenverteilung im Grundzustand ermöglichen sogenannte Schalenmodelle, in denen eine schalenartige Struktur a priori angenommen wird. Während bisherige Schalenmodelle die Teilchenverteilung nur innerhalb eines kleinen Bereiches der physikalischen Parameter beschreiben können, wird in der vorliegenden Arbeit ein Yukawa-Schalenmodell abgeleitet, das diesen Einschränkungen nicht unterliegt.

Die theoretische Untersuchung von Anregungseigenschaften der Yukawa-Balls ist im Rahmen von Normalmodenanalysen realisierbar, die eine spektrale Zerlegung von angeregten Bewegungen ermöglichen. Eine der grundlegenden Normalmoden ist die Breathing-Mode. Die ausführliche Analyse ihrer Existenzbedingungen ist das zweite zentrale Thema dieser Arbeit. Als unmittelbares Resultat wird gezeigt, dass diese Breathing-Mode, deren Existenz bisher für Yukawa-Balls und andere sphärische Cluster angenommen wurde, nur in einer kleinen Gruppe von Systemen vorkommen kann, zu der die Yukawa-Balls und viele andere Cluster im Allgemeinen nicht gehören. Eine Folge dieser Ergebnisse ist, dass die Antwort eines solchen Systems auf radiale Anregungen in charakteristischer Weise von den wesentlichen Systemeigenschaften abhängt und somit für deren experimentelle Untersuchung herangezogen werden kann.

Contents

1	Introduction	1
1.1	Strongly Correlated Systems	2
1.2	Yukawa Balls	7
1.3	Thesis Outline	10
2	Ground state theory of Yukawa balls	11
2.1	Variational Problem of the Energy Functional	12
2.2	Ground State Density Profile in Mean-Field Approximation	16
2.2.1	The Coulomb Limit and Electrostatics	17
2.2.2	General Solution	18
2.2.3	Density Profile for Harmonic Confinement	21
2.2.4	Force Equilibrium Within Yukawa Electrostatics	23
2.3	Simulation Results of Yukawa Balls	26
2.3.1	Ground State Simulations	27
2.3.2	Comparison of Simulation and Mean-Field Results	34
2.4	Inclusion of Correlations by Using the Local Density Approximation (LDA)	35
2.4.1	LDA Without Correlations	35
2.4.2	LDA with Correlations	43
2.4.3	Comparison of Simulation and LDA Results	46
2.5	Shell Models of Yukawa Balls	48
2.5.1	An Improved Yukawa Shell Model	51
2.6	Summary	56

3	Normal Modes of Finite Clusters	57
3.1	Recapitulation of Normal Modes	58
3.2	Normal Modes of Confined Coulomb Systems	59
3.3	Normal Modes of Confined Yukawa Systems	61
3.4	Breathing Mode	63
3.4.1	General Conditions for the Existence of the Breathing Mode	64
3.4.2	Breathing Modes in Lennard-Jones Systems	70
3.4.3	Breathing Modes of Yukawa Balls	72
3.4.4	Monopole Oscillations	76
3.5	Normal Modes in the Presence of Dissipation	79
3.6	Summary	82
4	Conclusions	83
	Bibliography	87
	List of the Author's Publications	97
	Danksagung	101
	Curriculum Vitae	105

CHAPTER 1

Introduction

The theoretical and experimental investigation of collective many-particle effects in systems of various scales and dimensionality ranks among the most promising challenges of contemporary physics. These effects are often called *strong correlation effects* and include the emergence of long range order, of liquid-like or crystalline structures, and of dynamic features, which are characterized by pronounced interactions between the particles and, therefore, by deviations from the ideal gas behavior.

The strength of many-particle correlations can be measured by the *coupling parameter* Γ (also referred to as correlation parameter¹[Dub88]), which is the ratio of the mean (nearest neighbor) interaction energy to the average kinetic energy of a system. Using the parameter Γ , the *universal trends* in correlated systems can very generally be quantified as ranging from ideal gas-like behavior for $\Gamma \ll 1$ and liquid-like short-range order for $\Gamma \gtrsim 1$ to crystalline long-range order for $\Gamma \gtrsim 100$. While the precise values depend on the form of the potential energy and quantum effects have to be considered as well, various imposing correlation phenomena can be observed in all many-particle systems, independently of their specific nature. This generality makes the analysis of correlation effects in one system very attractive also for other fields of physics.

¹ Strongly correlated systems are also often referred to as strongly coupled systems.

1.1 Strongly Correlated Systems

Historically, the first encounter of strong non-ideality effects is probably the gas-liquid phase transition. There, condensation effects clearly show a deviation from ideal gas behavior and the breakdown of the ideal equation of state, $p = nk_{\text{B}}T$. The phenomenological solution of this problem has been the introduction of a modified equation of state, such as the van der Waals equation, which incorporates interactions between the molecules (for a recent overview, see [Leb82] and the introductory essay in [Row88]). More systematic insights into non-ideal fluids are provided by modern statistical mechanics, which have put the theoretical analysis of correlations on a firm ground. Their statistical treatment is based on two groups of integral equations combined with approximating closure relations – the BBGKY hierarchy and the Ornstein-Zernike equation, see [Han91].

Correlations also play a central role in the description of the electronic properties of solids. While the physical properties of many materials like simple metals, semiconductors, and insulators are successfully explained by modern solid-state physics, there are, however, materials like transition metals and their oxides, in which electrons experience strong Coulomb interactions [Ima98]. The influence of these strongly interacting electrons among each other is pronounced to such an extent that an effective one-body description fails [Ess05]. Therefore, correlations must not be neglected, but are very important.

Materials consisting of strongly correlated electrons are often highly sensitive to small changes in external parameters. The corresponding effects include dramatic changes in the resistivity at the metal-insulator transition [Anz68, Spa68, Anz86], high transition temperatures of cuprate superconductors, and volume-collapse transitions of rare earth metals [McM98]. Furthermore, there are strongly correlated materials featuring a huge thermoelectric power [Wol65], and others showing colossal magnetoresistance, i.e., a very high sensitivity to changes in an applied magnetic field [Ram97]. The description of such strongly correlated electrons is often based on model Hamiltonians such as the (single band) Hubbard model [Ess05]. Compared to the full many-body problem this model takes into account only a few relevant degrees of freedom, but is effective (and complex) enough to retain the essential physical phenomena (see [Kot04] for a clear overview).

Deceptive in its simplicity, the Hubbard model is acknowledged as a paradigm of strongly correlated electron systems in condensed matter physics. Given the importance attached to this idealized description, it is remarkable that an almost perfect realization of this model is accessible by ultracold repulsive fermionic atoms exposed to the periodic potential of an optical lattice [Kö05]. The control over all relevant parameters in these systems provide a novel approach for the study of correlation effects on a quantitative level. The same holds for corresponding bosonic gases in optical lattices. They provide a realization of the Bose-Hubbard model including its quantum phase transition from a superfluid to a Mott-insulating phase [Gre02], even in the standard regime where the average interparticle spacing is much larger than the scattering length. Thus, by using optical lattices actually extremely dilute gases enter the regime of strong coupling, cf. figure 1.1. In addition, the exploration of strong correlations with ultracold gases is possible by using Feshbach resonances [Kö06]. Their ability to tune the pairwise interaction strength allows, e.g., for the exploration of the crossover, which takes place in two-component fermionic systems, from a molecular Bose-Einstein condensate of tightly bound pairs to a BCS superfluid of weakly bound Cooper pairs [Oha02]. This crossover promises insights into recent questions of quantum fluids and high-transition-temperature superconductors [Che05].

One of the biggest advantages of using ultracold atoms for the investigation of correlation phenomena is evidently the possibility of *dynamically* changing relevant parameters like the coupling parameter T , and thus studying the real-time dynamics of strongly correlated systems. However, this requires precise experiments in difficult conditions. In particular, additionally to the demanding creation of ultralow temperatures and preparation of adequate traps [Phi98], the detection methods essentially need to be correlation-sensitive. For a recent overview on the subject of ultracold gases covering this issue and, in general, many body correlations, see [Blo08a].

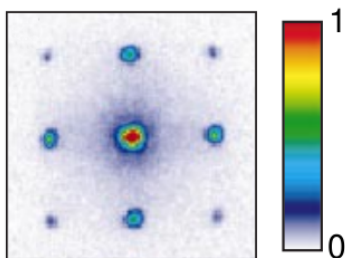


Figure 1.1: Absorption image of a matter-wave interference pattern after the ^{87}Rb atoms were released from an optical lattice potential. It reflects the strong coupling of the atoms within the optical lattice as well as the high degree of phase coherence. From reference [Gre02].

Further systems, also allowing for the investigation of strong coupling phenomena, are the ionic crystals [Win87, Dre98]. These systems consist of laser-cooled ions confined in electromagnetic traps. Due to the very low temperatures in the order of mK, the electrostatic energy of the mutual Coulomb interactions between the ions becomes much larger than the thermal energy ($\Gamma > 100$). As a result, the correlated ions show long-range order and form crystalline (shell-like) structures [Mor06], cf. figure 1.2.

Beside the appearance of correlation effects at low temperatures, strongly correlated systems can also be found at high temperatures. One of these systems, the quark-gluon-plasma, is subject to the probable most extreme conditions and is, at the same time, a recent research topic. This state of matter consisting of deconfined quarks and gluons has a major role in the description of the early universe and of neutron stars. Using highly relativistic particle collisions, it is experimentally studied¹ at the Relativistic Heavy Ion Collider (RHIC) at BNL [STA05, PHE05, PHO05, BRA05] and its investigation is one of the projected aims of the ALICE collaboration at the Large Hadron Collider (LHC) at CERN as well [ALI08]. Primarily expected to be a weakly interacting gas of quarks and gluons [Col75, Shu78], the experiments up to now give strong evidence that the quark-gluon plasma actually behaves like a strongly

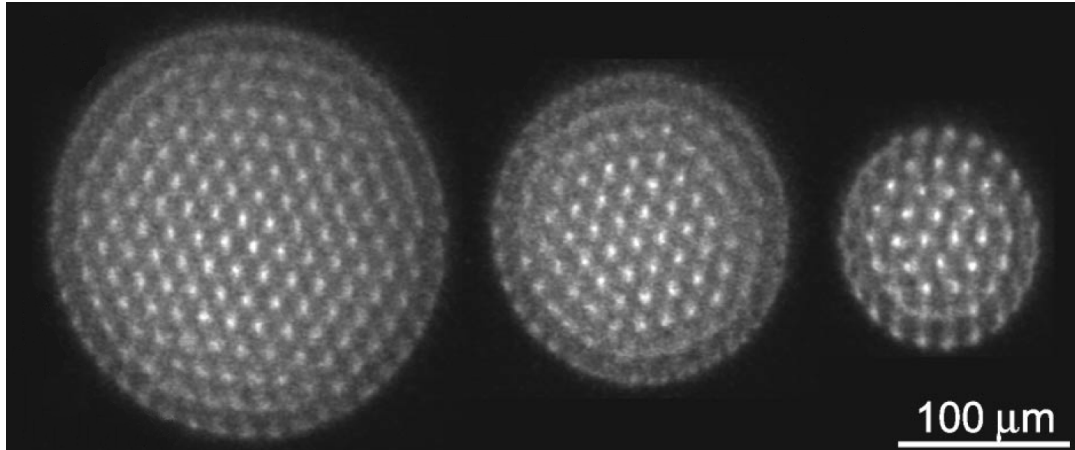


Figure 1.2: Recent observation of 1700, 770, and 290 $^{40}\text{Ca}^+$ ions confined in a radio-frequency Paul trap. The ordered structure of the three-dimensional spherical crystal is evident. From reference [Mor06].

¹ First experimental evidence was found at the Super Proton Synchrotron (SPS) at CERN [Abb00, NA500].

coupled fluid with extremely low viscosity [Hei09, Mü06]. After initial debate, this view is supported by first principle QCD lattice calculations as well [Shu04].

In spite of the differences from the quark-gluon plasma, classical systems may show similar properties regarding correlation effects [Tho05, Tho09]. Among the most promising classical strongly coupled systems are complex (dusty) plasmas (see, for example, [Mer04]). These are low-temperature plasmas containing, additionally to the electrons and ions, nano- or micrometer-sized particles of very high charges ($q \approx 10^3$ - 10^5 elementary charges). Directly linked to the high charges is one of the most fascinating aspects of complex plasmas. That is the formation of plasma crystals [Chu94, Hay94, Tho94], including three-dimensional spherical clusters (Yukawa balls) [Arp04], showing in an impressive manner correlated many-particle behavior, cf. figures 1.3 and 1.4.

A classification of these complex plasmas among other charged particle systems featuring strong coupling is given in the density-temperature diagram 1.5. There, additionally to the coupling parameter Γ , also the Brueckner parameter r_s is plotted, which is defined by the ratio of the mean interparticle distance and the effective Bohr radius. This quantum coupling parameter takes into account non-classical effects, which in the case of high densities prevent the formation of correlated structures. The transition from the classical to the quantum regime is quantified by the degeneracy

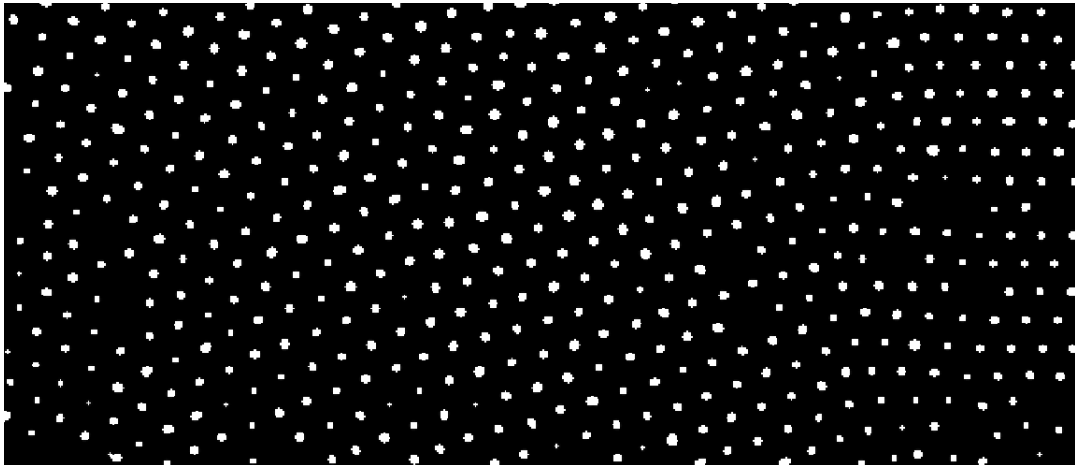


Figure 1.3: *Experimental image of an extended plasma crystal consisting of two layers. The bright spots correspond to the dust particles. From reference [Mel97].*

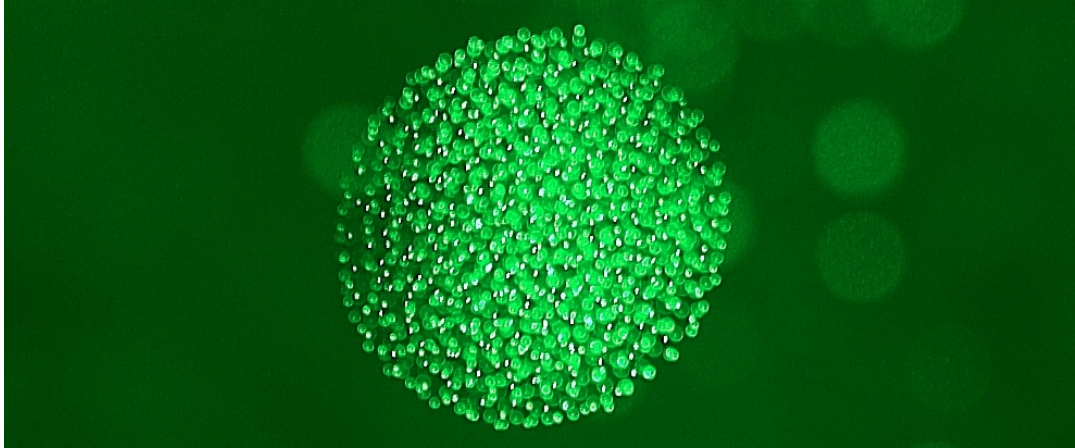


Figure 1.4: *Photograph of a laser light illuminated Yukawa ball consisting of several hundred dust particles. The spherical crystal with a diameter of about 7 mm shows a shell-like structure. Kindly provided by Dr. D. Block.*

parameter χ , which indicates the ratio of the quantum-mechanical particle extension and the mean distance of neighboring particles [Bon08]. In spite of the huge ranges of density and temperature, it is remarkable that, in consideration of the correlation effects, these systems (and many more) feature common properties, which can be characterized by only two parameters, Γ and r_s .

However, in most systems the observation and experimental analysis of strong correlations is difficult, requiring, in many cases, extreme conditions such as very low temperatures or specific densities. An exception are complex plasmas. As a consequence of the dust particles' high charge, they exhibit very strong correlations even at room temperature (Γ values exceeding 500 and above [Blo09]), and, due to the particles' high mass, they allow for high-precision experiments [Fen07, Iva07]. Many quantities such as crystal structure, pair distribution, normal modes, and even single particle trajectories can be directly observed in the experiment (even with the naked eye), making this field an ideal test case for the theoretical concepts of strongly correlated many-body systems. On grounds of this significant role, a basic understanding of the complex plasmas is indispensable. Therefore, particularly the recently discovered three-dimensional plasma crystals have already excited intensive experimental and theoretical activities (for a recent overview, see [Blo07b]).

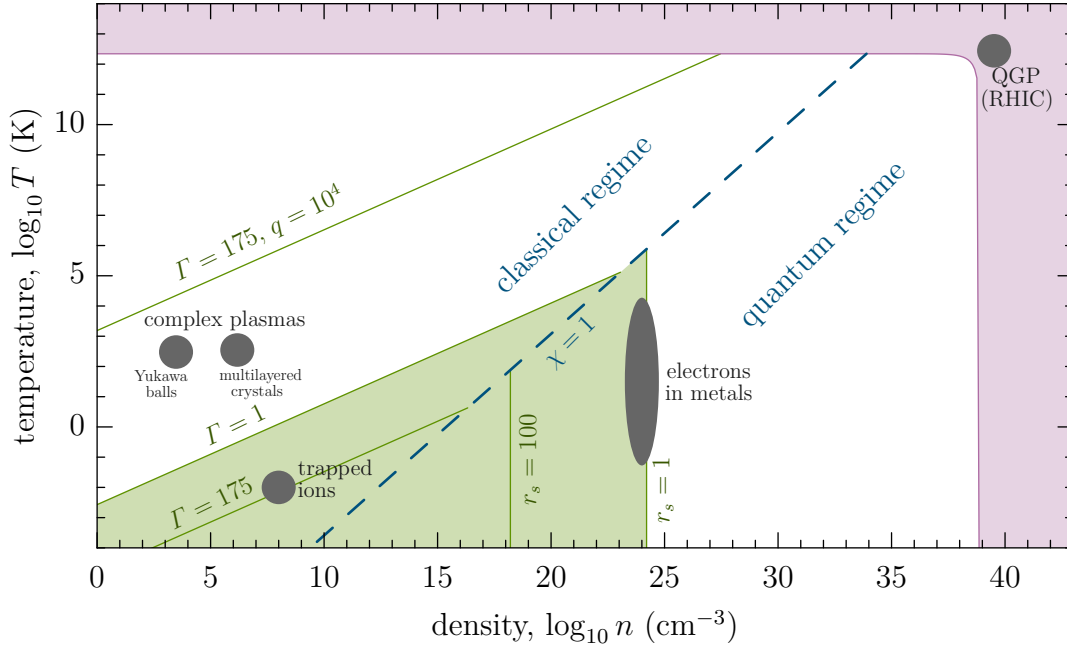


Figure 1.5: Density-temperature diagram of charged particle systems. The line $\chi = 1$ separates classical and quantum systems. Singly charged, strongly coupled systems can be found in the green shaded area enclosed by the lines $\Gamma = 1$ and $r_s = 1$. Higher charges q of the particles, as in complex plasmas, extend the area, where strong correlation effects are present. The red shaded area indicates the deconfined state of hadronic matter, i.e., the quark-gluon plasma. Several example systems are included, density and temperature values of which are gathered from [Dre98, Arp04, Tho04, Hay99].

1.2 Yukawa Balls

Experimental complex plasmas are generally produced in radio-frequency discharges by immersing, typically, micrometer-sized monodisperse (dust) particles. Similar to floating probes within a plasma, these dust particles acquire very high negative charges, leading to a strong electrostatic repulsion of the particles. However, without additional arrangements, these dust particles sediment towards the lower electrode until they are levitated by its electric field. Due to the monodisperse character of the particles, they can be considered identical, and hence, their height above the electrode will be almost equal. Therefore, they arrange themselves in nearly two-dimensional monolayered crystals, cf. figure 1.3.

The formation of three-dimensional crystals requires the switch-off or the compensation of gravitation in the laboratory frame, as possible by microgravity experiments [Mor99] or by using a thermophoretic force [Rot02]. However, in such experiments the formation of three-dimensional crystals is limited by an emerging void, i.e., dust-free region in the center of the discharge.

The possibility to create three-dimensional spherical dust crystals not subject to the formation of voids has been shown by Arp et al. [Arp04], and established a recent field of research. The generation of these three-dimensional crystals, which are called *Yukawa balls*, is enabled by surrounding the dust particles by dielectric (glass) walls, which reduce the plasma production in its inside and effectively prevents the void formation [Arp06]. The corresponding experimental setup is shown in figure 1.6. There, the basic forces acting on the dust particles are displayed as well. The confinement of the Yukawa balls, which results from these forces, was shown to be almost isotropically harmonic [Arp05] without significant contributions from a self-confinement mechanisms, as proposed in [Tot05].

Although the dust particles do not significantly influence their confinement, they have strong mutual impact due to their interaction, which is based on their high charge. However, as a consequence of the surrounding plasma, the interaction in complex

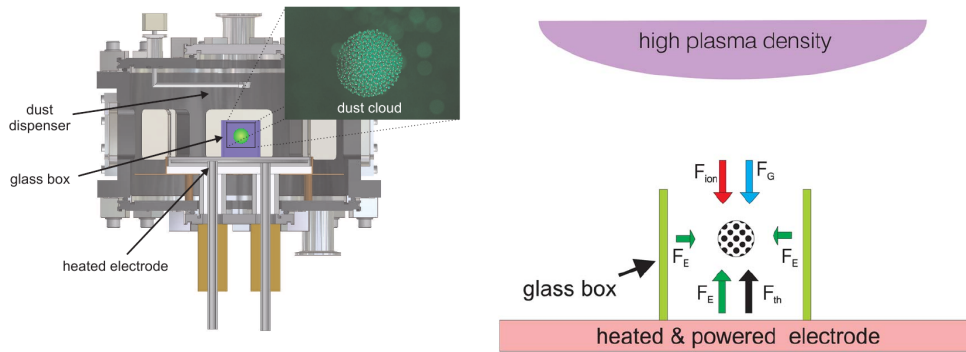


Figure 1.6: *Left:* Side view of the experimental setup used to create Yukawa balls. The arrangement consists of a heated lower electrode ($T < 90^\circ\text{C}$), a grounded vacuum vessel at room temperature, and a glass box, the upper and lower side of which is left open. Dust particles, injected from the top of the setup via a dust dispenser, can form a Yukawa ball inside this glass box. The inset shows an image of a such a Yukawa ball with 1cm in diameter. *Right:* The confinement of a Yukawa ball within the glass box is established by the superposition of gravity F_G , electric force F_E , thermophoretic force F_{th} , and ion-drag force F_{ion} . From references [Blo07b, Arp06].

plasmas is not pure Coulomb, but is dynamically screened. The specific form of this screening and, in particular, the effect of streaming ions is of great interest, and may result in unusual phenomena like attractive forces (see, for example, [Pie02]). For the Yukawa balls, this effect is negligible because the dust particles are situated in a subsonic ion flow regime [Arp06]. In this case the screening is static and well described by an isotropic Debye-Hueckel or Yukawa potential, $q^2 \exp(-\kappa r)/r$, which justifies the naming of the three-dimensional spherical crystals. Hence, the influence of the surrounding plasma on the interaction is specified only by the screening parameter κ , which is dependent on the densities $n_{e,i}$ and temperatures $T_{e,i}$ of the electrons and ions,

$$\kappa = \sqrt{4\pi e_0^2 \left(\frac{n_e}{k_B T_e} + \frac{n_i}{k_B T_i} \right)}. \quad (1.1)$$

Therefore, an effective theoretical model for the Yukawa balls is given by a 3-dimensional, classical system of N identical particles harmonically confined by the potential

$$\phi(\mathbf{r}) = \frac{m\omega_0^2}{2} \mathbf{r}^2, \quad (1.2a)$$

and interacting with an isotropic Yukawa-type pair potential

$$v(r) = q^2 \frac{\exp(-\kappa r)}{r}. \quad (1.2b)$$

The Hamiltonian of this system is then given by¹

$$H(\mathbf{r}, \mathbf{p}) = \underbrace{\sum_{i=1}^N \frac{\mathbf{p}_i^2}{2m}}_{K(\mathbf{p})} + \underbrace{\sum_{i=1}^N \phi(\mathbf{r}_i) + \frac{1}{2} \sum_{i \neq j}^N v(|\mathbf{r}_i - \mathbf{r}_j|)}_{U(\mathbf{r})}. \quad (1.3)$$

By using this model an adequate description of the Yukawa balls is given [Bon06a], allowing for their theoretical investigation, which, regarding essential ground state and excitation properties, is the aim of this thesis.

¹ In the following $3N$ -dimensional vectors are written upright, $\mathbf{r} = (\mathbf{r}_1, \mathbf{r}_2, \dots, \mathbf{r}_N)$.

1.3 Thesis Outline

After closing this introductory chapter, the thesis at hand is organized in two main parts:

Chapter 2: Ground state theory of Yukawa balls This chapter provides a statistical theory suitable to describe the ground state density profiles of Yukawa balls. Within the frame of this theory, two approximations are used, which yield analytical results for the average particle distribution. These results are compared with exact densities, which are obtained from numerical simulations. In doing so, particular attention is paid to the surprisingly strong influence of the screening parameter κ on the results. At the end of this chapter the so-called shell models, which provide an alternative approach towards the ground state structure of Yukawa balls, are investigated, and in conclusion a new shell model is derived.

Chapter 3: Normal Modes of Finite Clusters Within this chapter a detailed analysis of excitation properties based on normal modes is presented. Special attention is paid to one of the most important modes, the breathing mode, which is known from harmonically confined Coulomb systems. After deriving its existence conditions for isotropic clusters in general, the surprising result of a vanishing breathing mode is illustrated for Lennard-Jones clusters and for Yukawa balls, as well. Further, the direct consequences of these results are investigated – also in regard to the influence of dissipation.

In the final chapter the results of this thesis are summarized and complemented by suggestions for future work.

CHAPTER 2

Ground state theory of Yukawa balls

Probably the most striking forms of appearance of strong correlation effects are the liquid states and the crystal formation which were predicted and observed in various geometries. In particular, Yukawa balls show a three-dimensional crystal formation with a pronounced structure of interlaced spherical shells [Arp04], which is also known from spherically trapped ultracold ions [Mor06]. Contrary to the ultracold ions, properties of the Yukawa balls, like their shell population and their shell radii, can be easily measured [Arp04], and hence allow for a comparison with results from simulations and theories [Blo07a, Bon06a]. One of the main results expresses that the particle number on the shells is dependent on the screening of the interaction: with increasing κ of the Yukawa interaction (1.2b) more and more particles are located on inner shells, i.e., the average particle distribution is changed [Blo08b, Blo07a, Bon06a, Gol06]. Within the frame of the thesis at hand, this change of the average particle distribution could be understood from a theoretical point of view [Hen07, Hen06].

One approach for the description of the average particle distribution is provided by so-called Coulomb shell models [Has91, Tsu93, Kra06, Cio08] and Yukawa shell models [Tot05, Bau07], in which a shell-like structure is included a priori. The objective of these models, which are presented in section 2.5, is to achieve an accurate prediction of the shell populations and of the shell radii. However, the shell models are somewhat artificial due to their immanent shell structure and a completely analytical theory should replace them.

Therefore, another approach is used: thermal equilibrium statistical mechanics. It provides the theoretical foundation for the determination of the average particle distribution, i.e., the density profile, and allows for this determination by using a simple variational principle. The idea behind is very basic – the equilibrium density profile minimizes the corresponding Helmholtz free energy [Eva79]. For the case of zero temperature, as it is studied within this chapter, the free energy equals the energy, thus the ground state density profile can be obtained by minimizing the latter one [Hen07, Tot06a, Hen06, Tot01].

In order to accomplish the minimization, within the next section an expression for the energy depending on the density is derived. In principle, its variation provides an equation for the determination of the ground state density profile. However, due to the incomplete knowledge of particle correlations this is not possible in full generality. For this reason, within the subsequent sections 2.2 and 2.4, two of the most essential approximations, the mean-field and the local density approximation, are introduced, which yield analytical solutions for the ground state density. By means of these solutions, the effect of screening on the density profile is revealed. Finally, the quality of the approximations is investigated by comparison with simulation results, which are presented in section 2.3.

2.1 Variational Problem of the Energy Functional

In order to consider a statistical theory of Yukawa balls, of course, not only one such system but an ensemble of these has to be used. Due to the fixed particle number, the appropriate statistical ensemble is the canonical one, which also depends on the temperature T or rather its inverse $\beta = (k_{\text{B}}T)^{-1}$. The proper N -particle distribution of the equilibrium is then given by

$$f(\mathbf{r}, \mathbf{p}) = \frac{1}{h^{3N} N!} \frac{e^{-\beta H(\mathbf{r}, \mathbf{p})}}{Z}. \quad (2.1)$$

The quantity $f(\mathbf{r}, \mathbf{p}) \, d\mathbf{r} \, d\mathbf{p}$ represents the probability that the phase point describing the state of the system is included in the infinitesimal phase-space volume $d\mathbf{r} \, d\mathbf{p}$ at (\mathbf{r}, \mathbf{p}) . The factor $1/N!$ makes allowance for the indistinguishability of the particles, while the power of Planck's constant, h^{3N} , ensures the correct correspondence to

quantum statistics [Han91]. The partition function,

$$Z = \frac{1}{h^{3N} N!} \text{Tr} e^{-\beta H(\mathbf{r}, \mathbf{p})}, \quad (2.2)$$

then normalizes this probability density such that its 'classical' trace, i.e.,

$$\text{Tr} \equiv \int_{\mathcal{V}^N} d\mathbf{r} \int d\mathbf{p}, \quad (2.3)$$

yields unity. Within this trace, there is the constraint that only those states are considered, in which all particles are situated within the spatial region \mathcal{V} . While for unconfined, homogeneous systems only its volume is of importance, here indeed the actual region is decisive. Thus, all statistical quantities like the partition function or statistical averages are depending on T, N, \mathcal{V} .

The ensemble average of a physical quantity $O(\mathbf{r}, \mathbf{p})$ can be calculated using the N -particle distribution,

$$\langle O \rangle = \text{Tr} [f(\mathbf{r}, \mathbf{p}) O(\mathbf{r}, \mathbf{p})]. \quad (2.4)$$

For only space-dependent quantities $O(\mathbf{r})$ or only momentum-dependent quantities $O(\mathbf{p})$, the latter equation can be simplified due to the factorization into spatial and momentum distributions,

$$f(\mathbf{r}, \mathbf{p}) = f^s(\mathbf{r}) f^m(\mathbf{p}), \quad (2.5)$$

with

$$f^s(\mathbf{r}) = \frac{e^{-\beta U(\mathbf{r})}}{\int_{\mathcal{V}^N} d\mathbf{r} e^{-\beta U(\mathbf{r})}} \quad \text{and} \quad f^m(\mathbf{p}) = \frac{e^{-\beta K(\mathbf{p})}}{\int d\mathbf{p} e^{-\beta K(\mathbf{p})}}. \quad (2.6)$$

Hence, in those cases the ensemble averages can be written as

$$\langle O \rangle = \int_{\mathcal{V}^N} d\mathbf{r} f^s(\mathbf{r}) O(\mathbf{r}) \quad \text{and} \quad \langle O \rangle = \int d\mathbf{p} f^m(\mathbf{p}) O(\mathbf{p}), \quad (2.7)$$

respectively. This is applicable in the derivation of the ensemble average of the energy $E = \langle H \rangle$, which itself can be separated into momentum-dependent kinetic energy, $K(\mathbf{p})$, and into spatially dependent potential energy, $U(\mathbf{r})$. Thus, the average energy

is given by

$$\begin{aligned}
 E &= \langle H(\mathbf{r}, \mathbf{p}) \rangle = \langle K(\mathbf{p}) \rangle + \langle U(\mathbf{r}) \rangle \\
 &= \frac{\int d\mathbf{p} K(\mathbf{p}) e^{-\beta K(\mathbf{p})}}{\int d\mathbf{p} e^{-\beta K(\mathbf{p})}} + \int_{\mathcal{V}^N} d\mathbf{r} f^S(\mathbf{r}) U(\mathbf{r}).
 \end{aligned} \tag{2.8}$$

The first expression can be easily calculated by rewriting it as a derivate of a logarithm and then using the known integral of a Maxwellian distribution, which finally yields the well-known result $3Nk_B T/2$. To calculate the second expression, it is useful to introduce the *reduced spatial distribution functions*

$$f_k^S(\mathbf{r}_1, \dots, \mathbf{r}_k) = \int_{\mathcal{V}^{N-k}} d\mathbf{r}_{k+1} \dots d\mathbf{r}_N f^S(\mathbf{r}), \tag{2.9}$$

so that $f_k^S(\mathbf{r}_1, \dots, \mathbf{r}_k) d\mathbf{r}_1 \dots d\mathbf{r}_k$ represents the joint probability of finding one particle within a volume $d\mathbf{r}_1$ at \mathbf{r}_1 , and another particle within a volume $d\mathbf{r}_2$ at \mathbf{r}_2 , and so on, irrespective of the position of all the other $N - k$ particles. The most important reduced spatial distribution functions are f_1^S and f_2^S . While the former is related to the *ensemble averaged density*,

$$n(\mathbf{r}) = \left\langle \sum_{i=1}^N \delta(\mathbf{r} - \mathbf{r}_i) \right\rangle, \tag{2.10}$$

by

$$n(\mathbf{r}) = N f_1^S(\mathbf{r}), \tag{2.11}$$

f_2^S in turn is related to f_1^S by

$$f_2^S(\mathbf{r}_1, \mathbf{r}_2) = f_1^S(\mathbf{r}_1) f_1^S(\mathbf{r}_2) [1 + h(\mathbf{r}_1, \mathbf{r}_2)]. \tag{2.12}$$

At heart, the latter is given by the *pair correlation function* h , which measures deviations of this probability density from the case of a statistically independent (mean-field) distribution of \mathbf{r}_1 and \mathbf{r}_2 .

For binary interactions, all of the thermodynamic functions can be evaluated from knowledge of $n(\mathbf{r})$ and $h(\mathbf{r}_1, \mathbf{r}_2)$ [Dub99]. Accordingly, by using (2.8)-(2.12) and the

Hamiltonian (1.3), the ensemble averaged energy can be written as

$$\begin{aligned}
 E &= \frac{3}{2} N k_B T + \sum_{i=1}^N \int_{\mathcal{V}^N} d\mathbf{r} f^S(\mathbf{r}) \phi(\mathbf{r}_i) + \frac{1}{2} \sum_{i \neq j}^N \int_{\mathcal{V}^N} d\mathbf{r} f^S(\mathbf{r}) v(|\mathbf{r}_i - \mathbf{r}_j|) \\
 &= \frac{3}{2} N k_B T + \int_{\mathcal{V}} d\mathbf{r} n(\mathbf{r}) \phi(\mathbf{r}) \\
 &\quad + \frac{N-1}{2N} \int_{\mathcal{V}^2} d\mathbf{r} d\mathbf{r}' n(\mathbf{r}) n(\mathbf{r}') v(|\mathbf{r} - \mathbf{r}'|) [1 + h(\mathbf{r}, \mathbf{r}')], \tag{2.13}
 \end{aligned}$$

wherein the integral of interaction contains both, the mean-field and the correlation contribution. For the ground state energy ($T = 0$), which subsequently plays a central role, this expression reduces to

$$E = \int_{\mathcal{V}} d\mathbf{r} \left(u_{\text{trap}}(\mathbf{r}) + u_{\text{mf}}(\mathbf{r}) + u_{\text{corr}}(\mathbf{r}) \right), \tag{2.14}$$

with the energy densities of confinement, of mean-field interaction, and of the correlations

$$u_{\text{trap}}(\mathbf{r}) = n(\mathbf{r}) \phi(\mathbf{r}), \tag{2.15a}$$

$$u_{\text{mf}}(\mathbf{r}) = \frac{N-1}{2N} n(\mathbf{r}) \int_{\mathcal{V}} d\mathbf{r}' n(\mathbf{r}') v(|\mathbf{r} - \mathbf{r}'|), \tag{2.15b}$$

$$u_{\text{corr}}(\mathbf{r}) = \frac{N-1}{2N} n(\mathbf{r}) \int_{\mathcal{V}} d\mathbf{r}' n(\mathbf{r}') v(|\mathbf{r} - \mathbf{r}'|) h(\mathbf{r}, \mathbf{r}'), \tag{2.15c}$$

respectively. This expression for the ground state energy shows the dependence on n and h , which on their part are fixed by the equilibrium N -particle distribution f . Because this distribution yields the lowest value for the energy, n and h in turn have to minimize it. This fact provides the possibility to actually calculate the density profile. For this purpose, the generally unknown pair correlation function is approximated and the minimum of the energy with respect to the density has to be determined, what can be done by a *variational principle*¹. However, within this minimization, two

¹ This minimization of the approximated density-dependent ground state energy is similar to the procedure of the quantum mechanical density functional theory. The energy at hand is a statistical quantity and purely classical though.

restrictions have to be taken into consideration: the density is non-negative everywhere and it reproduces the total particle number, i.e.,

$$\int_{\mathcal{V}} d\mathbf{r} n(\mathbf{r}) = N. \quad (2.16)$$

While the former constraint requires restriction of the allowed variations, the latter constraint can be included by introducing a pertinent Lagrange multiplier μ .

Thus, in the following not the ground state energy (2.14), but a corresponding *energy functional* is considered, which depends not only on N , but also on a density function. In contrast, the dependence on \mathcal{V} is lapsed and the boundless space

$$\mathcal{V} = \mathbb{R}^3 \quad (2.17)$$

is used instead. This is because within this chapter not a volume restrictive density profile of confined dust crystals is considered, but a density profile which is restricted by its confinement only. Thus, the energy functional reads as

$$E[n] = \int d\mathbf{r} \left(u_{\text{trap}}(\mathbf{r}) + u_{\text{mf}}(\mathbf{r}) + u_{\text{corr}}(\mathbf{r}) \right) + \mu \left(N - \int d\mathbf{r} n(\mathbf{r}) \right). \quad (2.18)$$

2.2 Ground State Density Profile in Mean-Field Approximation

One of the most important approximations for the ensemble averaged energy of interaction is the *mean-field approximation*. It utilizes the full non-local mean-field energy density, completely neglects the correlation contributions, i.e., $u_{\text{corr}} \equiv 0$, and is associated with a structure-spanning averaging. The energy functional is then given by

$$E_{\text{mf}}[n] = N\mu_{\text{mf}} + \int d\mathbf{r} n(\mathbf{r}) \left(\phi(\mathbf{r}) - \mu_{\text{mf}} \right) + \frac{N-1}{2N} q^2 \int d\mathbf{r} d\mathbf{r}' n(\mathbf{r}) n(\mathbf{r}') \frac{\exp(-\kappa|\mathbf{r}-\mathbf{r}'|)}{|\mathbf{r}-\mathbf{r}'|}, \quad (2.19)$$

where the explicit form of the Yukawa interaction (1.2b) is being used. This expression is formally equivalent to the electrostatics' expression of a charge distribution with

fixed total charge in an external confinement [Jac99]. The factor $(N - 1)/N$ leads to an effective charge per particle of $q_{\text{eff}} = q\sqrt{(N - 1)/N}$. However, in contrast to electrostatics with its Coulomb interaction, $1/r$, the interaction in (2.19) is screened via $e^{-\kappa r}$. Nevertheless, the density profile in mean-field approximation can be seen as the electrostatic charge distribution in case of a Yukawa interaction. Especially in the limiting case of vanishing screening, this view allows for the solution of the density profile.

2.2.1 The Coulomb Limit and Electrostatics

To obtain the density profile of the harmonically confined system in the Coulomb limit, one can use the well-known textbook result of the electrostatic field of a homogeneously charged ball, which is shown in figure 2.1. If the ball is of radius R_C the density is given by

$$n(\mathbf{r}) = \begin{cases} n_C & |\mathbf{r}| \leq R_C \\ 0 & |\mathbf{r}| > R_C, \end{cases} \quad (2.20)$$

and the charge density is $q_{\text{eff}} \cdot n(\mathbf{r})$. The electric potential caused by this charge density can be obtained by using Gauss's law or by directly solving Poisson's equation.

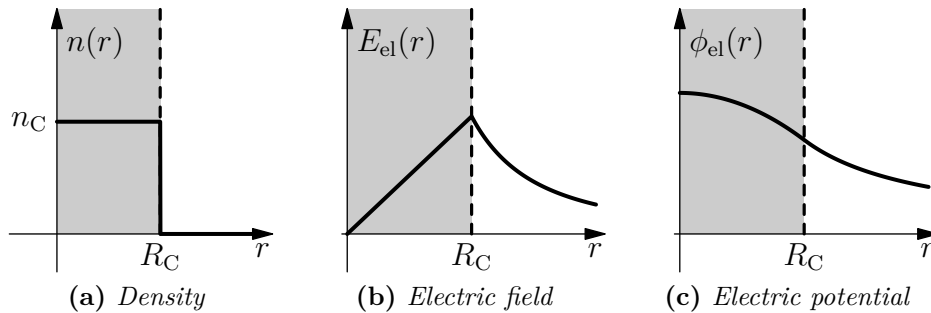


Figure 2.1: A homogeneously charged ball with radius R_C is related to a parabolic electric potential within the ball.

It yields

$$\phi_{\text{el}}(\mathbf{r}) = \frac{4\pi}{3} R_C^3 q_{\text{eff}} n_C \begin{cases} \frac{1}{R_C} \left(\frac{3}{2} - \frac{r^2}{2R_C^2} \right) & |\mathbf{r}| \leq R_C \\ \frac{1}{|\mathbf{r}|} & |\mathbf{r}| > R_C. \end{cases} \quad (2.21)$$

Hence, the electric potential ϕ_{el} is parabolic within the ball and consequently can compensate the external parabolic potential ϕ . This is the case if the density takes a specific value which can be calculated from the equilibrium condition. Namely, equilibrium is attained if the overall potential inside the ball is constant, i.e.,

$$q_{\text{eff}} \phi_{\text{el}}(\mathbf{r}) + \phi(\mathbf{r}) = \text{const.} \quad \forall \mathbf{r} : |\mathbf{r}| \leq R_C. \quad (2.22)$$

By using (1.2a) and (2.21) the equilibrium density results in

$$n_C = \frac{3m\omega_0^2}{4\pi q_{\text{eff}}^2}. \quad (2.23)$$

Additionally, normalization allows the determination of the ball's radius and yields

$$R_C = \sqrt[3]{\frac{q^2(N-1)}{m\omega_0^2}}. \quad (2.24)$$

In summary, from the electrostatic analogy it follows that the mean-field density profile of the harmonically confined system is homogeneous in the Coulomb limit. However, in general the Yukawa balls are not described by Coulomb interacting particles, but by Yukawa interacting ones. Thus, what is the effect of screening on the density profile?

2.2.2 General Solution

As outlined previously, the problem of ascertaining the density profile n_{mf} in the general case of screening is given by determining the minimum of the energy functional (2.19). The vanishing of its linear approximation at the minimum gives then rise to the variational problem

$$0 = \left. \frac{\delta E_{\text{mf}}[n]}{\delta n(\mathbf{r})} \right|_{n=n_{\text{mf}}}. \quad (2.25)$$

The explicit variation of the energy functional E_{mf} gives an inhomogeneous integral equation for the density,

$$0 = \phi(\mathbf{r}) - \mu_{\text{mf}} + q_{\text{eff}}^2 \int d\mathbf{r}' n_{\text{mf}}(\mathbf{r}') \frac{\exp(-\kappa|\mathbf{r} - \mathbf{r}'|)}{|\mathbf{r} - \mathbf{r}'|} \quad \forall \mathbf{r} \in \mathcal{V}_{\text{mf}}, \quad (2.26)$$

which is valid for all space points within the supporting region

$$\mathcal{V}_{\text{mf}} = \left\{ \mathbf{r} \in \mathbb{R}^3 | n_{\text{mf}}(\mathbf{r}) > 0 \right\}. \quad (2.27)$$

This is due to the restriction to non-negative densities. The region \mathcal{V}_{mf} is unrelated to the thermodynamic region \mathcal{V} which is already set by (2.17). The density outside of \mathcal{V}_{mf} vanishes, i.e.,

$$n_{\text{mf}}(\mathbf{r}) = 0 \quad \forall \mathbf{r} \notin \mathcal{V}_{\text{mf}}, \quad (2.28)$$

so that there is an explicit space separation of the density. This is outlined in figure 2.2a. In case of isotropic systems, as is given by the Hamiltonian (1.3), the density profile is isotropic as well. Thus, \mathcal{V}_{mf} has to be spherically symmetric, as shown by figure 2.2b. In this case the integral equation (2.26) can be solved for the density by successive integration, cf. [Hen06] for details.

However, an explicit solution for the density can be obtained more smartly as well, because the kernel of the integral equation (2.26), i.e., the Yukawa potential, is the

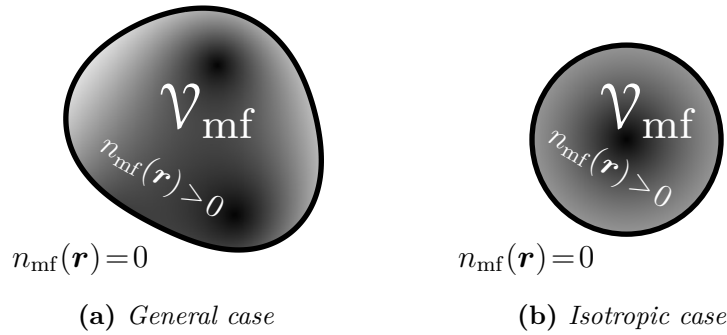


Figure 2.2: Spatial confinement of the ground state density.

Green's function of the Helmholtz operator. This means

$$(\Delta - \kappa^2) \frac{\exp(-\kappa|\mathbf{r} - \mathbf{r}'|)}{|\mathbf{r} - \mathbf{r}'|} = -4\pi\delta(\mathbf{r} - \mathbf{r}'). \quad (2.29)$$

Hence, application of the Helmholtz operator on equation (2.26) yields the explicit solution

$$n_{\text{mf}}(\mathbf{r}) = \frac{1}{4\pi q_{\text{eff}}^2} \left(\Delta\phi(\mathbf{r}) - \kappa^2\phi(\mathbf{r}) + \kappa^2\mu_{\text{mf}} \right) \quad \forall \mathbf{r} \in \mathcal{V}_{\text{mf}} \quad (2.30)$$

for the ground state density profile in mean-field approximation in case of an arbitrary confinement potential. However, within this expression the Lagrange multiplier μ_{mf} as well as the supporting region \mathcal{V}_{mf} are not yet determined.

The calculation of μ_{mf} can be performed by using the constraint of normalization (2.16). Taking into account the results (2.17), (2.28), and (2.30) this yields¹

$$\kappa^2\mu_{\text{mf}} = \frac{4\pi q_{\text{eff}}^2 N - \int_{\mathcal{V}_{\text{mf}}} d\mathbf{r} (\Delta - \kappa^2)\phi(\mathbf{r})}{|\mathcal{V}_{\text{mf}}|}, \quad (2.31)$$

whereas $|\mathcal{V}_{\text{mf}}|$ denotes the volume of the spatial region \mathcal{V}_{mf} . Therefore, only the determination of this region \mathcal{V}_{mf} has to be accomplished. This can be done by inserting the solution (2.30) into its integral equation (2.26), because the latter one contains additional boundary conditions, which are disregarded in (2.30) due to the application of the differential operator. However, the extraction of the supporting region out of the resulting equation

$$4\pi(\mu_{\text{mf}} - \phi(\mathbf{r})) = \int_{\mathcal{V}_{\text{mf}}} d\mathbf{r}' \left(\Delta\phi(\mathbf{r}') - \kappa^2\phi(\mathbf{r}') + \kappa^2\mu_{\text{mf}} \right) \frac{\exp(-\kappa|\mathbf{r} - \mathbf{r}'|)}{|\mathbf{r} - \mathbf{r}'|} \quad \forall \mathbf{r} \in \partial\mathcal{V}_{\text{mf}}, \quad (2.32)$$

is not at all simple.

For isotropically confined dust crystals, i.e. $\phi(\mathbf{r}) = \phi(r)$, the supporting region has to

¹ It should be noted that in the Coulomb case equation (2.31) results in $\int_{\mathcal{V}_{\text{mf}}} d\mathbf{r} \Delta\phi(\mathbf{r}) = 4\pi q^2(N-1)$.

be spherically symmetric, cf. figure 2.2b, and is specified by a ball

$$\mathcal{V}_{\text{mf}} = \mathcal{B}(R_{\text{mf}}), \quad (2.33)$$

which is centered at $\mathbf{r} = 0$, i.e., at the minimum of the trap, and which has a still unknown radius R_{mf} . This circumstance significantly simplifies the issue of determining \mathcal{V}_{mf} from (2.32), because only one parameter, the mean-field radius R_{mf} , has to be found. Indeed, using (2.33) within (2.32) yields, after some algebra,

$$\mu_{\text{mf}} = \phi(R_{\text{mf}}) + \frac{R_{\text{mf}} \phi'(R_{\text{mf}})}{1 + \kappa R_{\text{mf}}}, \quad (2.34)$$

which is an implicit equation for the radius for given μ_{mf} .

2.2.3 Density Profile for Harmonic Confinement

For the special case of harmonic confinement (1.2a), which is of particular interest for the investigation of Yukawa balls, the density profile (2.30) is spherically symmetric and reduces to

$$n_{\text{mf}}(r) = n_{\text{C}} \left(\frac{R_{\text{C}}^3}{R_{\text{mf}}^3} + \frac{\kappa^2 R_{\text{mf}}^2}{10} - \frac{\kappa^2 r^2}{6} \right) \Theta(R_{\text{mf}} - r), \quad (2.35)$$

where the definitions (2.23) and (2.24) of n_{C} and R_{C} have been used. The mean-field radius R_{mf} can be obtained from (2.34) together with the result of μ_{mf} , which yields the implicit equation

$$\kappa^3 R_{\text{mf}}^6 + 6\kappa^2 R_{\text{mf}}^5 = 15 \left(R_{\text{mf}}^3 + \kappa R_{\text{mf}}^4 \right) \left(\frac{R_{\text{C}}^3}{R_{\text{mf}}^3} - 1 \right) \quad (2.36)$$

for the radius. It has a unique positive solution for $R_{\text{mf}}/R_{\text{C}}$, which can be specified as a function of κR_{C} . The result is shown graphically in figure 2.3. While in the unscreened case ($\kappa = 0$) the mean-field radius equals the Coulomb radius R_{C} , for finite screening the mean-field radius is decreased. Thus, in comparison with Coulomb systems the considered Yukawa systems are compressed. This is comprehensible, because the exponential weakening of the interaction results in a reduced total force acting on the outer particles, which therefore move somewhat towards the center.

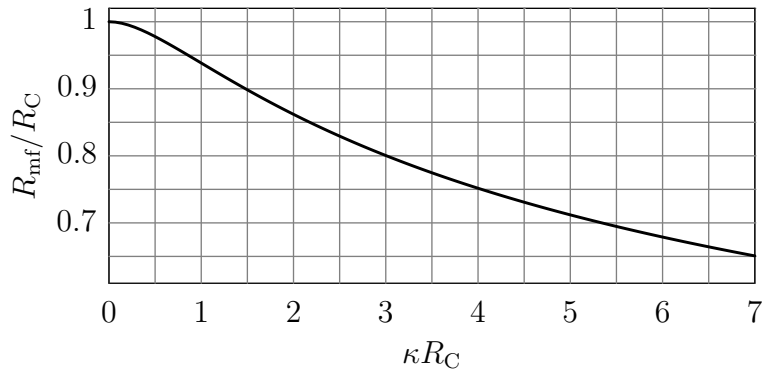


Figure 2.3: The mean-field radius R_{mf} in units of R_C as a function of the normalized screening parameter κR_C .

Often the screening parameter κ is given in units of d_C^{-1} , where d_C is the stable distance between two charged particles in the absence of screening [Bon06a]. One obtains

$$\kappa R_C = \kappa d_C \sqrt[3]{\frac{N-1}{2}}, \quad (2.37)$$

and therefore figure 2.3 shows that not only an increase of κ but also an increase of the particle number at small κ accounts for a stronger compression with respect to the Coulomb case.

With the determined radius the density profile can be calculated from (2.35). Corresponding results for various screening parameters are shown in figure 2.4. On the one hand, in the Coulomb limit ($\kappa R_C = 0$) the constant density profile obtained in section 2.2.1 is recovered. On the other hand, for finite screening inhomogeneous profiles emerge which are accompanied by the aforementioned compression. With increasing κR_C , the density values increase continuously, but most significantly in the center. As a result, the density profiles (2.35) are described by an inverted parabola which terminates in a discontinuity at $r = R_{\text{mf}}$ with a finite density value.

In summary, the mean-field density profile changes radically from a flat profile, in case of a long-range Coulomb interaction, to a profile rapidly decaying away from the trap center in the case of a screened Yukawa potential. This result joins the experimental

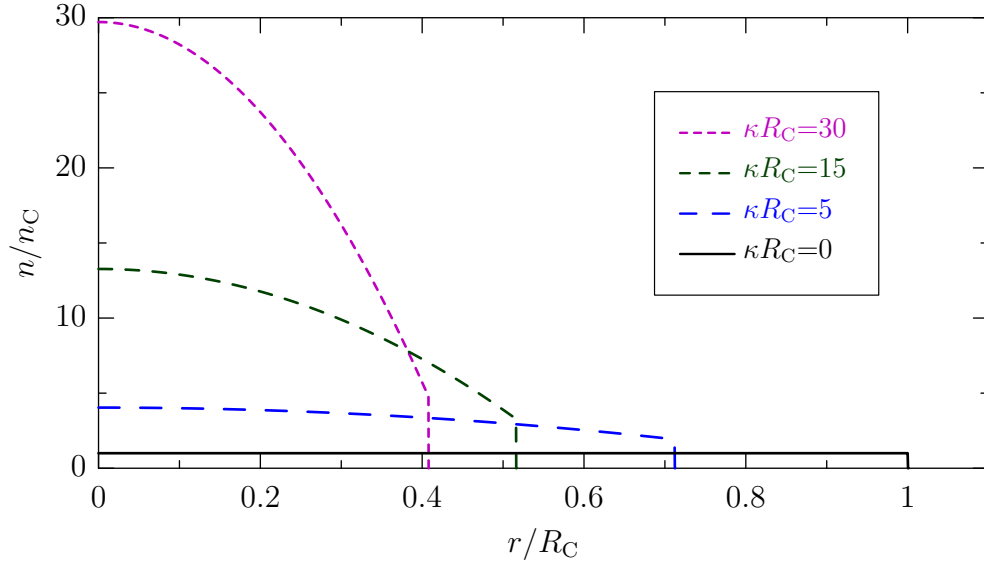


Figure 2.4: Density profile of harmonically confined dust crystals in mean-field approximation for four screening values (lines), from bottom to top: $\kappa R_C = 0$, $\kappa R_C = 5$, $\kappa R_C = 15$, $\kappa R_C = 30$.

and numerical findings [Blo08b, Blo07a, Bon06a, Gol06] and put these across from a theoretical point of view.

2.2.4 Force Equilibrium Within Yukawa Electrostatics

As mentioned previously, the density profile in mean-field approximation can be regarded as the electrostatic charge distribution in case of a Yukawa interaction. How can the parabolically decaying density profile be understood from that point of view?

The determination of the electrostatic charge distribution can not only be seen as a minimizing problem of the electrostatic energy, but equivalently as the question of a *local force equilibrium* for all points where the density is non-zero. The forces in case of a screened Coulomb interaction can be obtained from (2.26), which represents the total potential at the point $\mathbf{r} \in \mathcal{V}_>$. Thus, taking the gradient results in the corresponding force equation. For the harmonic confinement this equation is dependent on the radius

only and yields

$$m\omega_0^2 r = F_{<}(r) + F_{>}(r), \quad (2.38)$$

which means that for any spherical layer at a distance r from the center the external force of the confinement $F_\phi(r) = -m\omega_0^2 r$, which acts towards the center, is balanced by the internal force due to the Yukawa repulsion between the particles. The internal force contains two parts, which are outlined in figure 2.5. The force

$$F_{<}(r) = 4\pi q_{\text{eff}}^2 \frac{e^{-\kappa r}}{r} \left(1 + \frac{1}{\kappa r}\right) \int_0^r dr' r' n(r') \sinh(\kappa r') \quad (2.39a)$$

arises from the action of all particles inside the given layer, $r' \leq r$, and acts outwards, whereas

$$F_{>}(r) = 4\pi q_{\text{eff}}^2 \frac{1}{r} \left(-\cosh(\kappa r) + \frac{\sinh(\kappa r)}{\kappa r}\right) \int_r^{R_{\text{mf}}} dr' r' n(r') e^{-\kappa r'} \quad (2.39b)$$

results from the action of all particles located outside, $r' \geq r$, and acts inwards. The density within these equations has to guarantee the balance of the forces so that (2.38) is fulfilled.

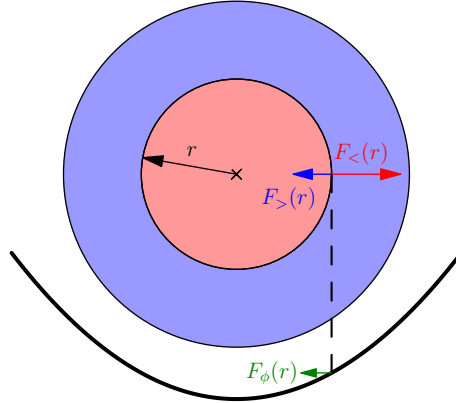


Figure 2.5: Forces within a Yukawa ball for a spherical layer at distance r : External confining force $F_\phi(r)$, Yukawa repulsion $F_{<}(r)$ of all inner particles, and Yukawa repulsion $F_{>}(r)$ of all outer particles.

In the Coulomb case the forces (2.39) simplify to

$$F_{<,C}(r) = \frac{q_{\text{eff}}^2 N_{<}(r)}{r^2}, \quad (2.40a)$$

$$F_{>,C}(r) = 0, \quad (2.40b)$$

with $N_{<}(r) = 4\pi \int_0^r dr' r'^2 n(r')$ being the particle number within the sphere of radius r . These two equations just represent two well known results of Coulomb electrostatics: a spherically symmetric charge distribution produces the same field in the outer region as a point charge at the center of the sphere and the inside of a hollow charged sphere is free of forces. From these equations and the force equilibrium (2.38) it follows that the equilibrated Coulomb density is the constant density $n(r) = n_c$.

In the general case of finite screening, the Coulomb results are not valid anymore, but the principle of equilibrium changes drastically. Now, a hollow charged sphere produces a force towards the center [Pie08], and in case of a constant density this is not balanced by the outward going force $F_{<}$. In order to balance the force an additional central charge, i.e., a higher central density, is required. Thus, the equilibrium density

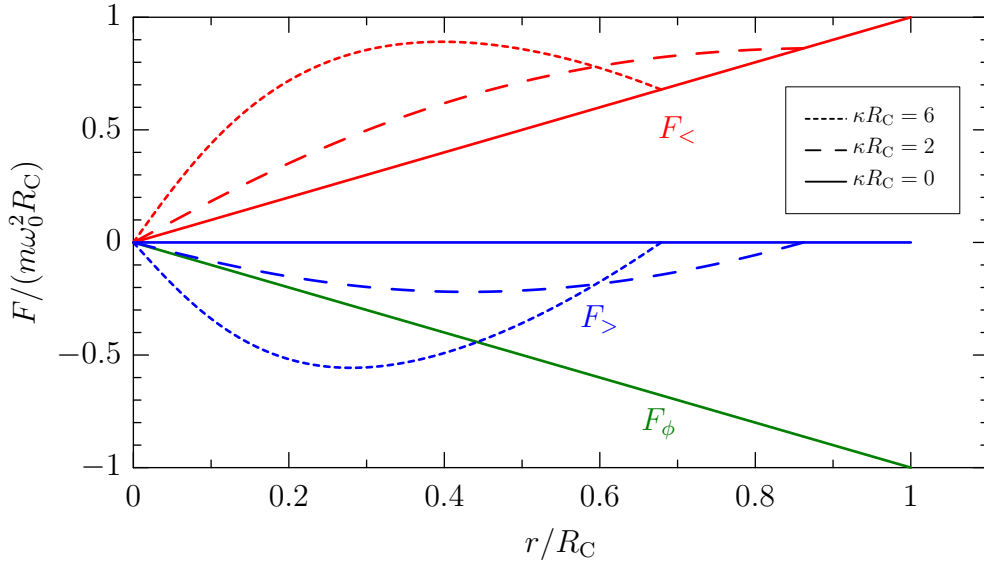


Figure 2.6: Local force equilibrium within a Yukawa ball. For each $r \leq R_{\text{mf}}$ the external force $F_{\phi}(r)$, the Yukawa repulsion $F_{<}(r)$ of all inner particles, and the Yukawa repulsion $F_{>}(r)$ of all outer particles result in a zero net force. In the Coulomb case ($\kappa R_C = 0$) the force $F_{>}(r)$ vanishes identically.

is not constant, but has to increase towards the center. The resulting equilibrated forces are displayed in figure 2.6 for some screening parameters showing the general differences between the Coulomb and the Yukawa principles of forces.

2.3 Simulation Results of Yukawa Balls

The density profiles obtained in the previous section utilize the mean-field approximation. In order to check the quality of this approximation, the density profiles can be compared with results of numerical simulations. One of the best methods for the simulation of the canonical ensemble is the Monte Carlo method with the Metropolis algorithm, which can accurately calculate ensemble averages of physical quantities for finite temperatures [Bon06b]. As an example of such a Monte Carlo simulation, figure 2.7 shows the ensemble averaged density of a Coulomb cluster with $N = 100$ particles for various small temperatures. One clearly sees the shell structure, which becomes more pronounced when the temperature is reduced. For very low temperatures, even a subshell structure emerges.

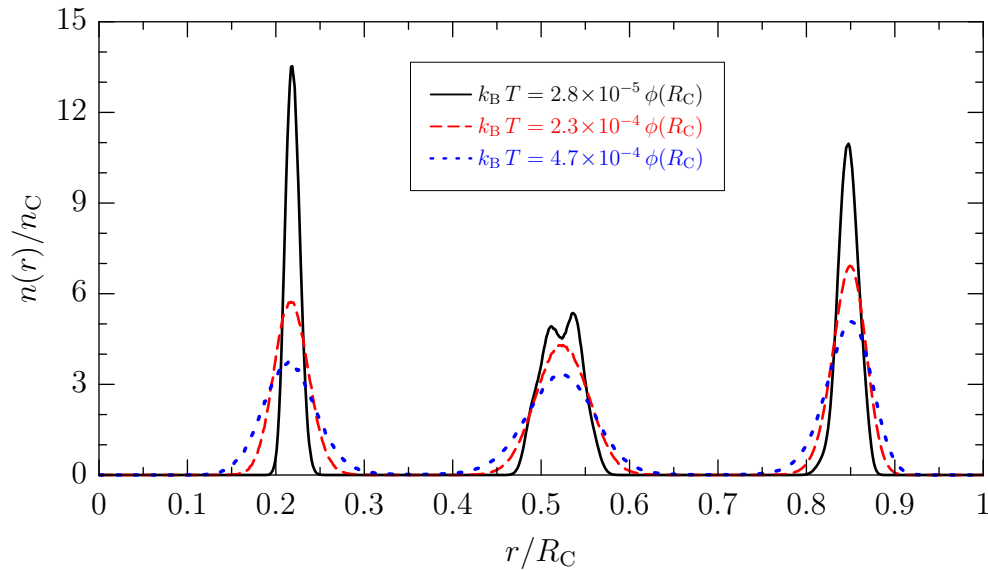


Figure 2.7: *Density profile of a Coulomb cluster with $N = 100$ particles for three low temperatures obtained from Monte-Carlo simulations.*

2.3.1 Ground State Simulations

In case of vanishing temperature the Metropolis algorithm requires more and more computing time to calculate the correct ensemble averages or rather to accurately determine the spatial distribution function f^s . Thus, this method is not appropriate for ground state density profiles.

On closer inspection it becomes apparent that the spatial distribution function at zero temperature may easily be achieved. In fact, it is pinpointed by the global minima, i.e., the ground states, of the Hamiltonian (1.3). This issue is depicted by figure 2.8. There, the configuration-dependent energy of some system is sketched and corresponding distribution functions for three different temperatures T are drawn. For high temperatures all low-energy configurations are nearly equally probable, while for low temperatures only the configurations with lowest energy have a finite probability. Therefore, only the global minima of the Hamiltonian have to be determined to obtain the spatial distribution function and the ensemble averaged density profile for $T = 0$, respectively.

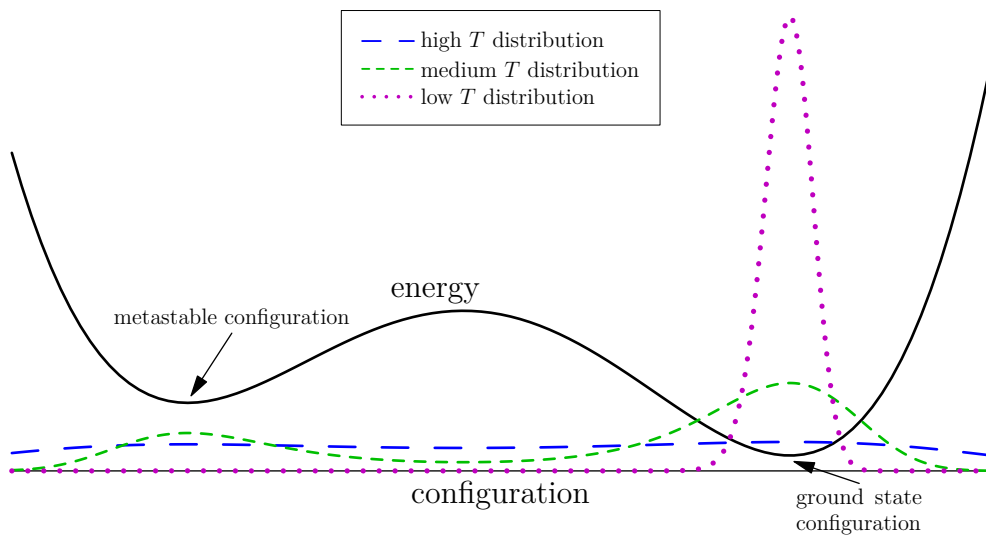


Figure 2.8: Sketch of the configuration-dependent energy of some system and the corresponding probability distribution functions for various temperatures. The low temperature distribution function is peaked at the global minimum, i.e., the ground state configuration.

The Exact Ensemble Averaged Ground State Density

The global minima of the Hamiltonian can be found by global optimization techniques like Basin-Hopping [Wal97] or simulated annealing [Lud05]. In doing so the isotropy of the system entails that each global minimum represents a two-dimensional manifold of global minima, which merge by spatial rotation¹. Let \mathbf{r}_{\min} denote one of these minima. The spatial distribution function is then given by

$$f^s(\mathbf{r}) = \frac{1}{4\pi} \int_0^\pi d\theta \sin \theta \int_0^{2\pi} d\phi \delta^3(\mathbf{r}_1 - \mathbf{R}_{\theta,\phi} \mathbf{r}_{\min,1}) \cdots \delta^3(\mathbf{r}_N - \mathbf{R}_{\theta,\phi} \mathbf{r}_{\min,N}), \quad (2.41)$$

where all global minima are obtained from \mathbf{r}_{\min} by rotation with respect to the spherical coordinates θ and ϕ via the rotational matrix $\mathbf{R}_{\theta,\phi}$. The ground state density

$$n(\mathbf{r}) = \sum_{i=1}^N \int d\mathbf{r}_1 \cdots d\mathbf{r}_N f^s(\mathbf{r}_1, \dots, \mathbf{r}_N) \delta(\mathbf{r} - \mathbf{r}_i), \quad (2.42)$$

which follows directly from the spatial distribution function, cf. (2.10), simplifies considerably by using (2.41), because the Dirac delta functions allow for carrying out all the spatial integrations. The resulting equation

$$n(\mathbf{r}) = \sum_{i=1}^N \frac{1}{4\pi} \int_0^\pi d\theta \sin \theta \int_0^{2\pi} d\phi \delta^3(\mathbf{r} - \mathbf{R}_{\theta,\phi} \mathbf{r}_{\min,i}) \quad (2.43)$$

can be further reduced by splitting up the Dirac delta function into its spherical components and carrying out the angle integrations as well.

Finally, the ground state density, which is expectedly spherically symmetric, can be written as

$$n(r) = \sum_{i=1}^N \frac{\delta(r - |\mathbf{r}_{\min,i}|)}{4\pi r^2}. \quad (2.44)$$

¹ The rotational merging defines an equivalence relation on the set of the global minima. Within the following only one corresponding equivalence class is assumed, i.e., barring the rotational symmetry there is only one global minimum. An extension to the general case of multiple equivalence classes is straightforward.

This equation represents the *exact*, i.e., non-approximated, ensemble averaged ground state density. It shows a delta-peaked shell structure, which is displayed for the Coulomb system of $N = 100$ particles in figure 2.9a.

However, naturally not the structure of all the delta-peaks is called the *shell structure* of the cluster, but the widespread structure of grouped delta-peaks. A clearer graphical representation of this widespread structure is possible by substituting for the point particles of the ground states spherical objects of small size with blurred¹ consistency. By this mollifying not only the shell structure but also the densities of the shells are revealed.

The Mollified Ensemble Averaged Ground State Density

The delta-peaked structure of the exact ground state density is based on the point-like structure of the particles and on the spatial distribution function (2.41), which contains basically a product of Dirac delta functions. In order to get a smoothed structure remaining the essential properties of the original structure, the exact density can be convolved with a mollifier, i.e., a special smooth function. It results in a substitution of the Dirac delta functions δ^3 within (2.43) by a mollifier j^2 . This corresponds either to smooth the Dirac delta functions of the spatial distribution function, and therefore extend the ground state ensemble into a vicinity of the ground states, or, equivalently, to smooth the point-like particles as is shown in figure 2.10.

In general, the mollifier j has to be a smooth, compactly supported, normalized function, and within the following the radially symmetric function

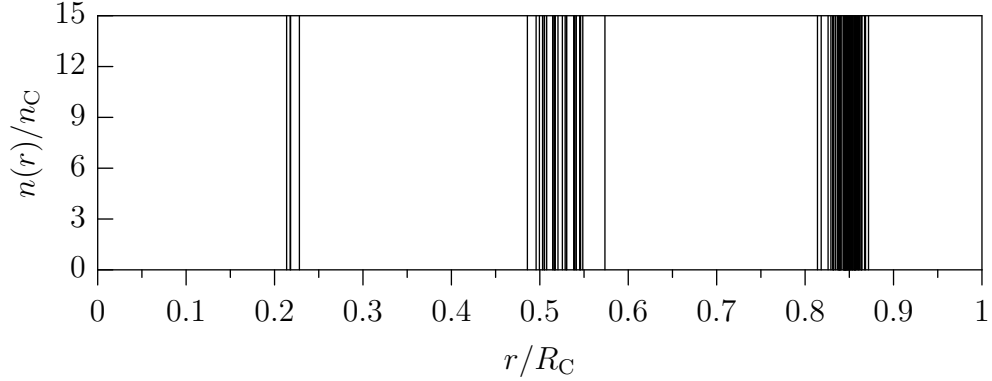
$$j_s(\mathbf{r}) = j_s(r) = c_s e^{(r^2/s^2-1)^{-1}} \Theta(s-r) \quad (2.45)$$

with normalization constant

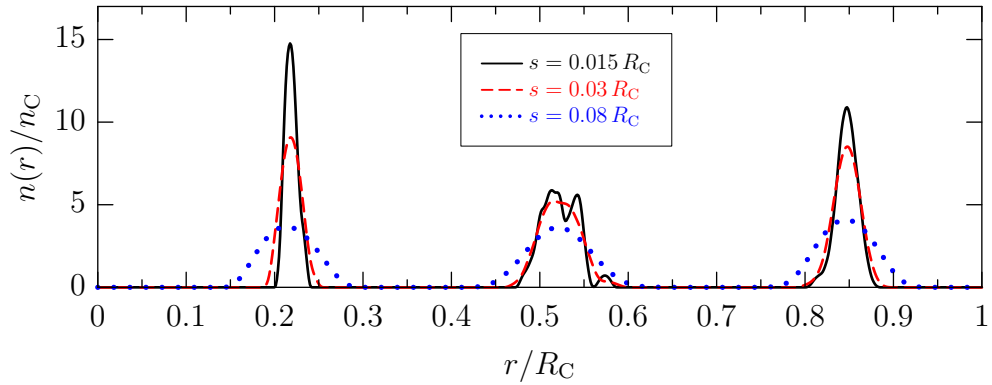
$$c_s = \left(4\pi s^3 \int_0^1 d\tau \tau^2 e^{1/(\tau^2-1)} \right)^{-1} \approx \frac{2.267}{s^3} \quad (2.46)$$

¹ Actually, a substitution by spherical objects with solid consistency is also possible and gives similar results, though the resulting density is not smooth.

² Contrary to this, mollifying expression (2.44) yields a density diverging at $r = 0$.



(a) Delta-peaked structure of the exact ensemble averaged ground state density. Each thin line represents a delta peak.



(b) Smooth structure of the mollified ensemble averaged ground state density. For the point particles expanded spherical objects with radius s were substituted. The three different lines correspond to three different radii of these objects.

Figure 2.9: Ground state density profile of a Coulomb cluster with $N = 100$ particles obtained from the global minima of the Hamiltonian.

will be used. The parameter s describes the support of the function and can be identified with the radius of the finite-sized particles.

The expression of the mollified ground state density, which is derived by using this mollifier within (2.43),

$$n(\mathbf{r}) = \sum_{i=1}^N \frac{1}{4\pi} \int_0^\pi d\theta \sin \theta \int_0^{2\pi} d\phi j_s(\mathbf{r} - \mathbf{R}_{\theta,\phi} \mathbf{r}_{\min,i}), \quad (2.47)$$

can be simplified. Therefore, without loss of generality within each summand of (2.43)

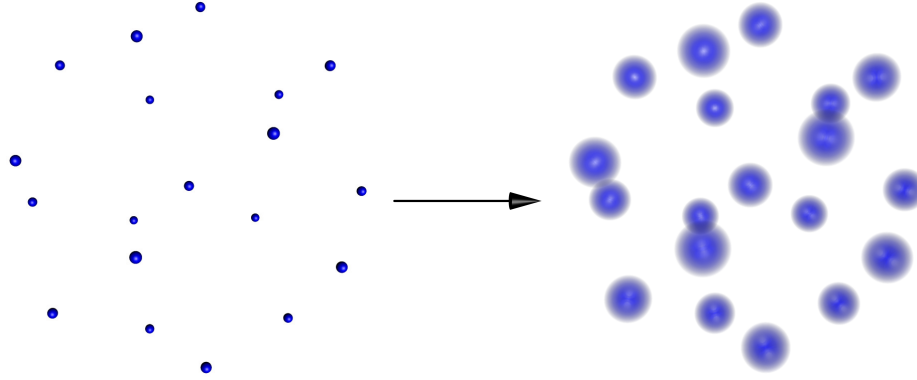


Figure 2.10: A smooth ground state density can be obtained by substituting blurred spherical objects for the point particles.

\mathbf{r}_{\min} is chosen out of the ground states so that its i th particle component $\mathbf{r}_{\min,i}$ is collinear with \mathbf{r} . Then, by putting the z -axis of the coordinate system in the same direction, the norm of $\mathbf{r} - \mathbf{R}_{\theta,\phi} \mathbf{r}_{\min,i}$ is given by $\sqrt{r^2 + r_{\min,i}^2 - 2r r_{\min,i} \cos \theta}$. As a result the mollified density, which is likewise spherically symmetric, yields¹

$$n(r) = \sum_{i=1}^N \mathcal{J}_s(r, r_{\min,i}) \quad (2.48)$$

with the function

$$\mathcal{J}_s(r, \tilde{r}) \equiv \frac{1}{2} \int_{-1}^1 dz j_s(\sqrt{r^2 + \tilde{r}^2 - 2r\tilde{r}z}), \quad (2.49)$$

which can be considered as the density at distance r of a mollified particle, which itself is located at distance \tilde{r} . While these equations give the solution for any symmetric mollifier, in case of (2.45) the integration within the function \mathcal{J}_s can be carried out

¹ For numerical purposes it is convenient to consider bins of N_i particles located at distance r_i from the center. Then (2.48) can be written as $n(r) = \sum_{i=1}^{\#bins} N_i \mathcal{J}_s(r, r_i)$.

and gives, after some algebra,

$$J_s(r, \tilde{r}) = \begin{cases} c_s e^{(\tilde{r}^2/s^2-1)^{-1}} \Theta(s - \tilde{r}) & \text{if } r = 0, \\ c_s e^{(r^2/s^2-1)^{-1}} \Theta(s - r) & \text{if } \tilde{r} = 0 \\ 0 & \text{if } (\tilde{r} - r)^2 \geq s^2 \\ \frac{c_s s^2}{4r\tilde{r}} \left(\text{Ei}\left(\frac{1}{\chi}\right) - \chi e^{\chi^{-1}} \right) & \text{if } (\tilde{r} - r)^2 < s^2, r > 0, \\ & \tilde{r} > 0, \text{ and } r + \tilde{r} \geq s \\ \frac{c_s s^2}{4r\tilde{r}} \left(\text{Ei}\left(\frac{1}{\chi}\right) - \chi e^{\chi^{-1}} - \text{Ei}\left(\frac{1}{\xi}\right) + \xi e^{\xi^{-1}} \right) & \text{else,} \end{cases} \quad (2.50a)$$

with the abbreviations

$$\chi = \frac{(r - \tilde{r})^2}{s^2} - 1 \quad \text{and} \quad \xi = \frac{(r + \tilde{r})^2}{s^2} - 1. \quad (2.50b)$$

In contrast to the first three cases of this expression, the conditions for the last two are maybe not evident. Therefore, within figure 2.11 these two cases are visualized providing a better understanding of (2.50a).

The explicit form of J_s allows for a very fast numerical calculation of the mollified

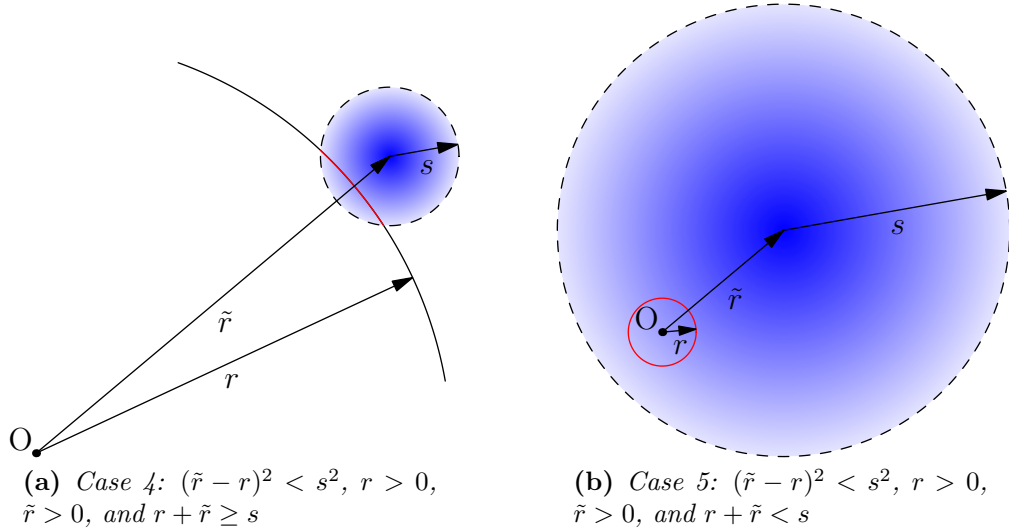


Figure 2.11: The last two cases of expression (2.50a) are visualized. The density J_s at distance r of the mollified particle (blue), which is located at distance \tilde{r} , is determined by the intersection (red) of the particle with a sphere of radius r .

ground state density. For the aforementioned Coulomb system three smoothed results corresponding to three different radii s are shown in figure 2.9b. By means of the mollifier method, there the shell structure, including finite density values within the shells, is evident. This shell structure bears a resemblance to the Monte-Carlo results of finite temperature, cf. figure 2.7. Nevertheless, finite temperature simulations with the Metropolis algorithm use distribution functions which have finite values in the vicinity of ground state and metastable configurations, as sketched in 2.8. The mollified ensemble instead only uses configurations in the vicinity of the ground state, and hence gives an accurate description of the ground state.

By using the mollifier method, the radius s of the particles is a free parameter in the calculation of the smooth density. Thus, different radii give different density profiles. However, the essential properties of the original structure, i.e., the positions and the average densities of the shells, are nearly independent on the choice of s . This is shown within figure 2.12 in more detail. There, the average densities of the shells are displayed in addition to the smoothed density profiles for various radii of the particles ranging from $s = 0.03R_C$ to $s = 0.05R_C$. This is the approximate range of

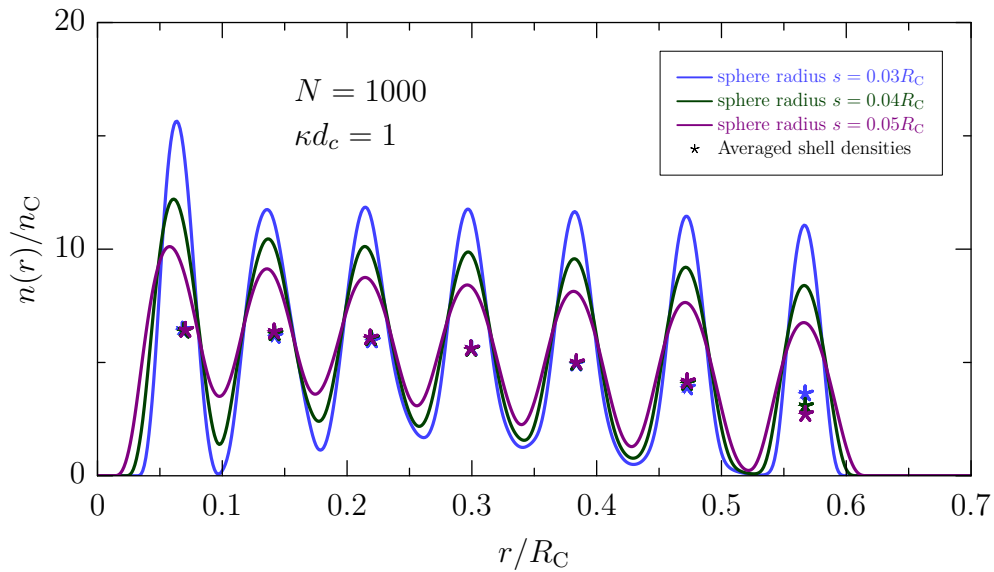


Figure 2.12: Smoothed density of the simulation results of a harmonically confined Yukawa crystal with $N = 1000$ and $\kappa d_C = 1$ with application of various sphere sizes for substitution of the particles: $0.03R_C$ (top curve), $0.04R_C$ and $0.05R_C$. The symbols show the averaged densities of the shells placed on the centers of mass of the shells.

reasonable radii: for smaller values of s the shells break up into subshells, whereas for larger values the amplitude of the oscillations decreases further without effect on the positions and on the average densities of the shells. It is in evidence that only the density of the outer shell is slightly sensitive to the sphere radius due to the increase of the shell's width with increasing s . For the following comparisons, sphere radii corresponding to the average of the possible density values of the outer shell will be used, which, in figure 2.12, is close to $s = 0.04R_C$.

2.3.2 Comparison of Simulation and Mean-Field Results

The mollified ground state density profiles give a possibility of comparison with analytical results like the ones from the mean-field approximation. The direct comparison of figures 2.4 and 2.9b then shows that the mean-field result does not possess any shell structure, what is caused by the neglect of correlations. However, the mean-field results should reflect the average behavior of the density profile, which itself is expressible by the average densities of the shells.

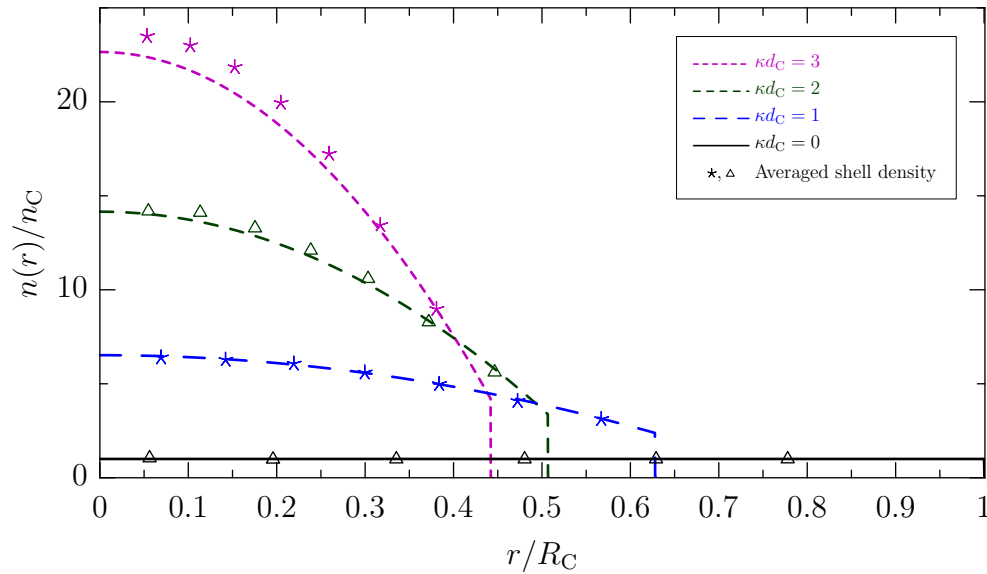


Figure 2.13: Mean-field density profile of a harmonically confined dust crystal for four screening values (lines), from bottom to top: $\kappa d_C = 0$, $\kappa d_C = 1$, $\kappa d_C = 2$, $\kappa d_C = 3$. The symbols denote the average shell densities, which are obtained from numerical simulations of a corresponding system with $N = 1000$ particles.

As an example, the mean-field density of a harmonically confined system with $N = 1000$ particles, which is large enough to exhibit several shells, is shown in figure 2.13. The symbols denote the average particle densities of the shells and are obtained from the mollified results of ground state simulations. The figure shows that the mean-field results not only reflect the average behavior of the density, but quantitatively reproduces the radially decreasing average density very well. However, there are also discrepancies in case of strong screening, cf. $\kappa d_C \gtrsim 2$. These are caused by disregarding the correlation contributions in the mean-field energy functional (2.19), which become important with increasing density. Hence, to remove these deviations the energy functional has to be extended by correlations.

2.4 Inclusion of Correlations by Using the Local Density Approximation (LDA)

One way to include correlations in a simple but very successful way is to use the *local density approximation* [Tot01, Hen07], which is well-known within the context of the density functional theory (see, for example, [Par03] or [Bon06b, chapter 3]). This approximation is based upon the idea of replacing complicated non-local terms within the energy density by simple local expressions using the known energy density of the corresponding homogeneous system. Therefore, this method works fine for nearly homogeneous systems, but it is suitable even in case of rapidly varying densities.

2.4.1 LDA Without Correlations

In order to familiarize with LDA and its characteristics it is advisable first to apply this method only to the energy density without correlations, which is given by $u_{\text{trap}} + u_{\text{mf}}$, cf. (2.15). To substitute this sum by the local density approximated energy density, one has to know the corresponding expression of the homogeneous system. This can be easily obtained by substituting the spatially dependent density $n(\mathbf{r})$ within the

proper energy density by a homogeneous density n_0 . This yields

$$u_{0,\text{trap}} = n_0 \phi(\mathbf{r}) \quad (2.51)$$

$$\begin{aligned} u_{0,\text{mf}} &= \frac{q_{\text{eff}}^2}{2} n_0 \int d\mathbf{r}' n_0 \frac{\exp(-\kappa|\mathbf{r} - \mathbf{r}'|)}{|\mathbf{r} - \mathbf{r}'|} \\ &= \frac{q_{\text{eff}}^2}{2} n_0^2 \int d\mathbf{r}' 4\pi r'^2 \frac{\exp(-\kappa r')}{r'} = q_{\text{eff}}^2 n_0^2 \frac{2\pi}{\kappa^2}, \end{aligned} \quad (2.52)$$

wherein the infinite homogeneous system is considered. Once the energy density of the homogeneous system is available, the energy density of LDA follows by the substitution $n_0 \rightarrow n(\mathbf{r})$

$$u_{\text{LDA},\text{trap}}(\mathbf{r}) = n(\mathbf{r}) \phi(\mathbf{r}) \quad (2.53)$$

$$u_{\text{LDA},\text{mf}}(\mathbf{r}) = q_{\text{eff}}^2 n(\mathbf{r})^2 \frac{2\pi}{\kappa^2}. \quad (2.54)$$

While the expression for $u_{\text{LDA},\text{trap}}$ is identical to the non-approximated expression (2.15a), this is not the case for the density of the mean-field energy. The LDA of the latter one is much simpler than its proper expression (2.15b) and additionally diverges in the long-range Coulomb limit. The reason for this divergence is the neglect of finite-size effects, which are discussed separately at the end of this section.

General Solution

By using the local approximated energy density, the LDA energy functional without correlations is given by

$$E_{\text{LDA}}[n] = N\mu_{\text{LDA}} + \int d\mathbf{r} n(\mathbf{r}) (\phi(\mathbf{r}) - \mu_{\text{LDA}}) + \frac{2\pi q_{\text{eff}}^2}{\kappa^2} \int d\mathbf{r} n(\mathbf{r})^2. \quad (2.55)$$

Its minimum, the LDA ground state density $n_{\text{LDA}}(\mathbf{r})$, is obtained in the same manner as the proper mean-field solution, cf. 2.2.2, and thus given by

$$n_{\text{LDA}}(\mathbf{r}) = \frac{1}{4\pi q_{\text{eff}}^2} (\kappa^2 \mu_{\text{LDA}} - \kappa^2 \phi(\mathbf{r})) \quad \forall \mathbf{r} \in \mathcal{V}_{\text{LDA}} \quad (2.56)$$

for all space points within the supporting region

$$\mathcal{V}_{\text{LDA}} = \left\{ \mathbf{r} \in \mathbb{R}^3 \mid n_{\text{LDA}}(\mathbf{r}) > 0 \right\}. \quad (2.57)$$

The Langrange multiplier μ_{LDA} within is obtain from normalization and given by

$$\kappa^2 \mu_{\text{LDA}} = \frac{4\pi q_{\text{eff}}^2 N + \kappa^2 \int_{\mathcal{V}_{\text{LDA}}} d\mathbf{r} \phi(\mathbf{r})}{|\mathcal{V}_{\text{LDA}}|}. \quad (2.58)$$

Both, the density equation and the equation for the Langrange multiplier, are very similar to the equations of the non-local mean-field solution (2.30) and (2.31), but show one important difference. The Laplacian of the potential $\Delta\phi(\mathbf{r})$ is missing. That is a reflection of the fact that this Laplacian contains derivatives and thus information about contiguous values of the potential, which are generally suppressed within LDA.

However, the determination the supporting region \mathcal{V}_{LDA} cannot be accomplished as in 2.2.2. This is because the LDA energy density is local, so that minimization does only give a local condition for the density in contrast to the non-local integral equation (2.26). The determination can be realized instead by inserting the solution (2.56) directly into the LDA energy functional (2.55) and minimizing the resulting expression with respect to \mathcal{V}_{LDA} , which yields, after some algebra,

$$\mu_{\text{LDA}} = \phi(\mathbf{r}) \quad \forall \mathbf{r} \in \partial\mathcal{V}_{\text{LDA}}. \quad (2.59)$$

Similar to (2.33), due to the symmetry of the isotropically confined Yukawa balls, the LDA supporting region is given by a ball

$$\mathcal{V}_{\text{LDA}} = \mathcal{B}(R_{\text{LDA}}). \quad (2.60)$$

The boundary of this ball is described solely by one parameter, the LDA radius R_{LDA} , so that (2.59) results in

$$\mu_{\text{LDA}} = \phi(R_{\text{LDA}}), \quad (2.61)$$

which is an implicit equation for this radius.

Harmonic Confinement

For the harmonic form of the confinement this implicit radius equation can be explicitly solved and yields

$$R_{\text{LDA}} = \sqrt[5]{15 \frac{R_{\text{C}}^3}{\kappa^2}}, \quad (2.62)$$

and the density profile is only radially dependent and reduces to

$$n_{\text{LDA}}(r) = n_{\text{C}} \frac{\kappa^2}{6} (R_{\text{LDA}}^2 - r^2) \Theta(R_{\text{LDA}} - r). \quad (2.63)$$

Corresponding results are shown in figure 2.14 for three screening parameters. The density profiles clearly possess a parabolic decrease away from the trap center until they vanish in a continuous manner. An increase of the screening parameter κR_{C} leads to a compression with respect to the Coulomb case. At the same time the density values increase continuously, most significantly in the center. Thus, in the

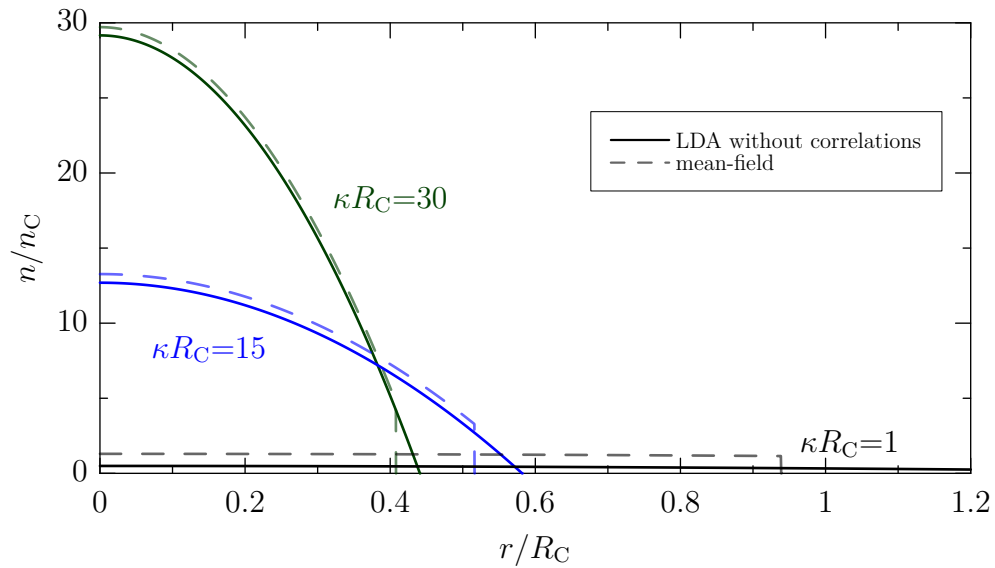


Figure 2.14: Density profile of harmonically confined dust crystals in local density approximation without correlations for three screening parameters (lines), from bottom to top: $\kappa R_{\text{C}} = 1$, $\kappa R_{\text{C}} = 15$, $\kappa R_{\text{C}} = 30$. For comparison, the corresponding non-local mean-field results are shown by the dashed lines.

case of the harmonic potential, the LDA density profile without correlations bears qualitative resemblance to the non-local mean-field density profile.

However, quantitatively in two points both approximations differ from one another as can also be seen in figure 2.14. Firstly, the density in the local density approximation does not show a discontinuity at $r = R_{\text{LDA}}$, in contrast to the mean-field result. This is due to the neglect of finite-size effects in the LDA derivation. Secondly, LDA yields too small values for the density – most evidently in the diverging Coulomb limit. However, this underrating of the density is reduced with increasing values of the parameter κR_C . The reason for this improved behavior with increasing κR_C is due to the fact that an increase of κ contracts the effective area of integration within (2.52). This contraction is in favor of the accuracy of the LDA, because the decreased integration volume contains a more homogeneous density. Additionally, an increase of the particle number N and consequently of R_C flattens the density profile, and will similarly improve LDA.

In summary, the local density approximation without correlations has shown that results of this kind of approximation will of course not be as accurate as their non-local counterparts, but give a good approximation, especially in the case of strong screening.

Improvement of LDA by Inclusion of Finite-Size Effects

Despite the strong results of the LDA density profile without correlations, the local density approximation breaks down in the Coulomb case as can be seen in figure 2.14 or directly from the density (2.63). Hence, the density cannot be normalized anymore, which is the same as in the two-dimensional case [Tot01]. However, the application of the local density approximation cannot be the reason for this breakdown, because this method is based upon the usage of results from the homogeneous system, and the Coulomb system in mean-field approximation is homogeneous with density n_C .

In fact, the cause of the breakdown is the use of the infinite homogeneous system as a reference system, which entails the neglect of any finite-size effects. This failure can be avoided by replacing the energy density of interaction (2.52) by the corresponding expression of the finite homogeneous system. In case of isotropically confined particles,

this system is a ball with radius R_{fs} and the energy density is given by

$$\begin{aligned}
 u_{0,\text{mf}} &= \frac{q_{\text{eff}}^2}{2} n_0 \int_{\mathcal{B}(R_{\text{fs}})} d\mathbf{r}' n_0 \frac{\exp(-\kappa|\mathbf{r} - \mathbf{r}'|)}{|\mathbf{r} - \mathbf{r}'|} \\
 &= \frac{q_{\text{eff}}^2}{2} n_0^2 \frac{2\pi}{\kappa r} \int_0^{R_{\text{fs}}} dr' r' \left\{ -\exp(-\kappa(r + r')) + \exp(-\kappa|r - r'|) \right\} \\
 &= q_{\text{eff}}^2 n_0^2 \frac{2\pi}{\kappa r} \left(e^{-\kappa r} \int_0^r dr' r' \sinh(\kappa r') + \sinh(\kappa r) \int_r^{R_{\text{fs}}} dr' r' e^{-\kappa r'} \right) \\
 &= q_{\text{eff}}^2 n_0^2 \frac{2\pi}{\kappa^2} \left(1 - e^{-\kappa R_{\text{fs}}} (1 + \kappa R_{\text{fs}}) \frac{\sinh(\kappa r)}{\kappa r} \right), \tag{2.64}
 \end{aligned}$$

including a finite-size contribution, which prevents the problem of divergence at $\kappa \rightarrow 0$. As a result, the finite-size effects lead to a corrected density profile

$$n(r) = \frac{1}{4\pi q_{\text{eff}}^2} \frac{\kappa^2 \mu - \kappa^2 \phi(r)}{1 - e^{-\kappa R_{\text{fs}}} (1 + \kappa R_{\text{fs}}) \sinh(\kappa r) / \kappa r} \Theta(R_{\text{fs}} - r), \tag{2.65}$$

instead of equation (2.63), which indeed yields the constant solution $n(r) = n_C$ in the harmonically confined Coulomb case.

As an example, the density profiles with (fs corrected) and without these finite-size contributions are shown in figure 2.15 for $N = 1000$, $\kappa d_C = 0.3$. One clearly sees that in the case of finite-size correction, the density profile shows a discontinuity at the boundary and, correspondingly, it yields increased values of the density. However, the density profile including those edge effects is not monotonically decreasing away from the trap center but has a density increasing part in the outer range due to the space dependence of the denominator in (2.65), cf. the dashed-dotted line. This is in contrast to the proper mean-field results.

A more accurate, monotonically decreasing density profile can also be obtained by taking the finite-size effects only partly into account (partly fs corrected) by using not the finite homogeneous sphere centered at the origin but centered at the point \mathbf{r}

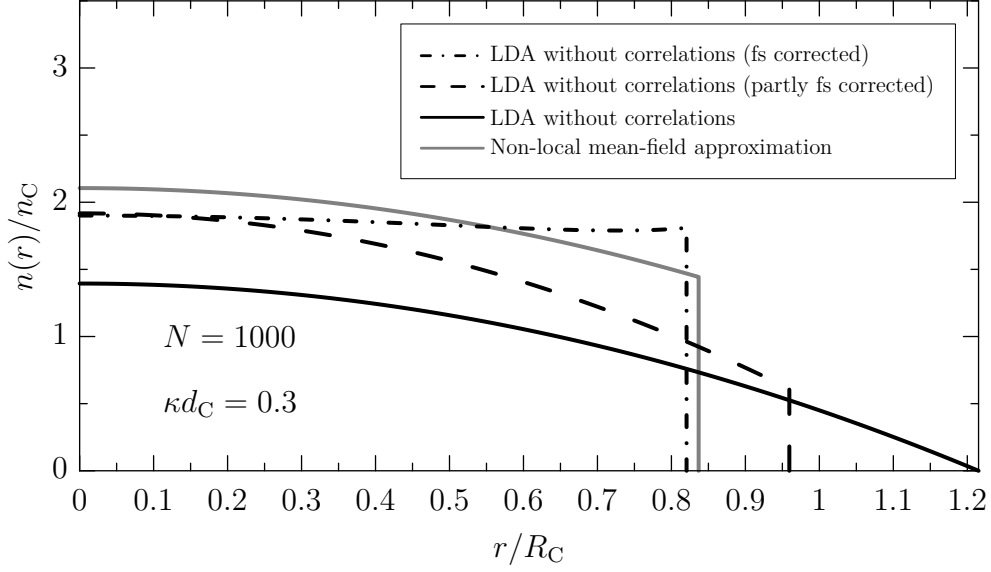


Figure 2.15: LDA density profiles of harmonically confined dust crystals with $N = 1000$ and $\kappa d_c = 0.3$ with and without finite-size effects included. For comparison the exact non-local mean-field result is also shown. The difference between the finite-size correction (fs corrected) and the partial finite-size correction (partly fs corrected) is described in the text.

where the energy density is calculated. This yields

$$\begin{aligned}
 u_{0,\text{mf}} &= \frac{q_{\text{eff}}^2}{2} n_0 \int_{\mathcal{B}(\mathbf{r}, R_{\text{fs}})} d\mathbf{r}' n_0 \frac{\exp(-\kappa|\mathbf{r} - \mathbf{r}'|)}{|\mathbf{r} - \mathbf{r}'|} \\
 &= q_{\text{eff}}^2 n_0^2 2\pi \int_0^{R_{\text{fs}}} dr' r' e^{-\kappa r'} \\
 &= q_{\text{eff}}^2 n_0^2 \frac{2\pi}{\kappa^2} \left(1 - e^{-\kappa R_{\text{fs}}} (1 + \kappa R_{\text{fs}})\right). \tag{2.66}
 \end{aligned}$$

This expression also has no divergent limit for $\kappa \rightarrow 0$, and, at the same time, yields monotonically decreasing density profiles

$$n(r) = \frac{1}{4\pi q_{\text{eff}}^2} \frac{\kappa^2 \mu - \kappa^2 \phi(r)}{1 - e^{-\kappa R_{\text{fs}}} (1 + \kappa R_{\text{fs}})} \Theta(R_{\text{fs}} - r), \tag{2.67}$$

as can be seen by the dashed line in figure 2.15.

The two methods to include finite-size effects as well as LDA with the infinite ho-

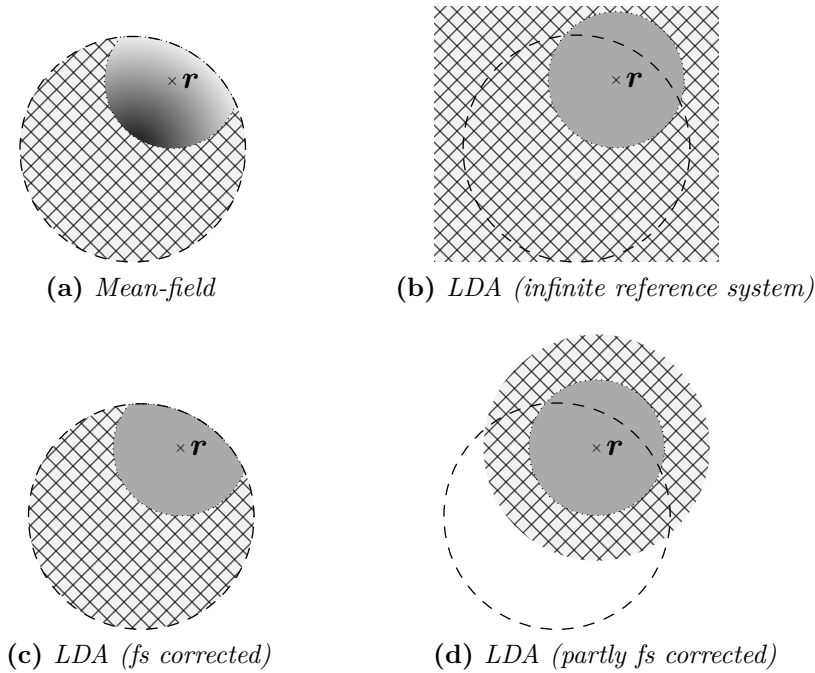


Figure 2.16: Comparison of the mean-field approximation and the various local density approximations for calculating the energy density of interaction $u_{0,\text{mf}}$ in the case of finite screening. Within the graphics the system is represented by the dashed line. The hatched region shows the integration area used within the method, whereas the solid gray region shows the effective integration area due to finite screening. The color gradient within (a) represents the non-constant density of the system which is taken into account within the proper mean-field approximation (dark colors correspond to high densities). In contrast, LDA uses the density at point \mathbf{r} for the whole integration area.

mogeneous reference system differ only in the (effective) integration area within the energy density of interaction. In order to comprehend these differences, the integration areas are compared, together with the corresponding mean-field area, in figure 2.16. First, consider the Coulomb case, i.e., where the solid regions fill out the hatched ones and where the density is constant within the proper mean-field approximation, too. There, the integration of 2.16a is equal to 2.16c, thus the density obtained by LDA (fs corrected) is equal to the mean-field one. In contrast to that, the effective integration area within 2.16b is infinite leading to the breakdown mentioned above. In the case of finite screening, where the integration area is effectively reduced, 2.16a and 2.16c still have the same region of integration. But the constant approximation within 2.16c, contrary to 2.16a, leads to an underestimation of the energy density in

the outer region of the system – the high values of density towards the center will be ignored. Eventually this leads to the non-monotonic density profile of LDA (fs corrected). By contrast, 2.16d features an additional effective integration area, which partly prevents the underestimation leading to the more accurate density profile of LDA (partly fs corrected).

Consequently, for isotropically confined Yukawa systems an improvement of LDA is possible by including finite-size effects. However, for small values of the screening parameter even the improved local density approximation does not approach the degree of accuracy obtained by the non-local mean-field approximation, cf. figure 2.15. On the other hand, for increased screening the finite-size effects do not alter the density profile significantly, what is shown in figure 2.17. Therefore, equation (2.52) of the infinite homogeneous system will be used in the following.

2.4.2 LDA with Correlations

The LDA energy functional $E_{\text{LDA}}[n]$ considered up to now contains only the energy densities of the confinement and of the mean-field interaction. The inclusion of particle correlations via LDA can be accomplished by using the energy density of correlations

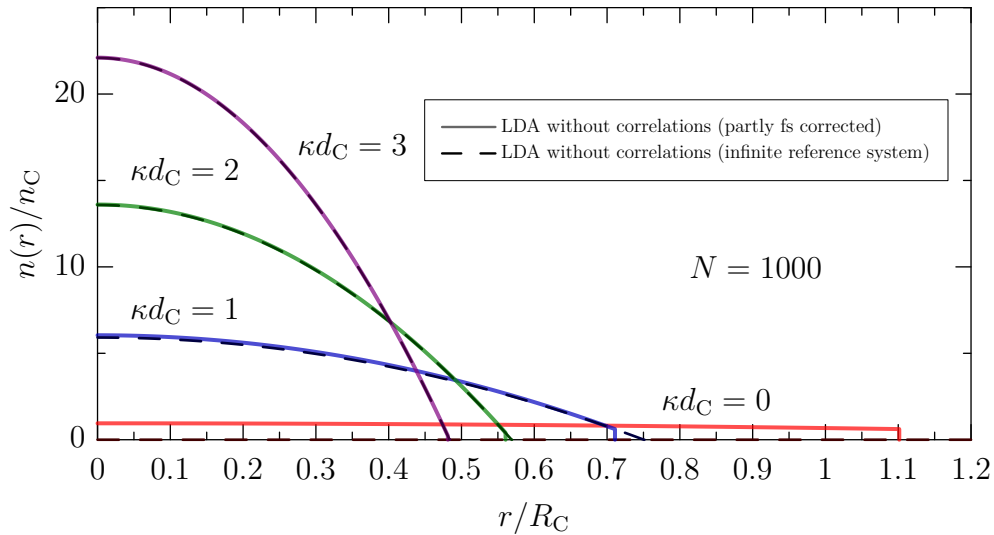


Figure 2.17: Comparison of LDA density profiles with the inclusion of finite-size effects (solid lines) and without the inclusion (dashed lines) for four screening parameters.

of the homogeneous system. An accurate approximation of this energy density is given for $n_0^{\frac{1}{3}} \geq 3\kappa/(20\pi)$ by

$$u_{0,\text{corr}} = -\gamma_1 q^2 n_0^{\frac{4}{3}} \exp\left(-\gamma_2 \kappa n_0^{-\frac{1}{3}} + \gamma_3 \left(\kappa n_0^{-\frac{1}{3}}\right)^4\right) \quad (2.68)$$

with

$$\gamma_1 = 1.444, \quad \gamma_2 = 0.375, \quad \gamma_3 = 7.4 \cdot 10^{-5}, \quad (2.69)$$

and was calculated by Totsuji et al. [Tot06b] from the (numerically obtained) Madelung energy of the corresponding Yukawa lattice. The local approximated energy density $u_{\text{LDA,corr}}(\mathbf{r})$ then follows by substituting the density of the homogeneous system n_0 by the local density $n(\mathbf{r})$ of the inhomogeneous system. Consequently, the complete ground-state energy functional in local density approximation reads as

$$E_{\text{LDA}}[n] = N \mu_{\text{LDA}} + \int d\mathbf{r} u(\mathbf{r}) \quad (2.70)$$

with the energy density

$$u(\mathbf{r}) = n(\mathbf{r}) \left(\phi(\mathbf{r}) - \mu_{\text{LDA}} \right) + q_{\text{eff}}^2 n(\mathbf{r})^2 \frac{2\pi}{\kappa^2} - \gamma_1 q^2 n(\mathbf{r})^{\frac{4}{3}} \exp\left(-\gamma_2 \kappa n(\mathbf{r})^{-\frac{1}{3}} + \gamma_3 \left(\kappa n(\mathbf{r})^{-\frac{1}{3}}\right)^4\right). \quad (2.71)$$

In order to assess the importance of the correlations within (2.71), the ratio of energy densities of correlations and of the mean-field interaction is plotted in figure 2.18. This ratio only depends on one parameter, $z(\mathbf{r}) = \sqrt[3]{n(\mathbf{r})}/\kappa$, and shows three different regions.

1. For $z \gtrsim 1$ the absolute of the ratio is very small and hence correlations are negligible.
2. For $z \lesssim 1$ the absolute of the ratio has higher values implying the importance of the correlations. This fact allows for a rough estimation of the screening values at which correlations become important. By approximating $n(\mathbf{r})$ by \bar{n}_{LDA} from (2.63) one obtains $\kappa R_C \gtrsim 0.5 (3N/4\pi)^{5/9}$. For the example of figure 2.19 with $N = 2000$ this yields screening values $\kappa R_C \gtrsim 15$, which indeed is a good estimation.

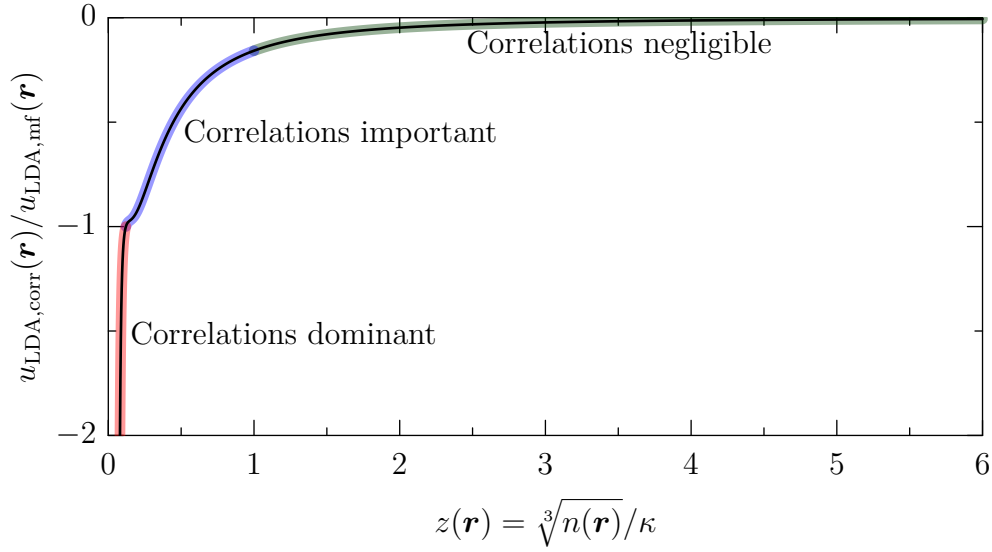


Figure 2.18: The ratio of the energy densities of correlations and of the mean-field interaction as a function of its local parameter $z(\mathbf{r}) = \sqrt[3]{n(\mathbf{r})}/\kappa$ is shown. Three regions are highlighted which display the different kinds of importance of the correlations.

3. For $z \lesssim 0.12$ the absolute of the ratio exceeds the value of one. Hence, the correlation energy dominates the mean-field energy.

As before, variation of the energy functional yields the LDA ground state density $n_{\text{LDA}}(\mathbf{r})$, but now with correlations included. Due to the correlations, the energy density is strongly non-linear and thus does not allow for an explicit solution. However, an implicit solution is possible and is conveniently given as a function of $z(\mathbf{r})$ by

$$0 = z(\mathbf{r})^3 + \frac{\phi(\mathbf{r}) - \mu_{\text{LDA}}}{4\pi\kappa q_{\text{eff}}^2} - \frac{N}{3\pi(N-1)} \left(\gamma_1 z(\mathbf{r}) + \frac{\gamma_1 \gamma_2}{4} - \gamma_1 \gamma_3 z(\mathbf{r})^{-3} \right) \quad (2.72)$$

$$\times \exp\left(-\gamma_2 z(\mathbf{r})^{-1} + \gamma_3 z(\mathbf{r})^{-4}\right) \quad \forall \mathbf{r} \in \mathcal{V}_{\text{LDA}}.$$

The solution of this density equation, the Lagrange parameter μ_{LDA} as well as the supporting region \mathcal{V}_{LDA} (respectively the LDA radius R_{LDA}) have to be determined numerically. For the case of a harmonic confinement, results are given in figure 2.19. There, the LDA ground state density profiles with correlations are shown for three different screening parameters. For comparison, the LDA results without correlations are shown, too. In case of low screening both density profiles are identical so that there is no effect of the particle correlations, in agreement with figure 2.18. But with

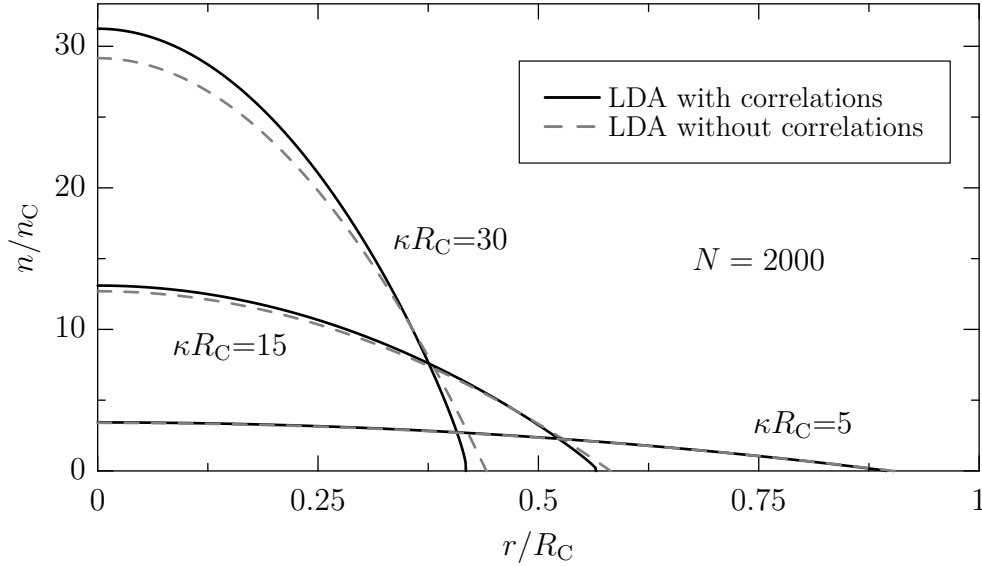


Figure 2.19: Density profiles of harmonically confined dust crystals with $N = 2000$ particles in local density approximation with correlations for three screening parameters (lines), from bottom to top: $\kappa R_C = 5$, $\kappa R_C = 15$, $\kappa R_C = 30$. For comparison, the corresponding LDA results without correlations are shown by the dashed lines.

increasing screening the correlation contributions within LDA alter the curvature of the profile, which rises more steeply towards the center. Hence, the particle correlations tend to increase the central density of the Yukawa balls.

On grounds of the limitation of (2.68), the resulting equation for the density, (2.72), is not valid for densities smaller than the limiting density $n^* = 9n_C(\kappa d_C)^3/(4000\pi^2)$. However, this limitation is irrelevant as this limiting density is in all cases much smaller than the average density. For example, the values of n^* , corresponding to the density profiles within figure 2.19, are $2.8 \cdot 10^{-5}n_C$, $7.7 \cdot 10^{-4}n_C$, and $6.2 \cdot 10^{-3}n_C$.

2.4.3 Comparison of Simulation and LDA Results

The comparison of simulation and mean-field results in section 2.3.2 revealed a very good agreement for weak screening, but some discrepancies for strong screening, which were attributed to the missing correlations within the mean-field approximation. The local density approximation, however, allows for the inclusion of such correlations in a simple manner and works accurately just in case of strong screening, as was shown in

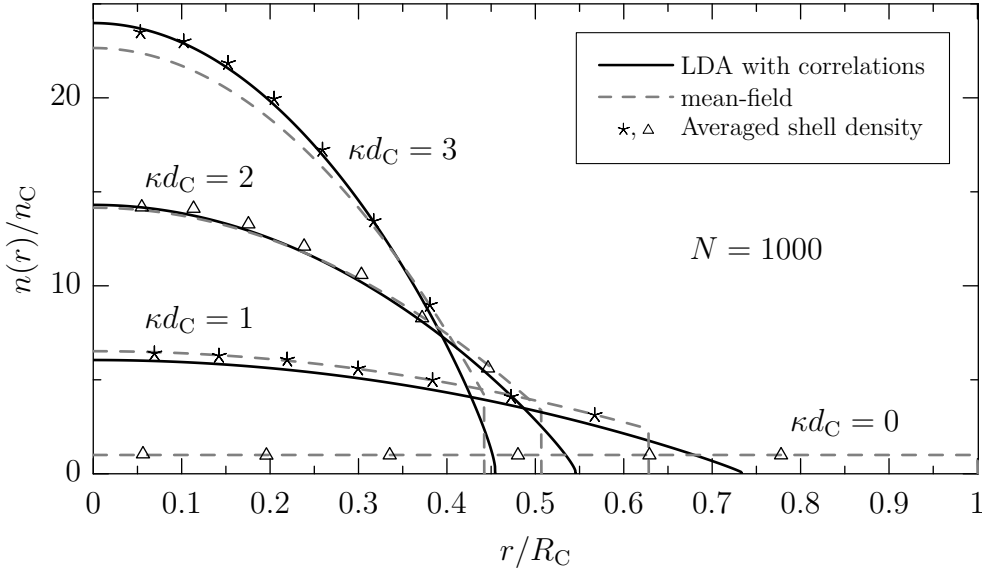


Figure 2.20: LDA density profiles with correlations of harmonically confined dust crystals with $N = 1000$ particles for four screening values (lines), from bottom to top: $\kappa d_C = 0$ (black), $\kappa d_C = 1$ (blue), $\kappa d_C = 2$ (green), and $\kappa d_C = 3$ (magenta). The symbols denote the average shell densities, which are obtained from corresponding numerical simulations. For comparison, the mean-field results are shown by dashed lines.

section 2.4.1. Consequently, in this case LDA results should be in good accordance with simulation results. As a matter of fact, this is the case as shown in figure 2.20.

Therein, LDA ground state density profiles with correlations are displayed for four different screening parameters together with the average particle densities of the shells, which are obtained from mollified results of ground state simulations. For comparison the mean-field density profiles are shown, too. The figure reveals that LDA allows for removing the discrepancies of the mean-field approximation, which arise in case of strong screening, but it does not feature the accuracy of the latter in case of weak screening. Therefore, both approximations complement one another in the description of the average density of the Yukawa balls, and the issue of the screening effect on the average particle distribution is satisfyingly settled for arbitrary screening.

In order to describe not only the average behavior of the density but also its shell structure, the local density approximation is not appropriate, because it is only useful within the study of long-range correlations [Han91]. The shell-causing short-range correlations, however, are not included. For a systematic treatment of these

correlations as well, the pair correlation function has to be involved in the energy expression, cf. (2.14). Therefore analytical solutions have to be abandoned, and schemes like the BBGKY hierarchy within equilibrium [Han91], or the Ornstein-Zernike relation including closure approximations [Han91, Ich94] are needed. However, for ground states the accurate applicability of available closure relations is not a foregone conclusion and subject of ongoing research.

2.5 Shell Models of Yukawa Balls

In order to describe the shell structure of the Yukawa balls the so-called *shell models*, in spite of their simplicity, proved to be very successful. These models possess an immanent shell structure by making the ansatz

$$n_{\text{sm}}(\mathbf{r}) = \sum_{\nu=1}^L N_{\nu} \frac{\delta(|\mathbf{r}| - R_{\nu})}{4\pi R_{\nu}^2} \quad (2.73)$$

for the ensemble averaged density. Thus, there are L infinitely thin origin centered shells with radii R_{ν} and “occupation numbers” N_{ν} . The occupation numbers count the number of particles on each shell and hence fulfill $\sum_{\nu=1}^L N_{\nu} = N$. A sketch of the structure is shown in figure 2.21 for $L = 3$. In spite of the similarities to the exact density (2.44), shell models attempt to reproduce only the global shell structure of the cluster. For this purpose, the parameters L , $\{R_{\nu}\}$, $\{N_{\nu}\}$ have to be determined, what is carried out by (numerically) minimizing a corresponding energy function

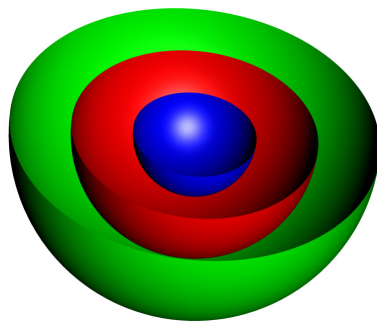


Figure 2.21: Sectorial view of a shell model structure with $L = 3$ shells.

$E_{\text{sm}}(L, \{R_\nu\}, \{N_\nu\})$ with respect to these parameters. This energy function then specifies the individual shell model.

The simplest shell model is the mean-field shell model, which neglects the contributions of the correlations. By analogy to electrostatics, it can be seen as a series of interlaced homogeneously charged capacitors. This model (or rather its energy function) can be easily obtained by evaluating the mean-field energy functional (2.19) at the density of the ansatz (2.73), i.e., $E_{\text{mf}}[n_{\text{sm}}]$. It yields, after some algebra [Hen06],

$$E_{\text{sm,mf}}(L, \{R_\nu\}, \{N_\nu\}) = \sum_{\nu=1}^L N_\nu \left\{ \phi(R_\nu) + q_{\text{eff}}^2 \frac{e^{-\kappa R_\nu}}{R_\nu} \right. \\ \left. \times \left(\frac{\sinh(\kappa R_\nu)}{\kappa R_\nu} \frac{N_\nu}{2} + \sum_{\mu < \nu}^L \frac{\sinh(\kappa R_\mu)}{\kappa R_\mu} N_\mu \right) \right\} \quad (2.74)$$

and consists of three parts, which are common to all shell models. Beside the energy of confinement, there are the intra-shell energy and the inter-shell energy, which take into account the interaction energy of the particles on the same shell and on different shells, respectively. The mean-field model can slightly be improved by allowing for the possibility of a single central particle without self-interaction [Tsu93] and by a counting correction $N_\nu \rightarrow N_\nu - 1$ in the intra-shell energy [Hen06]. In the Coulomb limit ($\kappa \rightarrow 0$) it reduces to

$$E_{\text{sm,HA}}(L, \{R_\nu\}, \{N_\nu\}) = \sum_{\nu=1}^L N_\nu \left\{ \phi(R_\nu) + \frac{q^2}{R_\nu} \left(\frac{N_\nu}{2} + \sum_{\mu < \nu}^L N_\mu \right) \right\}, \quad (2.75)$$

i.e., the shell model of Hasse and Avilov [Has91], which was designed to describe spherical ion crystals. Both mean-field models tend to the structure $L \rightarrow \infty$ with $N_\nu \rightarrow 0$ for all ν , what reflects the results of section 2.2 showing that n_{mf} yields the lowest mean-field energy. Therefore, in order to get improved results, correlations have to be included.

In the *Coulomb* case various extended models were proposed, which differ in the expression of the intra-shell energy E_{intra} . They are summarized in table 2.1. The first extension of the mean-field model was given by Tsuruta and Ichimaru [Tsu93]. They took into account intra-shell correlations by allocating a fixed domain to a given particle on a shell ν and distributing the $N_\nu - 1$ other particles uniformly on the shell except for that domain. The surrounding area of each particle not occupied by

Coulomb Shell Model	E_{intra}/q^2 of shell ν
Hasse, Avilov [Has91]	$N_\nu N_\nu / (2R_\nu)$
Tsuruta, Ichimaru [Tsu93]	$N_\nu(N_\nu - \sqrt{N_\nu}) / (2R_\nu)$
Kraeft, Bonitz [Kra06]	$N_\nu(N_\nu - \varepsilon\sqrt{N_\nu}) / (2R_\nu)$
Cioslowski, Grzebielucha [Cio08]	$E_{\text{Th}}(N_\nu) / R_\nu$ $\approx N_\nu(N_\nu - \varepsilon\sqrt{N_\nu} + \varepsilon' / \sqrt{N_\nu}) / (2R_\nu)$

Table 2.1: Coulomb shell models of various authors and their expression for the intra-shell energy of shell ν .

others was assumed to be equal to the total area of the shell divided by N_ν . This simple partitioning allows to reproduce the ground state energy within a relative error less than 5%, but produces systematic errors for the radii and occupation numbers [Kra06].

An improved shell model was given by Kraeft and Bonitz [Kra06], who generalized the simple partitioning: Because there is no obvious reason why the domain of a particle is given by the total area of its shell ν divided by N_ν , they introduced a parameter ε , which accounts for a different size of the domain. The parameter ε was obtained by fitting either the energy E_{sm} or the occupation numbers to results from numerical simulations. Both methods allow a reproduction of energies, radii and occupation numbers within very good accuracy. Interestingly, for large N the parameter converges to $\varepsilon \approx 1.104$. The reason for this convergence was identified by Cioslowski and Grzebielucha [Cio08]. They showed that the exact intra-shell energy is strongly related to the energy solution $E_{\text{Th}}(N_\nu)$ of the Thomson problem with N_ν particles [Why52], and they used a conjectured asymptote of the Thomson problem to reason the convergence. This asymptote of the Thomson problem and hence the large N_ν limit $\varepsilon \approx 1.104$ was first noted by Erber and Hockney [Erb91].

In case of *Yukawa* interaction the situation is more complex. In order to extend the mean-field shell model (2.74) by correlations, one ansatz was made by Totsuji et al. [Tot05]. They approximated the correlation energy by numerical results from calculations of a plane, two-dimensional Yukawa lattice and obtained for the intra-shell

energy of shell ν

$$E_{\text{intra},\nu}^{\text{Tot}} = \frac{q^2 N_\nu^2}{2R_\nu} \frac{e^{-\kappa R_\nu} \sinh(\kappa R_\nu)}{\kappa R_\nu} - \frac{q^2 N_\nu \sqrt{N_\nu}}{2R_\nu} f_{\text{corr}}^{\text{Tot}}\left(\frac{2\kappa R_\nu}{\sqrt{N_\nu}}\right) \quad (2.76a)$$

with

$$f_{\text{corr}}^{\text{Tot}}(x) = 1.9605 - 0.8930x + 0.1959x^2 - 0.01715x^3. \quad (2.76b)$$

While the results of this model are quite good for finite screening, the Coulomb limit, which is given by the Coulomb shell models, is missed. Additionally, for small particle numbers on a shell, the absolute value of the correlation energy may exceed the mean-field energy, what is not physical.

Another ansatz was made by Baumgartner et al. [Bau07]. In analogy to the Coulomb shell model of Kraeft and Bonitz, they substituted $N_\nu \rightarrow N_\nu - \varepsilon\sqrt{N_\nu}$ within the intra-shell energy E_{intra} of the Yukawa mean-field shell model. In further work, a function $\varepsilon(N_\nu)$, which is dependent on the particle number of the shell, was substituted for the single parameter ε [Kä08]. As a result, the shell model is able to reproduce energies, radii and occupation numbers with good accuracy for small screening values. However, in case of larger screening values deviations arise.

2.5.1 An Improved Yukawa Shell Model

A generally suitable Yukawa shell model can be obtained by applying the basic ideas of Tsuruta, Ichimaru [Tsu93] and Kraeft, Bonitz [Kra06] to the Yukawa case. That is, in order to account for the strong short-range repulsion and hence for the correlations of the particles, the Yukawa mean-field shell model can be improved by allocating a fixed circular domain to a given particle on a shell ν , which is, without loss of generality, placed on the z -axis at $R_\nu \hat{z}$. The $N_\nu - 1$ other particles are uniformly distributed on the remaining area

$$\mathcal{A}_{\tilde{\theta}} = \left\{ \mathbf{r} = (r, \theta, \phi) \in \mathbb{R}^3 \mid r = R_\nu, \tilde{\theta} \leq \theta \leq \pi, 0 \leq \phi \leq 2\pi \right\} \quad (2.77)$$

on that shell, where $\tilde{\theta}$ is the azimuthal angle describing the circular domain, which is visualized in figure 2.22. The uniform distribution of all the other particles on $\mathcal{A}_{\tilde{\theta}}$

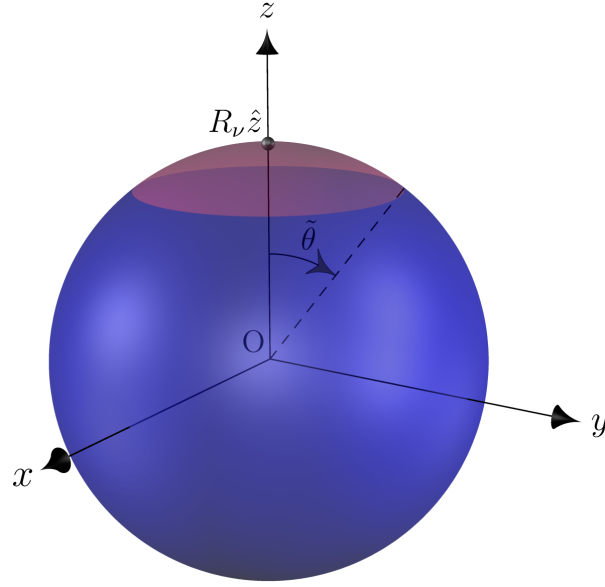


Figure 2.22: The circular domain (red) of a given particle placed on the z -axis at $R_\nu \hat{z}$ is shown in addition to the area $A_{\tilde{\theta}}$ (blue), where $N_\nu - 1$ other particles are distributed uniformly.

results in the density

$$n_{\tilde{\theta}}(\mathbf{r}) = \delta(r - R_\nu) \Theta(\theta - \tilde{\theta}) \frac{N_\nu - 1}{2\pi R_\nu^2 (1 + \cos \tilde{\theta})}, \quad (2.78)$$

at this area, which is normalized to

$$\int_{A_{\tilde{\theta}}} d\mathbf{r} n_{\tilde{\theta}}(\mathbf{r}) = N_\nu - 1. \quad (2.79)$$

The intra-shell energy of the shell is then given by

$$\begin{aligned} E_{\text{intra},\nu} &= q^2 \frac{N_\nu}{2} \int_{A_{\tilde{\theta}}} d\mathbf{r} n_{\tilde{\theta}}(\mathbf{r}) \frac{e^{-\kappa|\mathbf{r}-R\hat{z}|}}{|\mathbf{r}-R\hat{z}|} \\ &= q^2 \frac{N_\nu(N_\nu - 1)}{2R_\nu} \frac{e^{-\kappa R_\nu \sqrt{2-2\cos\tilde{\theta}}} - e^{-2\kappa R_\nu}}{\kappa R_\nu (1 + \cos\tilde{\theta})}. \end{aligned} \quad (2.80)$$

Adopting the idea of Kraeft and Bonitz, the area occupied by one particle, which is given by $4\pi R_\nu^2 - |\mathcal{A}_{\tilde{\theta}}| = 2\pi R_\nu^2(1 - \cos \tilde{\theta})$, need not to be the area obtained by simple partitioning but can be a multiple of it. Therefore, it is convenient to set

$$2\pi R_\nu^2(1 - \cos \tilde{\theta}) = \gamma \frac{4\pi R_\nu^2}{N_\nu}, \quad (2.81)$$

where the factor γ is formally allowed to be in the range $0 \leq \gamma \leq N_\nu$. Using this result the intra-shell energy of shell ν is written as

$$E_{\text{intra},\nu} = \frac{q^2 N_\nu (N_\nu - 1)}{2R_\nu(1 - \gamma/N_\nu)} \frac{e^{-2\kappa R_\nu \sqrt{\gamma/N_\nu}} - e^{-2\kappa R_\nu}}{2\kappa R_\nu}. \quad (2.82)$$

The factor γ within this expression is not determined yet. The simplest expression is obtained by choosing $\gamma = 0$. Then (2.82) reduces to the intra-shell energy of the Yukawa mean-field model including the counting correction $N_\nu \rightarrow N_\nu - 1$, cf. (2.74). Geometrically this choice means $\tilde{\theta} = 0$, i.e., there is no domain occupied by just one particle, and thus correlations are not included. On the contrary, the simple partitioning, which is obtained by setting $\gamma = 1$, includes correlations. In that case the intra-shell energy is given by

$$E_{\text{intra},\nu}^{\gamma=1} = \frac{q^2 N_\nu^2}{2R_\nu} \frac{e^{-2\kappa R_\nu/\sqrt{N_\nu}} - e^{-2\kappa R_\nu}}{2\kappa R_\nu}, \quad (2.83)$$

which in the Coulomb limit ($\kappa \rightarrow 0$) reduces to the corresponding expression of Tsuruta and Ichimaru [Tsu93]. In the general case of finite screening this expression is worth mentioning as well, because separation of the mean-field and the correlation energy yields

$$E_{\text{intra},\nu}^{\gamma=1} = \frac{q^2 N_\nu^2}{2R_\nu} \frac{e^{-\kappa R_\nu} \sinh(\kappa R_\nu)}{\kappa R_\nu} - \frac{N_\nu \sqrt{N_\nu}}{2R_\nu} f_{\text{corr}}\left(\frac{2\kappa R_\nu}{\sqrt{N_\nu}}\right) \quad (2.84a)$$

$$f_{\text{corr}}(x) = \frac{1 - e^{-x}}{x} \approx 1 - 0.5x + 0.167x^2 - 0.042x^3, \quad (2.84b)$$

which reveals the structure of the intra-shell energy of Totsuji's Yukawa shell model (2.76). By means of (2.84), now this structure can be understood from an analytical point of view and, at the same time, the expression for the correlation energy is improved by taking into account the non-flat geometry of the shell.

However, generally γ depends on N_ν and κR_ν ¹, and its analytical determination via a (generalized) Thomson problem, namely that of a weighted Riesz potential [Bor08], is currently not possible due to mathematical difficulties². Nevertheless, the calculation of $\gamma(\kappa R_\nu, N_\nu)$ can be achieved by comparing the analytical expression (2.82) with results from a numerical minimization of the shell's energy. Figure 2.23 shows the corresponding findings for various particle numbers on the shell.

In the Coulomb case ($\kappa R_\nu = 0$) γ corresponds to ϵ^2 of the Coulomb shell models. Hence, $\gamma(0, N_\nu)$ should converge for large N_ν to $\epsilon^2 \approx 1.219$, which indeed is observable. With increasing κR_ν , however, there is an almost linear slope of $\gamma(\kappa R_\nu, N_\nu)$, which have to attenuate for large κR_ν due to $\gamma \leq N_\nu$, and which seems to attenuate for large N_ν . Qualitatively, such a slope is comprehensible due to the assumption of a uniform distribution of the $N_\nu - 1$ particles on $\mathcal{A}_{\hat{\rho}}$: with increasing κR_ν , the uniform distribution yields an overestimated energy of interaction and, therefore, needs a

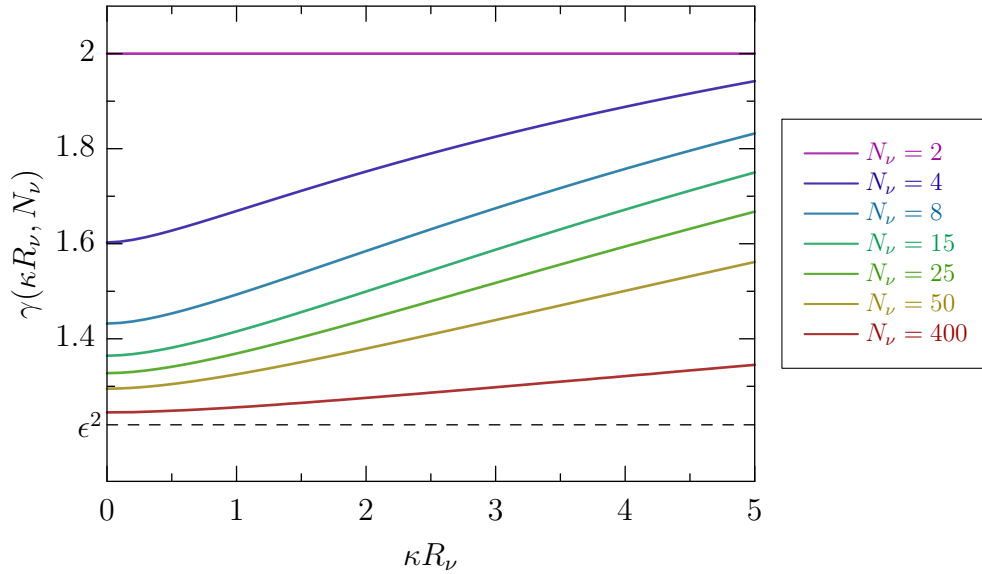


Figure 2.23: The function $\gamma(\kappa R_\nu, N_\nu)$, which is obtained by comparison of (2.82) with numerical minimization results, is shown as a function of κR_ν for various particle numbers. The dashed line, $\epsilon^2 \approx 1.219$, marks the limit in the Coulomb case.

¹ The dependence on the product κR_ν follows from a simple dimensional analysis.

² In fact, it can be shown that $\sqrt{\gamma(0, N_\nu)}$ corresponds to ϵ of the Coulomb shell models and even an analytical expression of this ϵ is so far only conjectured [Kui98]!

correction. Within the actual shell model (2.82), this correction is accomplished by reduction of $\mathcal{A}_{\tilde{\theta}}$ and, hence, by increasing γ . The estimation of the energy, however, is more correct for large N_ν , what explains the attenuation of the slope. A quantitative estimate of these slopes remains to be done, though.

In summary, by consistently adopting the basic ideas, which have been applied to the Coulomb shell models, a Yukawa shell model could be derived. It yields the correct Coulomb limit and, moreover, is applicable to the general case of finite screening, too. The accuracy of this Yukawa shell model, regarding the total energies, the shell radii, and the occupation numbers, still has to be analyzed in more detail by comparison with numerical simulations, what is topic of ongoing research.

Eventually, in table 2.2 all the previous Yukawa shell models are summarized showing their similarities and differences, also with regard to the Coulomb shell models of table 2.1.

Yukawa Shell Model	E_{intra}/q^2 of shell ν
Mean-field model	$\frac{N_\nu N_\nu}{2R_\nu} \frac{\exp(-\kappa R_\nu) \sinh(\kappa R_\nu)}{\kappa R_\nu}$
Totsuji et al. [Tot05]	$\frac{N_\nu N_\nu}{2R_\nu} \frac{\exp(-\kappa R_\nu) \sinh(\kappa R_\nu)}{\kappa R_\nu} - \frac{N_\nu \sqrt{N_\nu}}{2R_\nu} f_{\text{corr}}^{\text{Tot}} \left(\frac{2\kappa R_\nu}{\sqrt{N_\nu}} \right)$
Baumgartner et al. [Bau07]	$\frac{N_\nu (N_\nu - \varepsilon \sqrt{N_\nu})}{2R_\nu} \frac{\exp(-\kappa R_\nu) \sinh(\kappa R_\nu)}{\kappa R_\nu}$
Henning, equation (2.82)	$\frac{N_\nu (N_\nu - 1)}{2R_\nu (1 - \gamma/N_\nu)} \frac{\exp(-2\kappa R_\nu \sqrt{\gamma/N_\nu}) - \exp(-2\kappa R_\nu)}{2\kappa R_\nu}$

Table 2.2: Yukawa shell models of various authors and their expression for the intra-shell energy of shell ν .

2.6 Summary

Within this chapter a statistical theory suitable to describe the ground state of Yukawa balls was presented. By means of a variational principle the ground state density could be derived from the ensemble averaged energy. In order to obtain analytical results, two different approximations were used, the mean-field and the local density approximation. While the mean-field approximation takes into account the full non-local density of the mean-field energy but completely neglects the correlation contributions, the local density approximation simplifies the mean-field energy but allows for the inclusion of correlations. A comparison of the ground state densities resulting from both approximations with the numerically obtained exact density was possible by smoothing the exact density via the mollifier method. This comparison showed a very good agreement with the average density and also pointed out that both approximations complement one another in the description of the ground state density. The effect of screening on the density profile could therefore be understood from a theoretical point of view, offering a quantitative description.

The used approximations, however, are not capable for the description of the observed shell structure, which needs the inclusion of short-range correlations, cf. 2.4.3. Therefore, the pair correlation function has to be taken into account, what is subject of current research. A further subject is the extension to finite temperatures, which are accessible, e.g., by usage of the Helmholtz free energy instead of the energy (2.14). First results along this way have recently been obtained by Wrighton et al. [Wri09].

An alternative approach towards the ground state particle distribution of the Yukawa balls are artificial Yukawa shell models, which are an extension of the established Coulomb shell models. However, previous Yukawa shell models show wrong limits or yield unphysical results for small or large screening values. By using the basic concepts of successful Coulomb shell models, eventually a Yukawa shell model could be derived, which is able to overcome these limitations. A detailed investigation of this model regarding its descriptive power is topic of ongoing work.

CHAPTER 3

Normal Modes of Finite Clusters

Dynamical excitations, in addition to ground state properties, provide insight into correlation effects [Dub96a, Dub96b] and are particularly used to study melting behavior [Apo07, Sch95]. A successful approach to external excitations of a system is the normal mode analysis, i.e., the linearized theory of collective motions, which resolve every small movement into its spectral constituents. The normal mode analysis was already applied within the investigation of confined Coulomb systems [Cal07, Dub96a, Dub96b, Sch95], Yukawa systems [Bau07, She05a, Ami01, Mel01], and other types of finite clusters as well [Dyk08, vV01, Pos96, Wal91].

Within the previous investigations three unique spectral collective motions (modes) turned out to be of peculiar generality and seem to exist in all these systems: the rotational motions of the whole system, the center of mass oscillations (sloshing modes), and the uniform radial pulsation – the *breathing mode*. However, in frame of the thesis at hand it could be shown that the generality is not given for the breathing mode [Hen08], the existence of which requires the fulfillment of various strict conditions.

In order to clearly state the physical facts and their consequences, this chapter is organized as follows. After a brief recapitulation of normal modes in general, the normal modes of harmonically confined Coulomb systems and Yukawa systems are introduced. Upon detecting first irregularities of the breathing mode in Yukawa systems, the main part of this chapter covers the breathing mode, its general existence conditions, and resulting deviations, which are depicted by several examples. One of the important consequences, the possible existence of multiple monopole oscillations,

is treated subsequently. Finally, the effect of dissipation on the normal modes, which is crucial for dusty plasmas, is investigated.

3.1 Recapitulation of Normal Modes

In the following, properties of normal modes will be elaborated, which apply to harmonically confined dust crystals, but which are not restricted to these. Therefore, the Hamiltonian (1.3) is considered to describe d -dimensional systems, which are not restricted to the potentials (1.2), but allow for an arbitrary distance-dependent interaction $v(|\mathbf{r}_i - \mathbf{r}_j|)$ and for any isotropic confinement potential $\phi(|\mathbf{r}_i|)$. Then, small excitations from a ground state¹ $\mathbf{r}^* = (\mathbf{r}_1^*, \mathbf{r}_2^* \dots \mathbf{r}_N^*) \in \mathbb{R}^{dN}$ are analyzed. Such a ground state is a minimum of the potential energy U and thus fulfills the equations²

$$\mathbf{o} = \nabla_i U(\mathbf{r})|_{\mathbf{r}=\mathbf{r}^*} = \frac{\phi'(|\mathbf{r}_i^*|)}{|\mathbf{r}_i^*|} \mathbf{r}_i^* + \sum_{l=1}^N \frac{v'(|\mathbf{r}_{il}^*|)}{|\mathbf{r}_{il}^*|} \mathbf{r}_{il}^* \quad \forall i \leq N. \quad (3.1)$$

The small excitation is a time-dependent function $\mathbf{r}(t)$ in the configuration space with $|\mathbf{r}(t) - \mathbf{r}^*| \ll 1$. Due to the small amplitude the potential can be approximated harmonically by

$$U(\mathbf{r}) \approx U(\mathbf{r}^*) + \frac{1}{2}(\mathbf{r} - \mathbf{r}^*)^T \mathcal{H}^{\mathbf{r}^*} (\mathbf{r} - \mathbf{r}^*), \quad (3.2)$$

where (3.1) and the definition of the Hessian matrix $\mathcal{H}^{\mathbf{r}^*} = \nabla \nabla^T U(\mathbf{r})|_{\mathbf{r}=\mathbf{r}^*}$ are used. Because $\mathcal{H}^{\mathbf{r}^*}$ is a real symmetric $dN \times dN$ -matrix and positive semidefinite as well, its eigenvalue problem

$$\lambda m \hat{\mathbf{r}} = \mathcal{H}^{\mathbf{r}^*} \hat{\mathbf{r}} \quad (3.3)$$

defines dN eigenvalues $\lambda_j \geq 0$ and dN linearly independent eigenvectors $\hat{\mathbf{r}}_j$, which form a basis in the configuration space and are conveniently chosen to be orthonormal.

1 The following analysis works all the same for metastable states as well. For reasons of readability though only the ground states are mentioned.

2 \sum' indicates no summation over equal indices and a vector with two indices is an abbreviation for the difference of the corresponding single-indexed vectors, i.e., $\mathbf{r}_{il} = \mathbf{r}_i - \mathbf{r}_l$.

Within this basis the excitation can be expanded,

$$\mathbf{r}(t) = \mathbf{r}^* + \sum_{j=1}^{dN} c_j(t) \hat{\mathbf{r}}_j, \quad (3.4)$$

so that the time-dependence is fully determined by the coefficients $c_j(t)$ – the *normal coordinates*. These normal coordinates obey equations of motion, which follow from the Hamiltonian (1.3),

$$\begin{aligned} \mathbf{0} &\stackrel{(1.3)}{=} m\ddot{\mathbf{r}} + \nabla U(\mathbf{r}) \\ &\stackrel{(3.2)}{=} m\ddot{\mathbf{r}} + \mathcal{H}^{\mathbf{r}^*}(\mathbf{r} - \mathbf{r}^*) \\ &\stackrel{(3.4)}{=} m \sum_{j=1}^{dN} \ddot{c}_j(t) \hat{\mathbf{r}}_j + \sum_{j=1}^{dN} c_j(t) \mathcal{H}^{\mathbf{r}^*} \hat{\mathbf{r}}_j \\ &\stackrel{(3.3)}{=} m \sum_{j=1}^{dN} [\ddot{c}_j(t) + \lambda_j c_j(t)] \hat{\mathbf{r}}_j. \end{aligned} \quad (3.5)$$

Because the eigenvectors $\hat{\mathbf{r}}_j$ are linearly independent each normal coordinate $c_j(t)$ fulfills $0 = \ddot{c}_j(t) + \lambda_j c_j(t)$ with the solution

$$c_j(t) = A_j \cos(\sqrt{\lambda_j} t + B_j) \quad \forall j \leq dN, \quad (3.6)$$

in which the constants A_j and B_j have to be determined from the initial conditions $\mathbf{r}(0), \dot{\mathbf{r}}(0)$ of the excitation. Thus, the excitation relative to the ground state, $\mathbf{r}(t) - \mathbf{r}^*$, generally is a superposition of oscillating motions $A_j \cos(\sqrt{\lambda_j} t + B_j) \hat{\mathbf{r}}_j$, called *normal modes*. Each such normal mode describes a collective motion of all particles oscillating with the same frequency $\omega_j = \sqrt{\lambda_j}$ – the *normal frequency*. The respective displacements of the particles are given by the eigenvector $\hat{\mathbf{r}}_j$. Consequently, in order to investigate the excitations of finite clusters their normal modes have to be considered and with them the eigenvalue problem (3.3) of the Hessian $\mathcal{H}^{\mathbf{r}^*}$.

3.2 Normal Modes of Confined Coulomb Systems

For the investigation of the normal modes of harmonically confined Coulomb systems ($\kappa = 0$) detailed theoretical studies have been performed for $d = 1, 2, 3$ dimensions, see

[Cal07, Dub96b, Sch95] and references therein. It was shown that there exist three (partially degenerate) normal modes, which are *universal*, i.e., independent of the particle number N and independent of the configuration \mathbf{r}^* :

The rotational modes ($\lambda = 0$) correspond to a rotation of the whole system and which reflect the axial symmetries of the confinement potential.

The sloshing modes ($\lambda = \omega_0^2$) express that the motion of the center of mass is independent of the interparticle forces.

The breathing mode ($\lambda = 3\omega_0^2$) describes a uniform radial expansion and contraction of all particles.

The existence of these three universal modes is illustrated for the two-dimensional systems with $N = 3, 4, 5$ particles in figure 3.1, where all modes of these systems corresponding to the ground state configuration are shown.

While the ground states, i.e., the global minima of the Hamiltonians can be found by global optimization techniques like Basin-Hopping [Wal97] or simulated annealing [Lud05], the normal mode analysis, i.e., the computation of normal frequencies and normal vectors, can be done by numerical diagonalization of the corresponding Hessian. For large systems, however, special techniques, e.g., usage of reduced basis sets or iterative diagonalizations, have to be used to circumvent computational limitations [Bro95].

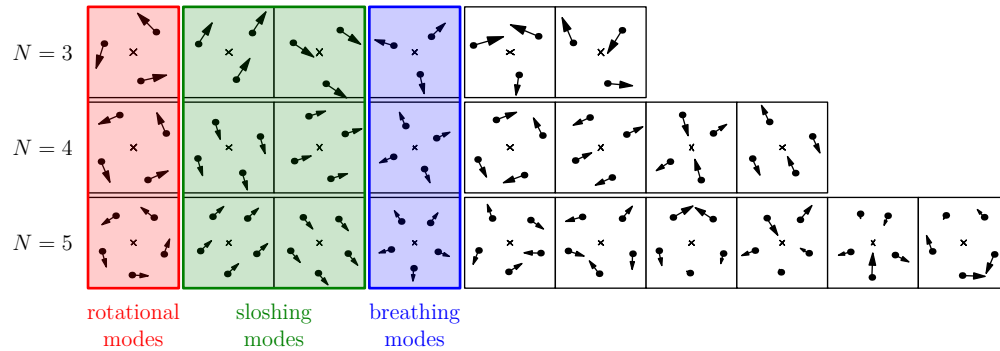


Figure 3.1: All normal modes of two-dimensional harmonically confined Coulomb systems with $N = 3, 4, 5$ particles. The dots picture the particles within the ground state configuration, and the arrows show the direction and amplitude of the oscillatory motion. The N -independent modes, i.e., the rotational modes, the sloshing modes, and the breathing modes are highlighted.

3.3 Normal Modes of Confined Yukawa Systems

For harmonically confined Yukawa systems the interaction potential and thus the Hessian \mathcal{H}^* depend on a screening parameter κ . Hence, in general, the normal modes will depend on this parameter as well. Within figure 3.2 this situation is displayed. There, the frequencies of all normal modes are shown for the ground state of harmonically confined Yukawa systems with $N = 16$ particles and a screening parameter ranging from $\kappa d_C = 0$ to $\kappa d_C = 20$.

The figure reveals that there are two mode frequencies independent of screening – corresponding to the rotational modes and the sloshing modes. These universal modes are existing in a Yukawa system as in Coulomb systems (and have κ -independent frequencies). They appear due to the symmetries of the system [Apo07, Par97]. In general, however, this is not the case for the breathing mode. Its extension to finite screening shows an increasing frequency, which, to some extent, can be understood from the functional behavior of the Yukawa interaction [Can98]. Based on this fact, an

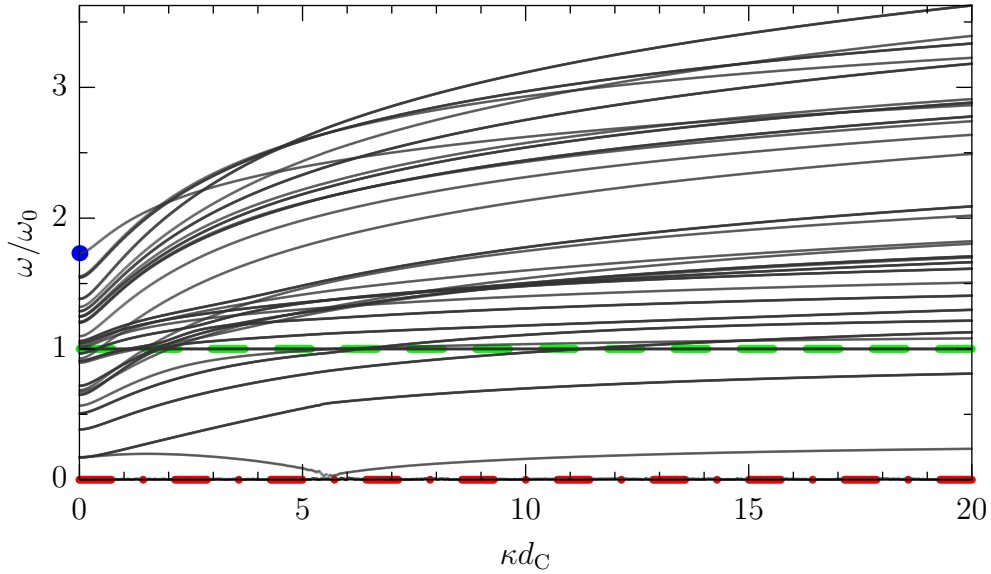


Figure 3.2: The κ -dependence of the normal mode frequencies of a harmonically confined two-dimensional Yukawa system with $N = 16$ particles on the screening parameter is shown. The rotational modes, the sloshing modes and the breathing mode are highlighted dash-dotted (red line) at $\omega = 0$, dashed (green) at $\omega = \omega_0$, and with a (blue) dot at $\omega = \sqrt{3}\omega_0$ and $\kappa = 0$, respectively.

intriguing question arises: is the κ -dependence of the frequency the only irregularity of the breathing mode in Yukawa systems?

3.4 Breathing Mode

The breathing mode, i.e., the mode of uniform radial expansion and contraction¹, is known from harmonically confined Coulomb systems. It is of special relevance since it can be easily excited selectively by variation of the confinement [Mel01] or by applying external fields [Dyk08]. In particular, the corresponding breathing frequency can often be precisely measured and may serve as a sensitive indicator of intrinsic system properties including the screening parameter and the particle charge in complex plasmas [Mel01].

The continuum analogon to the breathing mode is the *monopole oscillation* [Dub96b], which represents the lowest compressional mode within a hydrodynamic approach [Str96]. Due to the continuum character, this monopole oscillation is applicable to gas or fluid phases of classical [Gue99, Dub96b, She06b] or quantum systems [Kin04, Bau09, Mor03] where correlations are weak or moderate. In the strongly coupled crystalline state, however, where the particles become individually separated, the concept of the monopole oscillation is questionable. In order to use this concept also in case of strong correlations, the monopole oscillation is associated [Sch95, Par97, Mel01] with the oscillation of the mean square radius

$$R^2(t) := N^{-1} \mathbf{r}(t)^2. \quad (3.7)$$

It was then shown [Sch95, Dub96b] that this oscillation is universal in three-dimensional harmonically confined Coulomb systems, with its frequency, $\omega_{\text{MO}} = \sqrt{3} \omega_0$, equal to the breathing frequency, cf. 3.2. The same, i.e., a universal correspondence between the frequencies of the monopole oscillation and the breathing mode, also holds in harmonically confined two-dimensional systems if the interaction is a repulsive power law, $\propto 1/r^n$ ($n = 1, 2, \dots$), or logarithmic [Par97]. Due to this intimate connection of the breathing mode with the monopole oscillation a confusion of both concepts emerged [Par97].

However, while a monopole oscillation can appear in all types of finite clusters, a breathing mode can not be taken for granted. Nevertheless, the existence of this mode

¹ A normal mode $\hat{\mathbf{r}}$ is radial if all particle components are proportional to the equilibrium position $\hat{\mathbf{r}}_i \propto \mathbf{r}_i^*$, and uniform if the proportionality constants are equal for all particles.

was also assumed for non-Coulomb systems, like Lennard-Jones clusters [Cal07] or systems with Yukawa interaction [Kon03, She05b, For05]. In the context of this work it could be shown that these systems actually do not feature a breathing mode in general, which indeed is a special property of only Coulomb-like interactions [Hen08].

3.4.1 General Conditions for the Existence of the Breathing Mode

In order to find the conditions, at which a breathing mode can occur, the eigenvalue problem (3.3) of the Hessian has to be analyzed. The standard procedure to evaluate this equation is to find the roots of its characteristic polynomial yielding all eigenvalues and hence all eigenvectors. Subsequently an examination of these eigenvectors is possible regarding the existence an eigenvector $\hat{\mathbf{r}}_{\text{BM}}$ corresponding to a breathing mode. Such a vector has to describe a uniform and radial motion of all particles and therefore is of the form $\hat{\mathbf{r}}_{\text{BM}} \propto \mathbf{r}^*$.

However, the degree of the characteristic equation is $d \cdot N$ which prohibits an analytical calculation of the eigenvalues and -vectors in the general case and, consequently, prohibits general statements about the existence of the breathing mode. Therefore, one has to apply a different approach – the direct mode approach – which focuses on one mode only: the eigenvector of the breathing mode is directly used within the eigenvalue equation thus leading to the existence conditions of this mode.

To derive these conditions of the breathing mode's existence effectively, the eigenvalue equation has to be expressed within its particle components $i \leq N$, because the potentials ϕ and v are given for these. Then equation (3.3) reads

$$\lambda m \hat{\mathbf{r}}_i = \sum_{l=1}^N \mathcal{H}_{il}^{\mathbf{r}^*} \hat{\mathbf{r}}_l = \sum_{l=1}^N \nabla_i \nabla_l^T U(\mathbf{r})|_{\mathbf{r}=\mathbf{r}^*} \hat{\mathbf{r}}_l. \quad (3.8)$$

By using the isotropy of ϕ and the distance dependence of v , some algebra yields for

each particle-particle component of the Hessian

$$\begin{aligned} \nabla_i \nabla_l^T U(\mathbf{r})|_{\mathbf{r}=\mathbf{r}^*} &= \left[\frac{\phi'(|\mathbf{r}_l^*|)}{|\mathbf{r}_l^*|} \mathbf{I}_d + \frac{\mathbf{r}_l^* \mathbf{r}_l^{*T}}{|\mathbf{r}_l^*|^3} \left(|\mathbf{r}_l^*| \phi''(|\mathbf{r}_l^*|) - \phi'(|\mathbf{r}_l^*|) \right) \right] \delta_{il} \\ &+ \sum_{k=1}^N \left[\frac{v'(|\mathbf{r}_{lk}^*|)}{|\mathbf{r}_{lk}^*|} \mathbf{I}_d + \frac{\mathbf{r}_{lk}^* \mathbf{r}_{lk}^{*T}}{|\mathbf{r}_{lk}^*|^3} \left(|\mathbf{r}_{lk}^*| v''(|\mathbf{r}_{lk}^*|) - v'(|\mathbf{r}_{lk}^*|) \right) \right] (\delta_{il} - \delta_{ik}), \end{aligned} \quad (3.9)$$

where \mathbf{I}_d denotes the d -dimensional identity matrix. Thus (3.8) reduces to

$$\begin{aligned} \lambda m \hat{\mathbf{r}}_i &= \frac{\phi'(|\mathbf{r}_i^*|)}{|\mathbf{r}_i^*|} \hat{\mathbf{r}}_i + \frac{(\mathbf{r}_i^* \cdot \hat{\mathbf{r}}_i) \mathbf{r}_i^*}{|\mathbf{r}_i^*|^3} \left(|\mathbf{r}_i^*| \phi''(|\mathbf{r}_i^*|) - \phi'(|\mathbf{r}_i^*|) \right) \\ &+ \sum_{l=1}^N \left[\frac{v'(|\mathbf{r}_{il}^*|)}{|\mathbf{r}_{il}^*|} \hat{\mathbf{r}}_{il} + \frac{(\mathbf{r}_{il}^* \cdot \hat{\mathbf{r}}_{il}) \mathbf{r}_{il}^*}{|\mathbf{r}_{il}^*|^3} \left(|\mathbf{r}_{il}^*| v''(|\mathbf{r}_{il}^*|) - v'(|\mathbf{r}_{il}^*|) \right) \right]. \end{aligned} \quad (3.10)$$

Now the aforementioned direct mode approach can be applied. Therefore the eigenvector $\hat{\mathbf{r}}$ is substituted by the eigenvector of the breathing mode $\hat{\mathbf{r}}_{\text{BM}} = |\mathbf{r}^*|^{-1} \mathbf{r}^*$, which consequently leads to the existence conditions of this mode

$$\lambda_{\text{BM}} m \mathbf{r}_i^* = \phi''(|\mathbf{r}_i^*|) \mathbf{r}_i^* + \sum_{l=1}^N v''(|\mathbf{r}_{il}^*|) \mathbf{r}_{il}^* \quad \forall i \leq N. \quad (3.11)$$

These N existence equations of the breathing mode have the meaning that the linearized force on each particle from the confinement and from the pair interactions (right side) has to be purely *radial and uniform*, i.e., proportional to \mathbf{r}_i^* . To find their solutions, a separation into the two conditions is appropriate.

First, the condition of radially is equivalent to the tangential components¹ of (3.11)

$$\mathbf{o} = \mathbf{r}_i^* \wedge \sum_{l=1}^N v''(|\mathbf{r}_{il}^*|) \mathbf{r}_{il}^* \quad \forall i \leq N, \quad (3.12a)$$

¹ While the normal components of these equations denote the projections onto \mathbf{r}_i^* respectively, the tangential components correspond to projections perpendicular to \mathbf{r}_i^* , which in three dimensions find expression by the cross products $\mathbf{r}_i^* \times \dots$ and in general dimensions by the exterior products $\mathbf{r}_i^* \wedge \dots$

which can also be rewritten as

$$\sum_{l=1}^N v''(|\mathbf{r}_{il}^*|) \mathbf{r}_{il}^* = s_i \mathbf{r}_i^* \quad \forall i \leq N \quad (3.12b)$$

with some coefficients s_i . These *radiality equations* have two classes of solutions:

- R1) The ground state configuration is of special kind featuring, e.g., a rotational symmetry with respect to all \mathbf{r}_i^* . In this case, independently of the interaction, the sum in (3.12b) is proportional to \mathbf{r}_i^* . Hence, there are numbers s_i which fulfill the radiality equations. An example showing such a rotational symmetry is given in figure 3.4b.
- R2) The pair interaction v has a specific form, which can be obtained by adding a multiple of the tangential components of equations (3.1) to equations (3.12a). Thus v fulfills the differential equation

$$v''(r) = -(\gamma + 1) \frac{v'(r)}{r}, \quad (3.13)$$

where γ is an arbitrary real number, and whose solutions are¹

$$v(r) \propto \begin{cases} 1/r^\gamma & \gamma \neq 0 \\ \log(r) & \gamma = 0. \end{cases} \quad (3.14)$$

If the pair interaction has such a form, the condition of radiality follows directly for every ground state configuration from the property of minimizing the potential energy, (3.1). In this case the coefficients s_i are given by

$$s_i = (\gamma + 1) \frac{\phi'(|\mathbf{r}_i^*|)}{|\mathbf{r}_i^*|}. \quad (3.15)$$

In order to fulfill the existence equations (3.11), the radiality solutions R1) and R2) also have to meet the condition of uniformity which is equivalent to the normal components of (3.11)

$$\lambda_{\text{BM}} m = \phi''(|\mathbf{r}_i^*|) + s_i. \quad (3.16)$$

¹ In fact, the general solution has a second additive constant, which, however, is irrelevant.

These *uniformity equations* also have two kinds of solutions:

- U1) The ground state configuration features some special symmetry, e.g., a single shell configuration, where the coefficients s_i are independent of i .
- U2) In case of the radially solution R2), the confinement potential ϕ fulfills the configuration-independent equation

$$\lambda_{\text{BM}} m = \phi''(r) + (\gamma + 1) \frac{\phi'(r)}{r}, \quad (3.17)$$

which is obtained by using the coefficients (3.15) within (3.16). The solutions of this differential equation are

$$\phi(r) = \begin{cases} \frac{\lambda_{\text{BM}} m}{2(2+\gamma)} r^2 + c v(r) & \gamma \neq -2 \\ \frac{\lambda_{\text{BM}} m}{2} r^2 \log(r) + c r^2 & \gamma = -2, \end{cases} \quad (3.18)$$

where γ describes the pair interaction, cf. (3.14), and c is an arbitrary constant.

Consequently, there are two basically different possibilities for the existence of a breathing mode – a universal breathing mode and a non-universal breathing mode.

Universal Breathing Mode

The previous analysis shows that a universal, i.e., a configuration- and N -independent, breathing mode exists on the one hand in case of harmonically confined systems, $\phi(r) = m\omega_0^2 r^2/2$, with particles interacting via potentials $v(r)$ proportional to $1/r^\gamma$ or to $\log(r)$. In these cases the breathing frequency is generally given by

$$\omega_{\text{BM}} = \sqrt{2 + \gamma} \omega_0. \quad (3.19)$$

On the other hand, a universal breathing mode also exists for interaction potentials proportional to r^2 if the confinement has the form $r^2 \log(r)$. In this case also the prefactor of the confinement determines the breathing frequency. In both cases the confinement can be modified by an additional term $c v(r)$ without changing the results, what corresponds to the addition of particles located in the trap origin.

These results of the universal breathing mode are valid for any real γ and any dimension and coincide, as mentioned previously, in special cases with the results of the monopole

oscillation [Par97]. Furthermore, the conclusion follows that no universal breathing mode exists for exponential interaction potentials (such as Yukawa, Morse etc.) or non-monotonic ones (e.g., Lennard-Jones).

Non-Universal Breathing Mode

Beside the universal breathing modes there is a second class of solutions of the existing conditions (3.11). These are the configuration-dependent solutions, which exist in case of special highly symmetric configurations. For instance, two-dimensional equally spaced single shell systems fulfill the conditions (3.11) independently from v and ϕ . The same holds for three-dimensional single shell systems, which form Platonic solids (with or without particle in the center), cf. figure 3.3. In these cases the system looks the same from every particle's view. Thus, all existence conditions (3.11) are identical. Then, since no direction is preferred, the sum has to be proportional to \mathbf{r}_i^* , and a unique value $\lambda_{\text{BM}} \geq 0$ exists fulfilling the existence equations. However, it should be emphasized that the resulting breathing mode is *non-universal* and its frequency ω_{BM} depends on the configuration and on N .

In order to derive an expression for the frequency of non-universal breathing modes, the existence conditions (3.11) can be multiplied by \mathbf{r}_i^* and subsequently added up resulting in

$$\omega_{\text{BM}}^2 = \frac{1}{m|\mathbf{r}^*|^2} \left(\sum_{i=1}^N \phi''(|\mathbf{r}_i^*|)|\mathbf{r}_i^*|^2 + \frac{1}{2} \sum'_{i,l=1}^N v''(|\mathbf{r}_{il}^*|)|\mathbf{r}_{il}^*|^2 \right). \quad (3.20)$$

For *harmonically confined systems*, by using the equilibrium conditions (3.1), this expression can finally be written

$$\frac{\omega_{\text{BM}}^2}{\omega_0^2} = 1 - \frac{\sum'_{i,l} v''(|\mathbf{r}_{il}^*|)|\mathbf{r}_{il}^*|^2}{\sum'_{i,l} v'(|\mathbf{r}_{il}^*|)|\mathbf{r}_{il}^*|}, \quad (3.21)$$

which, in the special case of Yukawa interaction, was published by Sheridan [She06a, She06b].

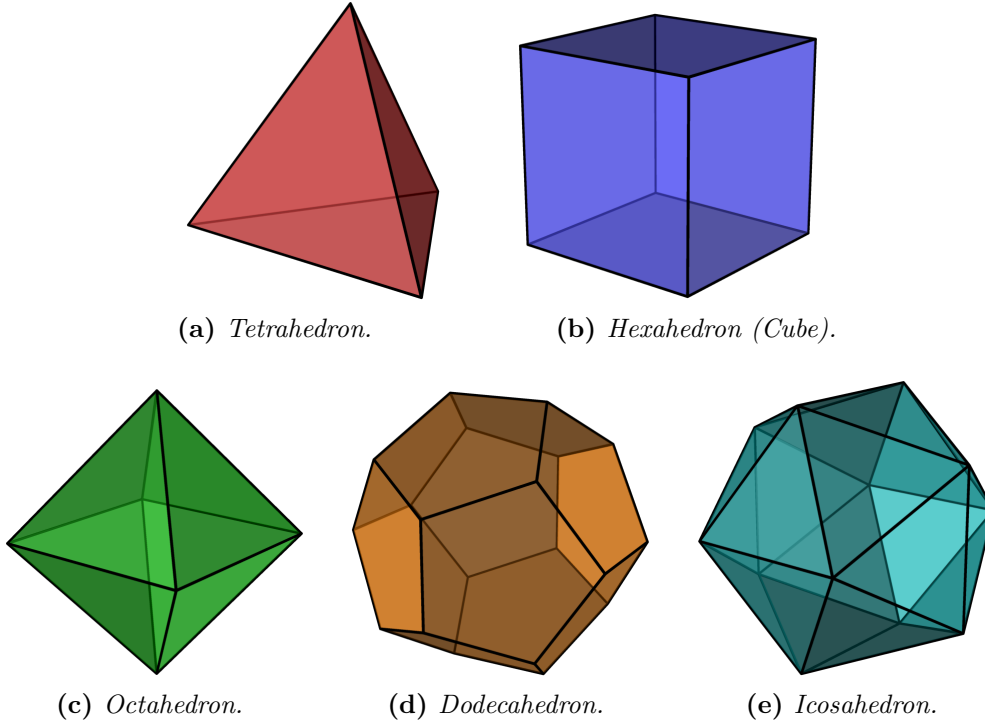


Figure 3.3: *The five Platonic solids. Systems with a configuration, in which the particles are located at the corners of a Platonic solid (with or without particle in the center), feature a breathing mode.*

Quasi-Breathing Mode

In order to exemplify the given results, a numerical normal mode analysis is performed for systems without a breathing mode and compared to harmonically confined Coulomb systems. To this end, starting from the ground state configurations of i) Lennard-Jones clusters [Wal97] and ii) harmonically confined Yukawa systems the normal modes are calculated for various N and κ , respectively. For each of the systems the deviation of every mode from a breathing mode, i.e., the deviation from the proportionality $\hat{\mathbf{r}} \propto \mathbf{r}^*$, is analyzed. The deviation is quantified by the absolute value of the projection onto the normalized ground state configuration

$$\mathcal{P}(\hat{\mathbf{r}}) = \left| \hat{\mathbf{r}} \cdot \frac{\mathbf{r}^*}{|\mathbf{r}^*|} \right|, \quad (3.22)$$

which has a value of one in case of the breathing mode and a value lower than one in all other cases. If, for a given system, there is no breathing mode, the mode with the smallest deviation is referred to as the *quasi-breathing mode*.

It should be noted that the measure (3.22) gives no direct insights separately into the uniformity or into the radially of a mode. On grounds of the proportionality of $\hat{\mathbf{r}}_{\text{BM}}$ and \mathbf{r}^* , *non-uniformity* of a mode $\hat{\mathbf{r}}$ arises if $\hat{\mathbf{r}}_i = c_i \mathbf{r}_i^*$, with different c_i for different particles. *Non-radiality* exists if there is no proportionality for all particles, i.e., there exist finite tangential velocity components. Finally, there is also the possibility of *anti-phase oscillating particles*, i.e., particles, which move inward while the majority moves outward and vice versa. These deviations from the breathing mode can be measured by corresponding distribution widths normalized to the mean,

$$\sigma_{\mathbf{r}} = \frac{|\max_i \sigma_{\mathbf{r},i} - \min_i \sigma_{\mathbf{r},i}|}{|\bar{\sigma}_{\mathbf{r},i}|} \quad \text{with } \sigma_{\mathbf{r},i} = \frac{\hat{\mathbf{r}}_i \cdot \mathbf{r}_i^*}{|\hat{\mathbf{r}}_i| |\mathbf{r}_i^*|} \quad (3.23a)$$

$$\sigma_{\mathbf{u}} = \frac{\max_i \sigma_{\mathbf{u},i} - \min_i \sigma_{\mathbf{u},i}}{\bar{\sigma}_{\mathbf{u},i}} \quad \text{with } \sigma_{\mathbf{u},i} = \frac{|\hat{\mathbf{r}}_i|}{|\mathbf{r}_i^*|}, \quad (3.23b)$$

in addition to the number N_{ap} of anti-phase oscillating particles. Figure 3.4 shows three examples of quasi-breathing modes together with their values of these measures.

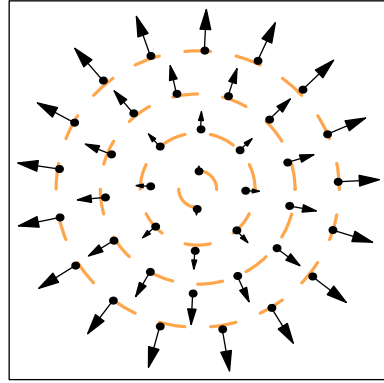
3.4.2 Breathing Modes in Lennard-Jones Systems

As a first example, the breathing-type modes of unconfined systems with Lennard-Jones interaction

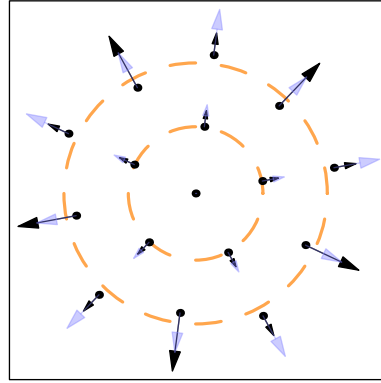
$$\phi(r) \equiv 0 \quad (3.24a)$$

$$v(r) = 4\epsilon \left[\left(\frac{\sigma}{r} \right)^{12} - \left(\frac{\sigma}{r} \right)^6 \right], \quad (3.24b)$$

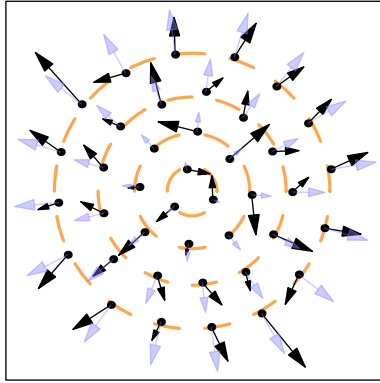
are examined. This type of interaction is (frequently) used for the theoretical description of molecules and atomic clusters [Bal05, Pro06]. While the eigenvalues of the corresponding normal modes are dependent on the chosen energy and length scale, ϵ and σ respectively, the eigenvectors are not. Thus, regarding the displacement pattern of the normal modes, unconfined Lennard-Jones systems only depend on the particle number. Therefore a systematic calculation of the (quasi)-breathing modes depending



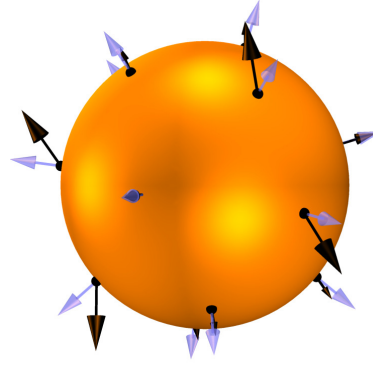
(a) Perfect breathing mode for $N = 40$ and $\kappa d_C = 0$.



(b) Purely radial but non-uniform quasi-breathing mode for $N = 16$ and $\kappa d_C = 20.0$, ($\sigma_r = 0, \sigma_u = 1.1, N_{ap} = 0$).



(c) Non-radial and non-uniform quasi-breathing mode for $N = 40$ and $\kappa d_C = 1.99$, ($\sigma_r = 2.77, \sigma_u = 2.11, N_{ap} = 4$).



(d) Quasi-breathing mode of a Yukawa ball for $N = 16$ and $\kappa d_C = 4.43$, ($\sigma_r = 0.41, \sigma_u = 0.93, N_{ap} = 0$).

Figure 3.4: Visualization of a perfect breathing mode in contrast to quasi-breathing modes in harmonically confined Yukawa systems. The dashed lines and the sphere mark the shells respectively and the light arrows visualize a hypothetical breathing mode.

on N can be performed. The corresponding results are shown in figure 3.5, where σ_r , σ_u and N_{ap} of the (quasi)-breathing mode are plotted for particle numbers N in the range from 3 to 150.

It is apparent that most of the systems does not possess a breathing mode, and that in these cases the quasi-breathing mode show substantial deviations from radially and uniformity. Very small even though non-vanishing deviations are observed for $N = 55, 135, 147$, which are highly symmetric multiple shell systems with full icosahedral symmetry [Wal97] (see dashed-dotted lines). The deviations are quantified by $\sigma_r = 0, N_{ap} = 0$ and $\sigma_u = 0.2, 0.24, 0.23$ respectively pointing out that the corresponding quasi-breathing modes showing perfect radiality but not uniformity. Additionally, figure 3.5 shows the occurrence of non-universal breathing modes for $N = 3, 4, 6, 13$ (see dashed lines in Fig. 3.5). These particle numbers correspond, in accordance with the previous analysis, to single-shell configurations, which are either planar and equally spaced ($N = 3$), or which form Platonic solids: tetrahedron ($N = 4$), octahedron ($N = 6$) and icosahedron with a central particle ($N = 13$), cf. figure 3.3.

3.4.3 Breathing Modes of Yukawa Balls

As a second example of broad practical interest, e.g., for Yukawa balls, two-dimensional confined dusty plasmas and for colloidal systems, the (quasi)-breathing modes in parabolically confined one-component Yukawa systems, (1.2), are considered. In case of vanishing screening, $\kappa \rightarrow 0$, these systems are Coulomb systems and, in agreement with the previous analysis, breathing modes as in figure 3.4a are always observed. In contrast, for finite screening, $\kappa > 0$, the normal mode analyses confirm that no universal breathing mode exists. In fact, there are single shell configurations, which show non-universal breathing modes [Mel01]. But most of all systems only possess quasi-breathing modes with deviations from a radial and uniform motion¹. Two typical examples of these quasi-breathing modes in case of two-dimensional Yukawa systems are presented in figure 3.4. While in figure 3.4b still a purely radial motion is observed, in figure 3.4c, the mode closest to the breathing mode shows striking

¹ Deviations from uniformity of a breathing mode have previously been reported by Sheridan [She06a].

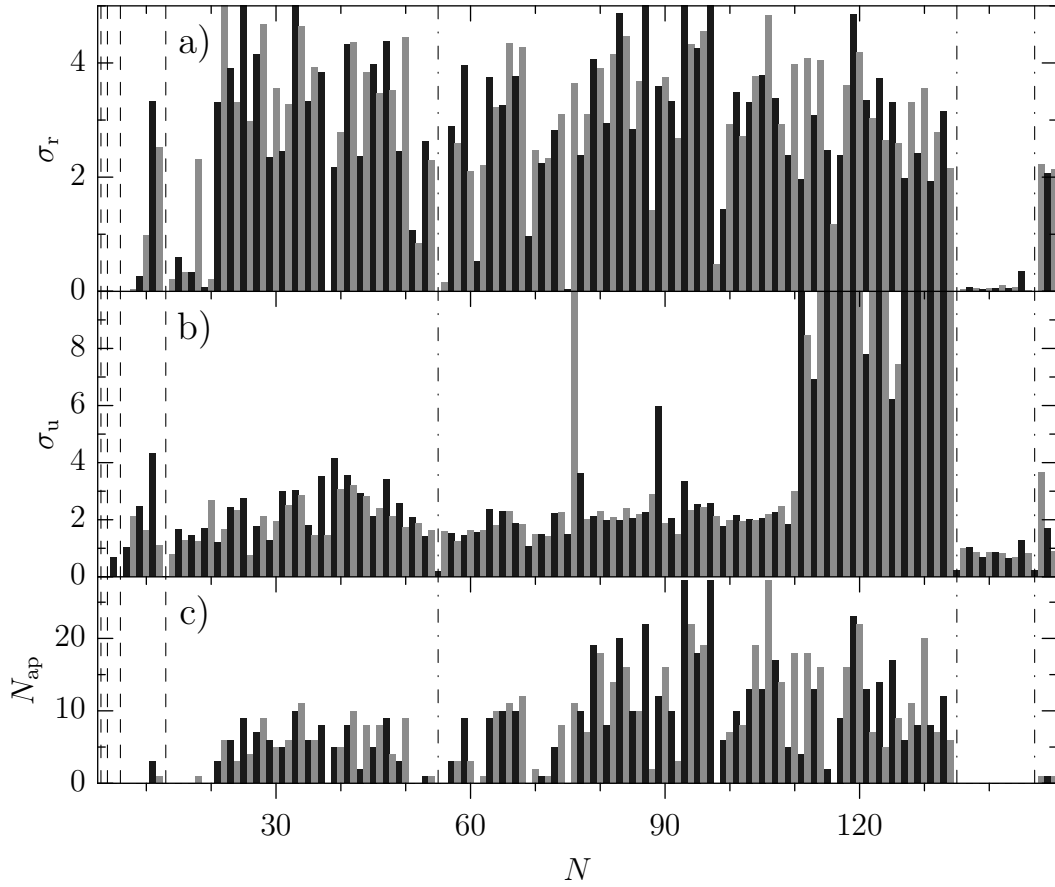


Figure 3.5: *Quasi-breathing modes of (externally) unconfined Lennard-Jones systems against the particle number. a) Deviations σ_r from radiality. b) Deviations σ_u from uniformity. c) Number N_{ap} of anti-phase oscillating particles. Cases of non-universal breathing modes are marked by dashed lines and the quasi-breathing modes of the icosahedral symmetric systems by dashed-dotted lines.*

deviations, including several particles moving in nearly tangential direction. For three-dimensional Yukawa balls the same types of deviations are observed as is shown in figure 3.4d.

In contrast to the previously considered Lennard-Jones systems, whose eigenvectors only depend on N , Yukawa systems feature a dependence on the screening parameter κ , and so their eigenvectors do. The investigation of the quasi-breathing mode regarding this dependence displays a very interesting structure, which is shown in figure 3.6

for the two-dimensional Yukawa systems with $N = 40$ particles within the range $0 \leq \kappa d_C \leq 2$.

Surprisingly, a small variation of κ leads to an irregular behavior of σ_r and/or σ_u with very sharp peaks. At first sight, such a structure contradicts the smooth κ -dependence of the Yukawa potential (1.2b), due to which all eigenvectors have to show a smooth κ -dependence too. However, a closer inspection reveals a κ -dependent direction of the eigenvectors within \mathbb{R}^{dN} . The change of this direction with changing κ involves that not one fixed mode has smallest deviations from the breathing mode, but with increasing κ this property may swap from one mode to another. This swap of the quasi-breathing mode, which is observable in the inset of figure 3.6 and additionally sketched in figure 3.7, is the reason for the peaked structure.

The κ -dependent deviations from the breathing mode are most evident in the non-uniform or non-radial moving directions of the particles. In addition, these deviations may also become noticeable in the behavior of the quasi-breathing mode's frequency ω_{QBM} . This frequency is displayed as a function of the screening parameter κ (by the

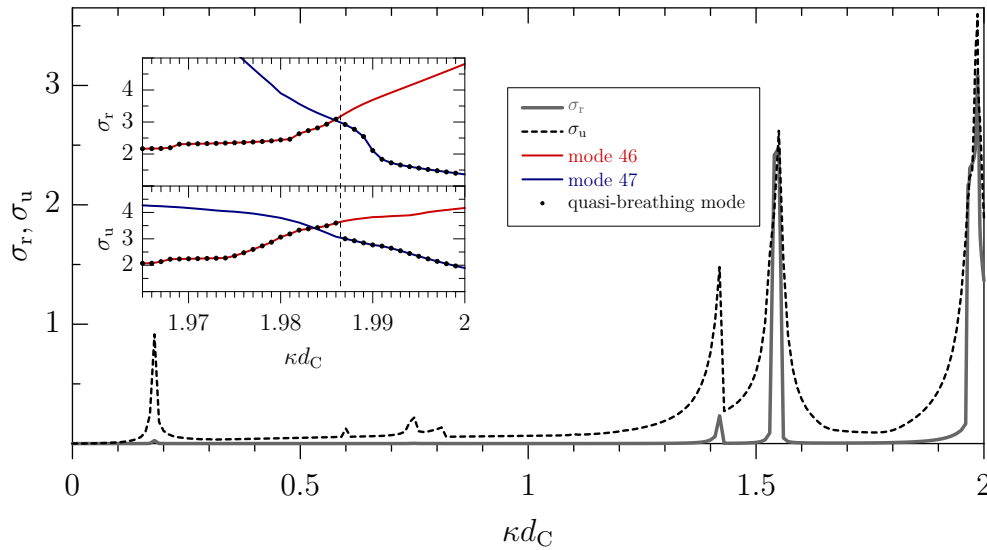


Figure 3.6: The properties σ_r and σ_u of the quasi-breathing mode depending on screening for harmonically confined two-dimensional Yukawa systems with $N = 40$ particles. The inset shows σ_r and σ_u of modes 46 (red line, numbers correspond to the mode frequencies in descending order) and 47 (blue line), which have the smallest deviations. The actual quasi-breathing mode is presented by dots.

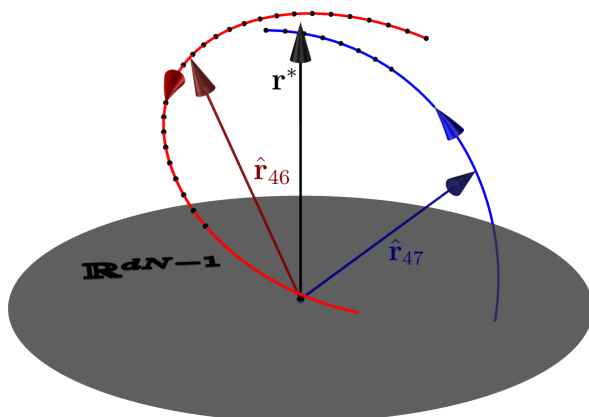


Figure 3.7: The direction of the eigenvectors, e.g., $\hat{\mathbf{r}}_{46}$ and $\hat{\mathbf{r}}_{47}$, within \mathbb{R}^{dN} may change with increasing screening. Therefore the property of having the largest projection onto \mathbf{r}^* , which defines the (by dots indicated) quasi-breathing mode, may swap abruptly from one mode to another mode.

black line) in figure 3.8 and clearly shows a raising frequency for increasing screening values, cf. 3.2. The deviations from the breathing mode are far less explicit but still observable in the peaked structure within this function, which is also caused by the swap of the quasi-breathing mode and which therefore emerge at the same screening values, cf. 3.6. As a result of the small amplitude of the peaks, the frequency of the quasi-breathing mode can be very well approximated by the frequency (3.21) of the (non-existing!) breathing mode. The relative error of this approximation is displayed (by the blue line) in figure 3.8, as well. The use of this approximation was first proposed by Sheridan [She06a], who also suggested a continuum model to analytically derive the behavior of this approximated frequency function [She06b]. It is worth mentioning that his model was based on the assumption of constant density profiles of Yukawa balls. By taking into account the non-constant density profiles, which were derived in chapter 2 of the thesis at hand, this model can be improved. However, both models disregard the pair correlation function, which is crucial for the determination of the breathing frequency (3.21). The future determination of density profiles, which take into account approximations of this pair correlation function, may improve these frequency models.

In summary, it can be stated that the confined Yukawa systems in consequence of their κ -dependence allow for the investigation of the breathing mode to quasi-breathing

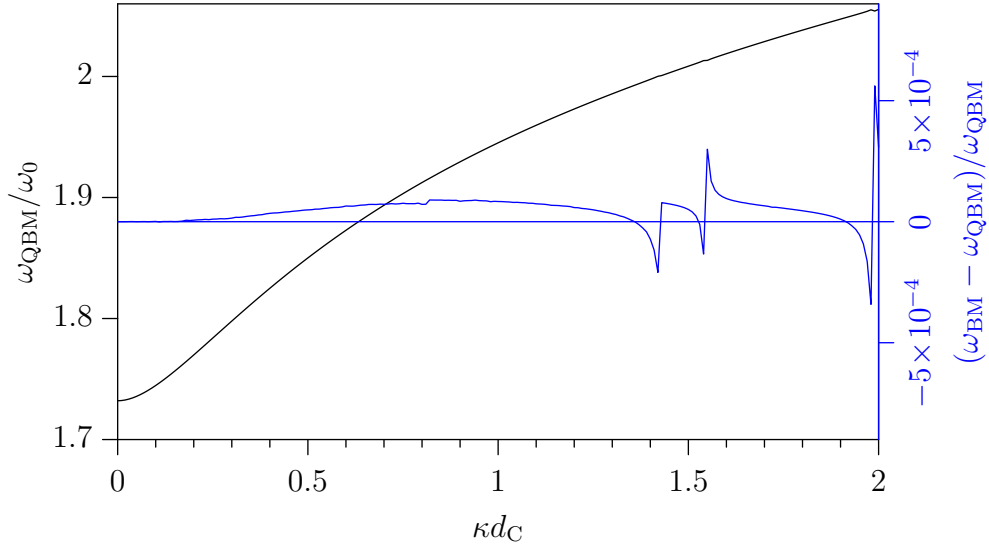


Figure 3.8: The frequency ω_{QBM} of the quasi-breathing mode (black line, left axis) as a function of the screening parameter for harmonically confined two-dimensional Yukawa systems with $N = 40$ particles. Additionally, the relative error of its breathing mode approximation ω_{BM} , (3.21), is shown (blue line, right axis).

mode transition in many details. This transition, geometrically speaking, corresponds to the κ -dependent motion $\hat{\mathbf{r}}_j(\kappa)$ of the eigenvectors, which in their entirety rotate within \mathbb{R}^{dN} . The κ -dependent motion, however, not only entails a change of the breathing mode but also a change of the associated monopole oscillation.

3.4.4 Monopole Oscillations

In the beginning of this section it was noted that the monopole oscillation, which in the strongly coupled regime is defined by (3.7), is closely connected with the breathing mode. Indeed, like the breathing mode it can be easily excited by variation of the trap frequency ω_0 , e.g., by a rapid change of the frequency ω_0 of the equilibrated system corresponding to the excitation given by $\mathbf{r}(0) = (1 + \xi)\mathbf{r}^*$ and $\dot{\mathbf{r}}(0) = \mathbf{0}$, which in turn corresponds to the normal coordinates

$$c_j(t) = \xi \mathbf{r}^* \cdot \hat{\mathbf{r}}_j \begin{cases} 1 & t < 0 \\ \cos(\omega_j t) & t \geq 0. \end{cases} \quad (3.25)$$

However, while this variation of the frequency excites always a monopole oscillation, the breathing mode is thereby only excited if there is a breathing mode. In this case, the monopole oscillation and the breathing mode describe the same motion and thus have the same frequency. Contrary, if the breathing mode does not exist, as in most Yukawa systems, then it follows, that there are *several* monopole oscillations with *different* frequencies. This property is directly apparent by using the normal mode expansion (3.4) in the definition (3.7) of the monopole oscillation. It yields

$$R^2(t) = N^{-1} \mathbf{r}^{*2} + 2N^{-1} \sum_{j=1}^{dN} c_j(t) \hat{\mathbf{r}}_j \cdot \mathbf{r}^* \quad (3.26)$$

for small excitations, i.e., for small amplitudes of the normal coordinates (3.25). If a breathing mode exists, one of the eigenvectors $\hat{\mathbf{r}}_j$ is given by $\hat{\mathbf{r}}_{\text{BM}}$, which is parallel to \mathbf{r}^* , whereas all other eigenvectors are orthogonal to \mathbf{r}^* . Thus, due to (3.25), all normal coordinates but the one of the breathing mode are vanishing. Hence, in this case the monopole oscillation, for $t \geq 0$, is given by

$$R^2(t) = N^{-1} \mathbf{r}^{*2} (1 + 2\xi \cos(\omega_{\text{BM}} t)) \quad (3.27)$$

and therefore oscillates with only the breathing frequency. In contrast, if no breathing mode exists, there are many eigenvectors $\hat{\mathbf{r}}_j$ with non-vanishing projection on \mathbf{r}^* , cf. figure 3.7. Then, the monopole oscillation contains several different frequencies $\omega_{\text{MO}} = \omega_j$ or, alternatively, there are different monopole oscillations [Hen09]. The mostly pronounced one corresponds to the quasi-breathing mode, which has the largest projection onto \mathbf{r}^* .

The multiplicity of the monopole oscillation in systems with a non-existing breathing mode is also apparent in its spectrum $\Phi_{R^2}(\omega)$ or rather in the spectrum $\Phi_{\dot{R}^2}(\omega)$ ¹, which is derived by the absolute square of the Fourier transform

$$\mathcal{F}_{\dot{R}^2}(\omega) = \frac{1}{\sqrt{2\pi}} \int_{-\infty}^{\infty} dt \dot{R}^2(t) e^{-i\omega t} . \quad (3.28)$$

By using the derivative of (3.26) an explicit calculation of the spectrum is possible

¹ While the general structure of both spectra is identical, the constant within (3.26) yields a more intricate expression for $\Phi_{R^2}(\omega)$ than for $\Phi_{\dot{R}^2}(\omega)$.

and yields, after some algebra,

$$\Phi_{\dot{R}^2}(\omega) = \frac{2\xi^2}{\pi N^2} \sum_{j,k=1}^{dN} \frac{(\hat{\mathbf{r}}_j \cdot \mathbf{r}^*)^2 \omega_j^2 (\hat{\mathbf{r}}_k \cdot \mathbf{r}^*)^2 \omega_k^2}{(\omega^2 - \omega_j^2)(\omega^2 - \omega_k^2)}. \quad (3.29)$$

In figure 3.9 this spectrum, obtained from numerical normal mode analysis, is shown for a Yukawa ball with $N = 16$ particles and a screening strength of $\kappa d_C = 4.42$. The two eye-catching peaks are caused by the poles of (3.29) and thus correspond to two different monopole oscillations. The corresponding frequencies are $\omega_{\text{MO}}^{(1)} = 2.349 \omega_0$ and $\omega_{\text{MO}}^{(2)} = 2.360 \omega_0$.

The emergence of multiple monopole oscillations is a direct consequence of the system's interaction and confinement potentials and of the system's configuration, if they are not fulfilling the strict conditions of the breathing mode. Therefore, the monopole oscillations should allow for the investigation of these important system properties.

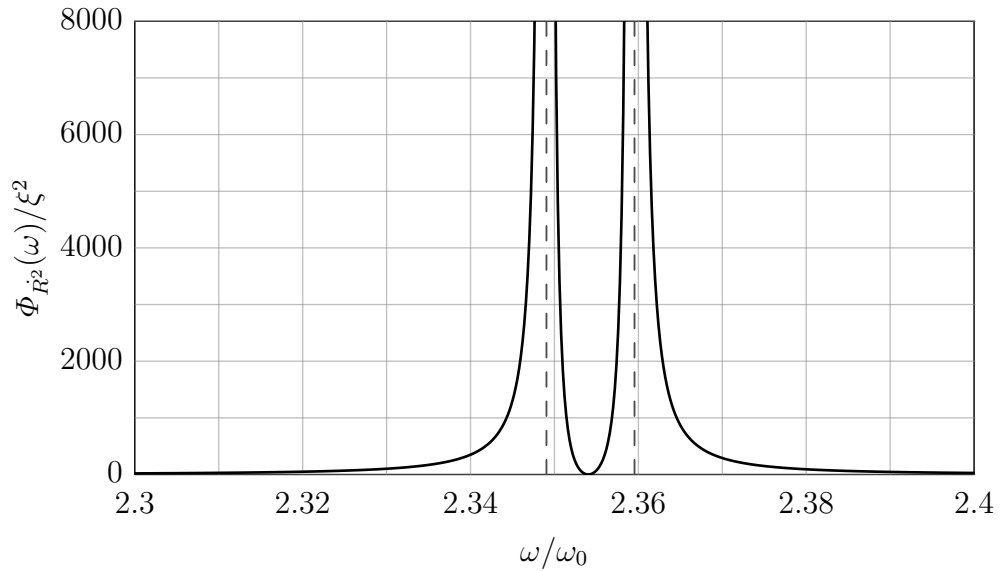


Figure 3.9: The spectrum $\Phi_{\dot{R}^2}(\omega)$ of a Yukawa ball with $N = 16$ particles and a screening strength of $\kappa d_C = 4.42$ contains two monopole modes, the frequencies of which are indicated by dashed lines.

3.5 Normal Modes in the Presence of Dissipation

While the problem of the breathing mode, its existence, and the relation to the monopole oscillation is figured out theoretically, its experimental investigation is still outstanding, e.g., in the case of Yukawa balls [Hen09]. Beside the required accuracy of the particle positions and motions, also dissipation effects make this a demanding task. Dissipation effects damp down the motion of all normal modes as can be seen by extending Newton's equation (3.5) of the excitation \mathbf{r} by a friction force $-m\nu\dot{\mathbf{r}}$ with $\nu > 0$, which results in

$$\mathbf{0} = m\ddot{\mathbf{r}} + m\nu\dot{\mathbf{r}} + \nabla U(\mathbf{r}) = m \sum_{j=1}^{dN} [\ddot{c}_j(t) + \nu\dot{c}_j(t) + \lambda_j c_j(t)] \hat{\mathbf{r}}_j. \quad (3.30)$$

Then, each normal coordinate fulfills an equation of motion

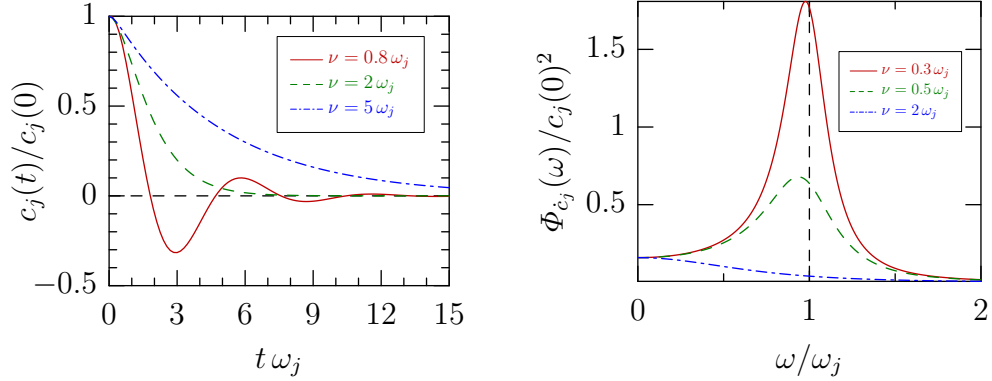
$$0 = \ddot{c}_j(t) + \nu\dot{c}_j(t) + \lambda_j c_j(t) \quad (3.31)$$

analogous to the single damped harmonic oscillator, and thus depends on the damping strength ν . The solution of this differential equation reads [Kä08]

$$c_j(t) = A_j \begin{cases} e^{-\nu t/2} \cos\left(\sqrt{\omega_j^2 - \nu^2/4} t + B_j\right) & \nu < 2\omega_j \\ e^{-\nu t/2} (1 + B_j t) & \nu = 2\omega_j \\ e^{-\nu t/2} \left(e^{\sqrt{\nu^2/4 - \omega_j^2} t} + B_j e^{-\sqrt{\nu^2/4 - \omega_j^2} t} \right) & \nu > 2\omega_j, \end{cases} \quad (3.32)$$

where the constants A_j and B_j have to be determined from the initial conditions $\mathbf{r}(0), \dot{\mathbf{r}}(0)$ of the excitation. The three cases correspond to normal modes, which are underdamped, critically damped, and overdamped, respectively. The corresponding dynamics of a mode are illustrated in figure 3.10a using the condition $\dot{c}_j(0) = 0$.

While thus the normal frequencies change due to dissipation, the displacement patterns of the normal modes, i.e., the eigenvectors, are not affected by it. Therefore, the issue of the breathing mode is still present in dissipative systems. However, the experimental investigation of the normal modes, and particularly (quasi)-breathing modes, is constrained by a short oscillation time of the particles – especially by consideration of experimental damping parameters, which are estimated to be $\nu \approx 2\omega_0$ [Hen09].



(a) Dynamics of a normal mode $c_j(t)$ for three values of the damping strength ν using the condition $\dot{c}_j(t \leq 0) = 0$.

(b) The corresponding spectra $\Phi_{c_j}(\omega)$ of the normal mode. The vertical dashed line indicates the peak position in the undamped case.

Figure 3.10: The dynamics and the spectrum of a normal mode as a function of friction corresponding to (3.32) and (3.33), respectively.

Similar constrains become noticeable within an experimental analysis of the monopole oscillation by means of the corresponding spectrum (3.29). There, dissipation causes a red-shift of the frequency peaks as well as a flattening and a relative broadening, as can be seen in the spectrum of a normal mode. For the aforementioned variation of the trap frequency, cf. (3.25), such a spectrum is given by

$$\Phi_{\dot{c}_j}(\omega) = \frac{\xi^2(\mathbf{r}^* \cdot \mathbf{r}_j)^2 \omega_j^4}{2\pi(\nu^2 \omega^2 + (\omega^2 - \omega_j^2)^2)}. \quad (3.33)$$

In the undamped case ($\nu = 0$) this spectrum contains a single distinct peak centered at the normal mode frequency¹. Contrary, for $\nu > 0$ dissipation causes an attenuation of higher frequencies, what eventually entails a red-shift. Additionally, the peak is flattened and therefore relatively broadened. All these effects are shown in figure 3.10b.

The same effects are present within complete power spectra, which are often used in experimental investigations of normal modes [Iva09, Mel03, Mel01]. For a Yukawa ball

¹ Also in the undamped case the peak is not a delta peak. This is caused by the variation of the trap frequency at $t = 0$, so that there is no harmonic oscillation for $t \leq 0$.

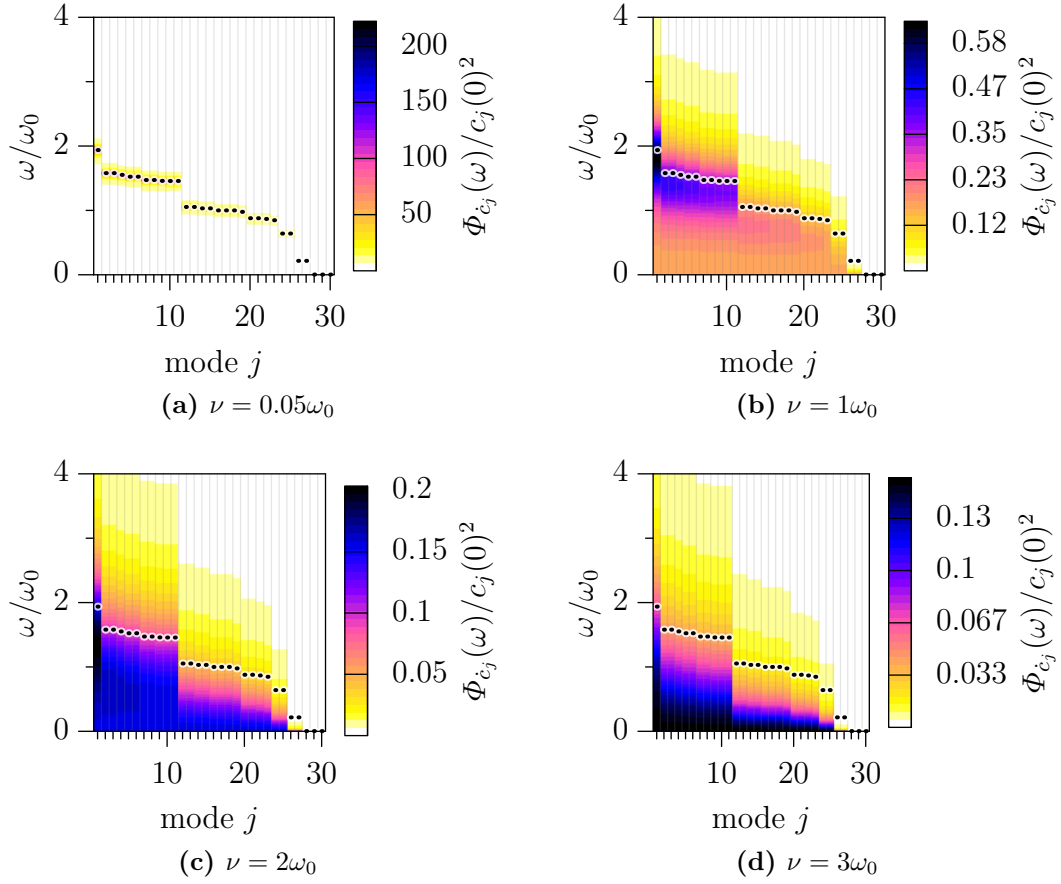


Figure 3.11: Theoretical normal mode spectra (3.33) for a Yukawa ball with $N = 10$ and $\kappa d_c = 1$ for four damping values. For comparison, the undamped spectrum is shown in all figures by black dots.

with $N = 10$ particles and the screening parameter $\kappa d_C = 1$ such power spectra are shown in figure 3.11 for various damping parameters. It is evident, that at sufficiently large damping more and more normal modes vanish, i.e., an increasing fraction of the power density is concentrated around $\omega = 0$. Eventually, due to dissipation effects the resolution of monopole oscillation spectra is constrained making an observation of multiple proximate peaks difficult.

It should be mentioned that dissipation effects, otherwise, allow for a sensitive diagnostics of relevant experimental parameters, including particle charge and trap frequency as suggested in [Hen09].

3.6 Summary

Within this chapter an analysis of the normal modes of finite clusters were presented. Starting from the known universal modes of harmonically confined Coulomb systems, which are the rotational modes, the sloshing modes, and the breathing mode, the universal modes of other finite clusters were investigated. As a result, it could be shown that the existence of the breathing mode, which may serve as a sensitive indicator of intrinsic system properties, is restricted to a small class of systems. On the one hand, there is this mode for harmonically and to some extent harmonic-logarithmically trapped systems in any dimension with a power law or logarithmic interaction potential. On the other hand, this mode exists also for other systems in case of particular, highly symmetric configurations. Therefore, systems with exponential or non-monotonic potentials (including Yukawa, Morse or Lennard-Jones systems), not being in such a special configuration, do not feature a breathing mode. In these systems all normal modes exhibit non-uniform and/or non-radial motion, which has been illustrated for several representative examples.

As a consequence, in this case an external perturbation of the system, which excites radial particle motions (e.g., by rapid change of the trap frequency), will excite not one but several monopole oscillations at once. The resulting complex spectrum represents the internal properties of the system, in particular the form of the pair interaction and the confinement, and is expected to be a sensitive experimental diagnostics of strongly correlated systems [Hen08]. In this context, dissipation effects must not be neglected, the influence of which on normal modes was discussed in the final part of this chapter. Thereby, it was shown that the issue of the breathing mode is still present in dissipative systems, although its experimental investigation is made challenging.

Additionally to the presented results, also their extension to strong excitations is of topical interest for experiments and theory. For this purpose, the normal mode analysis has to be based on a non-harmonic approximation, cf. (3.2), and, as a consequence, non-linearity effects (like mode coupling) are expected to occur. At the same time, also the extension of the breathing mode properties to quantum mechanical systems is subject of current interest. In this context, first results have already revealed fascinating non-classical phenomena [Bau09].

CHAPTER 4

Conclusions

The thesis at hand was concerned with the theoretical investigation of essential ground state and excitation properties of Yukawa balls.

The ground state of Yukawa balls is characterized by a pronounced structure of nested spherical shells, each of which has a specific population of dust particles. Based on the findings of experimental and numerical analyses, one of the basic goals of this thesis was to understand, from a theoretical point of view, the dependence of the particle distribution on the screening of the interaction. Therefore, a statistical theory was used, which is suitable to determine the ground state density profiles of Yukawa balls by minimizing their ground state energy. In order to accomplish this minimization, two essential approximations were applied – the mean-field and the local density approximation. By means of these approximations, analytical results for the density profiles could be derived. These results demonstrated the dramatic influence of the screening on the average particle distribution from a theoretical point of view.

The quality of the approximations was investigated by comparison with simulation results. This comparison revealed an excellent quantitative accordance with the average particle distribution showing the efficiency of the chosen approach. However, the used approximations are not capable for the description of the distinct shells of the Yukawa balls. For that purpose, more sophisticated approximations are needed, which take into account the particle correlations more properly. An additional question of topical interest is the extension of the density profiles to finite temperatures, which is of relevance for experiments and which, moreover, provides a powerful approach

to a thermodynamic theory of the Yukawa balls. Both the description of the shell structure and the finite temperature extension are subject of ongoing work.

An alternative approach to the shell structure of the Yukawa balls is given by Yukawa shell models. These artificial models possess an immanent shell structure and try to explain the properties of the shells. However, previous Yukawa shell models had strong limitations regarding the potential screening values and yield wrong or unphysical results beyond these limitations. By using the essential concepts of the similar Coulomb shell models, within this thesis a decisively improved Yukawa shell model could be derived, which is not subject of such screening value based limitations. Moreover, it includes the previous shell models as limiting cases. Further investigations of this model will reveal its descriptive capabilities and is topic of current research.

The other aspect of the thesis at hand was the investigation of the normal modes of Yukawa balls and other finite clusters. These normal modes provide an important approach to the external excitations of a system by resolving small oscillatory motions into their spectral constituents. In previous investigations three normal modes turned out to be of peculiar generality and were assumed to exist in Yukawa balls and other systems, as well. One of these modes is the breathing mode. It describes a uniform radial pulsation and is of special relevance for the experimental investigation of, e.g., the particle charge in complex plasmas. However, in the frame of this thesis the general existence conditions of the breathing mode could be derived. Their analysis revealed that this mode is existing only in a small class of systems, to which Yukawa balls and many other clusters do not generally belong to. For clarification of these findings, several representative examples have been showed, illustrating in an impressive manner various deviations from the breathing mode.

The direct consequences of the results, which particularly arise for Yukawa balls, were investigated in detail. Among them is a characteristic change in the response of the system to radial perturbations, which previously were expected to excite one characteristic (monopole) oscillation. However, for most systems actually not one but several of such oscillations are excited at once. Interestingly enough, the resulting spectrum represents internal properties of the system, in particular the form of the pair interaction and the confinement, and may serve as a sensitive experimental diagnostics of strongly correlated finite clusters. The quantification of this fact deserves a closer attention and should be of significance for future work. Thereby, the influence of

dissipation effects on the normal modes has to be taken into consideration, which is of relevance for most experiments and which was discussed in the final part of this thesis. Beyond that, also non-linear effects, like mode coupling, may emerge in this context as a consequence of strong (anharmonic) excitations. Finally, it should be mentioned that the extension of the presented classical breathing mode properties to quantum mechanical systems is of current interest as well, and first corresponding results have already revealed exciting phenomena.

Bibliography

- [Abb00] A. Abbott: CERN claims first experimental creation of quark-gluon plasma. *Nature* (2000), vol. 403(6770):p. 581
- [ALI08] ALICE Collaboration: The ALICE experiment at the CERN LHC. *Journal of Instrumentation* (2008), vol. 3(08):p. S08002
- [Ami01] S. G. Amiranashvili, N. G. Gusein-Zade, and V. N. Tsytovich: Spectral properties of small dusty clusters. *Physical Review E* (2001), vol. 64(1):p. 016407
- [Anz68] S. Anzai and K. Ozawa: Effect of Pressure on the Magnetic and Electrical Transition Point of the NiAs-Type NiS. *Journal of the Physical Society of Japan* (1968), vol. 24:pp. 271–274
- [Anz86] S. Anzai, M. Matoba, M. Hatori, and H. Sakamoto: Effect of Se-Substitution on the Magnetic and Electrical Transition in the NiAs-Type NiS. *Journal of the Physical Society of Japan* (1986), vol. 55:pp. 2531–2534
- [Apo07] S. W. S. Apolinario and F. M. Peeters: Melting transitions in isotropically confined three-dimensional small Coulomb clusters. *Physical Review E* (2007), vol. 76(3):pp. 031107–13
- [Arp04] O. Arp, D. Block, A. Piel, and A. Melzer: Dust Coulomb Balls: Three-Dimensional Plasma Crystals. *Physical Review Letters* (2004), vol. 93(16):p. 165004
- [Arp05] O. Arp, D. Block, M. Klindworth, and A. Piel: Confinement of Coulomb balls. *Physics of Plasmas* (2005), vol. 12(12):pp. 122102–9
- [Arp06] O. Arp: *Coulomb balls - Structure and confinement of spherical dust crystals in a plasma*, Doctoral thesis, Christian-Albrechts-Universität, Kiel (2006)

- [Bal05] F. Baletto and R. Ferrando: Structural properties of nanoclusters: Energetic, thermodynamic, and kinetic effects. *Reviews of Modern Physics* (2005), vol. 77(1):pp. 371–53
- [Bau07] H. Baumgartner, H. Kählert, V. Golobnychiy, C. Henning, S. Käding, A. Melzer, and M. Bonitz: Shell Structure of Yukawa Balls. *Contributions to Plasma Physics* (2007), vol. 47(4-5):pp. 281–290
- [Bau09] S. Bauch, K. Balzer, C. Henning, and M. Bonitz: Quantum breathing mode of trapped bosons and fermions at arbitrary coupling. *ArXiv: 0903.1993* (2009)
- [Blo07a] D. Block, M. Kroll, O. Arp, A. Piel, S. Käding, Y. Ivanov, A. Melzer, C. Henning, H. Baumgartner, P. Ludwig, and M. Bonitz: Structural and dynamical properties of Yukawa balls. *Plasma Physics and Controlled Fusion* (2007), vol. 49(12B):pp. B109–B116
- [Blo07b] D. Block: *Experiments on structural formation in plasmas*, Habilitation treatise, Christian-Albrechts-Universität, Kiel (2007)
- [Blo08a] I. Bloch, J. Dalibard, and W. Zwerger: Many-body physics with ultracold gases. *Reviews of Modern Physics* (2008), vol. 80(3):pp. 885–80
- [Blo08b] D. Block, S. Käding, A. Melzer, A. Piel, H. Baumgartner, and M. Bonitz: Experiments on metastable states of three-dimensional trapped particle clusters. *Physics of Plasmas* (2008), vol. 15(4):pp. 040701–4
- [Blo09] D. Block: private communication (2009)
- [Bon06a] M. Bonitz, D. Block, O. Arp, V. Golubnychiy, H. Baumgartner, P. Ludwig, A. Piel, and A. Filinov: Structural Properties of Screened Coulomb Balls. *Physical Review Letters* (2006), vol. 96(7):pp. 075001–4
- [Bon06b] M. Bonitz and D. Semkat: *Introduction to Computational Methods in Many Body Physics*, Rinton Press (2006)
- [Bon08] M. Bonitz, P. Ludwig, H. Baumgartner, C. Henning, A. Filinov, D. Block, O. Arp, A. Piel, S. Käding, Y. Ivanov, A. Melzer, H. Fehske, and V. Filinov: Classical and quantum Coulomb crystals. *Physics of Plasmas* (2008), vol. 15(5):p. 055704
- [Bor08] S. V. Borodachov, D. P. Hardin, and E. B. Saff: Asymptotics for discrete

- weighted minimal Riesz energy problems on rectifiable sets. *Transactions of the American Mathematical Society* (2008), vol. 360(3):pp. 1559–1580
- [BRA05] BRAHMS Collaboration: Quark-gluon plasma and color glass condensate at RHIC? The perspective from the BRAHMS experiment. *Nuclear Physics A* (2005), vol. 757(1-2):pp. 1–27
- [Bro95] B. R. Brooks, D. Janežič, and M. Karplus: Harmonic analysis of large systems. I. Methodology. *Journal of Computational Chemistry* (1995), vol. 16(12):pp. 1522–1542
- [Cal07] F. Calvo and E. Yurtsever: Non-monotonic size effects on the structure and thermodynamics of Coulomb clusters in three-dimensional harmonic traps. *The European Physical Journal D - Atomic, Molecular, Optical and Plasma Physics* (2007), vol. 44(1):pp. 81–91
- [Can98] L. Candido, J. Rino, N. Studart, and F. M. Peeters: The structure and spectrum of the anisotropically confined two-dimensional Yukawa system. *Journal of Physics: Condensed Matter* (1998), vol. 10(50):pp. 11627–11644
- [Che05] Q. Chen, J. Stajic, S. Tan, and K. Levin: BCS-BEC crossover: From high temperature superconductors to ultracold superfluids. *Physics Reports* (2005), vol. 412(1):pp. 1–88
- [Chu94] J. H. Chu and L. I: Direct observation of Coulomb crystals and liquids in strongly coupled rf dusty plasmas. *Physical Review Letters* (1994), vol. 72(25):p. 4009
- [Cio08] J. Cioslowski and E. Grzebielucha: Parameter-free shell model of spherical Coulomb crystals. *Physical Review E* (2008), vol. 78(2):pp. 026416–4
- [Col75] J. C. Collins and M. J. Perry: Superdense Matter: Neutrons or Asymptotically Free Quarks? *Physical Review Letters* (1975), vol. 34(21):p. 1353
- [Dre98] M. Drewsen, C. Brodersen, L. Hornekær, J. S. Hangst, and J. P. Schiffer: Large Ion Crystals in a Linear Paul Trap. *Physical Review Letters* (1998), vol. 81(14):p. 2878
- [Dub88] D. H. E. Dubin and T. M. O’Neil: Computer simulation of ion clouds in a Penning trap. *Physical Review Letters* (1988), vol. 60(6):p. 511
- [Dub96a] D. H. E. Dubin: Effect of correlations on the thermal equilibrium and normal modes of a non-neutral plasma. *Physical Review E* (1996), vol. 53(5):p. 5268

- [Dub96b] D. H. E. Dubin and J. P. Schiffer: Normal modes of cold confined one-component plasmas. *Physical Review E* (1996), vol. 53(5):p. 5249
- [Dub99] D. H. E. Dubin and T. M. O’Neil: Trapped nonneutral plasmas, liquids, and crystals (the thermal equilibrium states). *Reviews of Modern Physics* (1999), vol. 71(1):p. 87
- [Dyk08] E. C. Dykeman and O. F. Sankey: Low Frequency Mechanical Modes of Viral Capsids: An Atomistic Approach. *Physical Review Letters* (2008), vol. 100(2):pp. 028101–4
- [Erb91] T. Erber and G. M. Hockney: Equilibrium configurations of N equal charges on a sphere. *Journal of Physics A: Mathematical and General* (1991), vol. 24(23):pp. L1369–L1377
- [Ess05] F. H. L. Essler, H. Frahm, F. Göhmann, A. Klümper, and V. E. Korepin: *The One-Dimensional Hubbard Model*, Cambridge University Press (2005)
- [Eva79] R. Evans: The nature of the liquid-vapour interface and other topics in the statistical mechanics of non-uniform, classical fluids. *Advances in Physics* (1979), vol. 28(2):p. 143
- [Fen07] Y. Feng, J. Goree, and B. Liu: Accurate particle position measurement from images. *Review of Scientific Instruments* (2007), vol. 78(5):pp. 053704–10
- [For05] V. E. Fortov, A. V. Ivlev, S. A. Khrapak, A. G. Khrapak, and G. E. Morfill: Complex (dusty) plasmas: Current status, open issues, perspectives. *Physics Reports* (2005), vol. 421(1-2):pp. 1–103
- [Gol06] V. Golubnychiy, H. Baumgartner, M. Bonitz, A. Filinov, and H. Fehske: Screened Coulomb balls—structural properties and melting behaviour. *Journal of Physics A: Mathematical and General* (2006), vol. 39(17):pp. 4527–4531
- [Gre02] M. Greiner, O. Mandel, T. Esslinger, T. W. Hänsch, and I. Bloch: Quantum phase transition from a superfluid to a Mott insulator in a gas of ultracold atoms. *Nature* (2002), vol. 415(6867):pp. 39–44
- [Gue99] D. Guery-Odelin, F. Zambelli, J. Dalibard, and S. Stringari: Collective oscillations of a classical gas confined in harmonic traps. *Physical Review A* (1999), vol. 60(6):p. 4851

-
- [Han91] J. P. Hansen and I. R. McDonald: *Theory of simple liquids*, Academic Press, 2. (reprint) edn. (1991)
- [Has91] R. W. Hasse and V. V. Avilov: Structure and Madelung energy of spherical Coulomb crystals. *Physical Review A* (1991), vol. 44(7):p. 4506
- [Hay94] Y. Hayashi and K. Tachibana: Observation of Coulomb-Crystal Formation from Carbon Particles Grown in a Methane Plasma. *Japanese Journal of Applied Physics* (1994), vol. 33(6A):pp. L804—L806
- [Hay99] Y. Hayashi: Structure of a Three-Dimensional Coulomb Crystal in a Fine-Particle Plasma. *Physical Review Letters* (1999), vol. 83(23):p. 4764
- [Hei09] U. Heinz: The strongly coupled quark–gluon plasma created at RHIC. *Journal of Physics A: Mathematical and Theoretical* (2009), vol. 42(21):p. 214003
- [Hen06] C. Henning, H. Baumgartner, A. Piel, P. Ludwig, V. Golubnichiy, M. Bonitz, and D. Block: Ground state of a confined Yukawa plasma. *Physical Review E* (2006), vol. 74(5):pp. 056403–6
- [Hen07] C. Henning, P. Ludwig, A. Filinov, A. Piel, and M. Bonitz: Ground state of a confined Yukawa plasma including correlation effects. *Physical Review E* (2007), vol. 76(3):pp. 036404–7
- [Hen08] C. Henning, K. Fujioka, P. Ludwig, A. Piel, A. Melzer, and M. Bonitz: Existence and Vanishing of the Breathing Mode in Strongly Correlated Finite Systems. *Physical Review Letters* (2008), vol. 101(4):pp. 045002–4
- [Hen09] C. Henning, H. Kahlert, P. Ludwig, A. Melzer, and M. Bonitz: Spectral properties of spherically confined dusty plasma crystals. *Journal of Physics A: Mathematical and Theoretical* (2009), vol. 42(21):p. 214023
- [Ich94] S. Ichimaru: *Statistical Plasma Physics, Volume II: Condensed Plasmas*, vol. Statistical plasma physics of *Frontiers in physics*, Addison-Wesley, Redwood City, Calif. (1994)
- [Ima98] M. Imada, A. Fujimori, and Y. Tokura: Metal-insulator transitions. *Reviews of Modern Physics* (1998), vol. 70(4):p. 1039
- [Iva07] Y. Ivanov and A. Melzer: Particle positioning techniques for dusty plasma experiments. *The Review of Scientific Instruments* (2007), vol. 78(3):p. 033506

- [Iva09] Y. Ivanov and A. Melzer: Modes of three-dimensional dust crystals in dusty plasmas. *Physical Review E* (2009), vol. 79(3):pp. 036402–7
- [Jac99] J. D. Jackson: *Classical electrodynamics*, Wiley, New York (1999)
- [Kin04] J. Kinast, A. Turlapov, and J. E. Thomas: Breakdown of hydrodynamics in the radial breathing mode of a strongly interacting Fermi gas. *Physical Review A* (2004), vol. 70(5):p. 051401
- [Kon03] M. Kong, B. Partoens, and F. M. Peeters: Structural, dynamical and melting properties of two-dimensional clusters of complex plasmas. *New Journal of Physics* (2003), vol. 5:p. 23
- [Kot04] G. Kotliar and D. Vollhardt: Strongly Correlated Materials: Insights From Dynamical Mean-Field Theory. *Physics Today* (2004), vol. 57(3):p. 53
- [Kra06] W. D. Kraeft and M. Bonitz: Thermodynamics of a correlated confined plasma II. Mesoscopic system. *Journal of Physics: Conference Series* (2006), vol. 35:pp. 94–109
- [Kui98] A. B. J. Kuijlaars and E. B. Saff: Asymptotics for minimal discrete energy on the sphere. *Transactions of the American Mathematical Society* (1998), vol. 350:pp. 523–538
- [Kä08] H. Kählert: *First-principle simulation of classical charged particles in traps*, Diploma thesis, Christian-Albrechts-Universität, Kiel (2008)
- [Kö05] M. Köhl, H. Moritz, T. Stöferle, K. Günter, and T. Esslinger: Fermionic Atoms in a Three Dimensional Optical Lattice: Observing Fermi Surfaces, Dynamics, and Interactions. *Physical Review Letters* (2005), vol. 94(8):p. 080403
- [Kö06] T. Köhler, K. Góral, and P. S. Julienne: Production of cold molecules via magnetically tunable Feshbach resonances. *Reviews of Modern Physics* (2006), vol. 78(4):pp. 1311–51
- [Leb82] J. L. Lebowitz and E. M. Waisman: *On the equilibrium theory of fluids*, Studies in statistical mechanics VIII, North-Holland Publishing Company, Amsterdam (1982), p. 440
- [Lud05] P. Ludwig, S. Kosse, and M. Bonitz: Structure of spherical three-dimensional Coulomb crystals. *Physical Review E* (2005), vol. 71(4):pp. 046403–5

-
- [McM98] A. K. McMahan, C. Huscroft, R. T. Scalettar, and E. L. Pollock: Volume-collapse transitions in the rare earth metals. *Journal of Computer-Aided Materials Design* (1998), vol. 5(2):pp. 131–162
- [Mel97] A. Melzer: *Der Plasmakristall: Phasenübergang und Stabilität*, Doctoral thesis, Christian-Albrechts-Universität, Kiel (1997)
- [Mel01] A. Melzer, M. Klindworth, and A. Piel: Normal Modes of 2D Finite Clusters in Complex Plasmas. *Physical Review Letters* (2001), vol. 87(11):p. 115002
- [Mel03] A. Melzer: Mode spectra of thermally excited two-dimensional dust Coulomb clusters. *Physical Review E* (2003), vol. 67(1):p. 016411
- [Mer04] R. L. Merlino and J. A. Goree: Dusty Plasmas in the Laboratory, Industry, and Space. *Physics Today* (2004), vol. 57:pp. 32—38
- [Mor99] G. E. Morfill, H. M. Thomas, U. Konopka, H. Rothermel, M. Zuzic, A. Ivlev, and J. Goree: Condensed Plasmas under Microgravity. *Physical Review Letters* (1999), vol. 83(8):p. 1598
- [Mor03] H. Moritz, T. Stöferle, M. Köhl, and T. Esslinger: Exciting Collective Oscillations in a Trapped 1D Gas. *Physical Review Letters* (2003), vol. 91(25):p. 250402
- [Mor06] A. Mortensen, E. Nielsen, T. Matthey, and M. Drewsen: Observation of Three-Dimensional Long-Range Order in Small Ion Coulomb Crystals in an rf Trap. *Physical Review Letters* (2006), vol. 96(10):pp. 103001–4
- [Mü06] B. Müller and J. L. Nagle: Results from the Relativistic Heavy Ion Collider. *Annual Review of Nuclear and Particle Science* (2006), vol. 56:pp. 93–135
- [NA500] NA50 Collaboration: Evidence for deconfinement of quarks and gluons from the J/ψ suppression pattern measured in Pb-Pb collisions at the CERN-SPS. *Physics Letters B* (2000), vol. 477(1-3):pp. 28–36
- [Oha02] Y. Ohashi and A. Griffin: BCS-BEC Crossover in a Gas of Fermi Atoms with a Feshbach Resonance. *Physical Review Letters* (2002), vol. 89(13):p. 130402
- [Par97] B. Partoens and F. M. Peeters: Classical artificial two-dimensional atoms: the Thomson model. *Journal of Physics: Condensed Matter* (1997), vol. 9(25):pp. 5383–5393

- [Par03] R. G. Parr: Density Functional Theory. *Annual Review of Physical Chemistry* (2003), vol. 34:pp. 631–656
- [PHE05] PHENIX Collaboration: Formation of dense partonic matter in relativistic nucleus-nucleus collisions at RHIC: Experimental evaluation by the PHENIX Collaboration. *Nuclear Physics A* (2005), vol. 757(1-2):pp. 184–283
- [Phi98] W. D. Phillips: Nobel Lecture: Laser cooling and trapping of neutral atoms. *Reviews of Modern Physics* (1998), vol. 70(3):p. 721
- [PHO05] PHOBOS Collaboration: The PHOBOS perspective on discoveries at RHIC. *Nuclear Physics A* (2005), vol. 757(1-2):pp. 28–101
- [Pie02] A. Piel and A. Melzer: Dynamical processes in complex plasmas. *Plasma Physics and Controlled Fusion* (2002), vol. 44(1):pp. R1–R26
- [Pie08] A. Piel, O. Arp, D. Block, I. Pilch, T. Trottenberg, S. Käding, A. Melzer, H. Baumgartner, C. Henning, and M. Bonitz: Complex plasmas: forces and dynamical behaviour. *Plasma Physics and Controlled Fusion* (2008), vol. 50(12):p. 124003
- [Pos96] A. Posada-Amarillas and I. L. Garzon: Vibrational analysis of Nin clusters. *Physical Review B* (1996), vol. 54(15):p. 10362
- [Pro06] A. Proykova and R. S. Berry: Insights into phase transitions from phase changes of clusters. *Journal of Physics B: Atomic, Molecular and Optical Physics* (2006), vol. 39(9):pp. R167–R202
- [Ram97] A. P. Ramirez: Colossal magnetoresistance. *Journal of Physics: Condensed Matter* (1997), vol. 9(39):pp. 8171–8199
- [Rot02] H. Rothermel, T. Hagl, G. E. Morfill, M. H. Thoma, and H. M. Thomas: Gravity Compensation in Complex Plasmas by Application of a Temperature Gradient. *Physical Review Letters* (2002), vol. 89(17):p. 175001
- [Row88] J. S. Rowlinson, editor: *J.D. van der Waals: On the continuity of the gaseous and liquid states*, Studies in statistical mechanics XIV, North-Holland Publishing Company, Amsterdam (1988)
- [Sch95] V. A. Schweigert and F. M. Peeters: Spectral properties of classical two-dimensional clusters. *Physical Review B* (1995), vol. 51(12):p. 7700
- [She05a] T. E. Sheridan: Center-of-mass and breathing oscillations in small complex plasma disks. *Physical Review E* (2005), vol. 72(2):pp. 026405–7

-
- [She05b] T. E. Sheridan: Chaos in a complex plasma. *Physics of Plasmas* (2005), vol. 12(8):pp. 080701–4
- [She06a] T. E. Sheridan: Accuracy of theory for the breathing oscillation of a complex plasma disc. *Journal of Physics D: Applied Physics* (2006), vol. 39(4):pp. 693–699
- [She06b] T. E. Sheridan: Continuum model for the breathing oscillation of a spherical complex plasma. *Physics of Plasmas* (2006), vol. 13(2):pp. 022106–7
- [Shu78] E. V. Shuryak: Theory of hadron plasma. *Zhurnal Eksperimental noi i Teoreticheskoi Fiziki* (1978), vol. 74:pp. 408–420
- [Shu04] E. Shuryak: A strongly coupled quark–gluon plasma. *Journal of Physics G: Nuclear and Particle Physics* (2004), vol. 30(8):pp. S1221–S1224
- [Spa68] J. T. Sparks and T. Komoto: Metal-to-Semiconductor Transition in Hexagonal NiS. *Reviews of Modern Physics* (1968), vol. 40(4):p. 752
- [STA05] STAR Collaboration: Experimental and theoretical challenges in the search for the quark-gluon plasma: The STAR Collaboration’s critical assessment of the evidence from RHIC collisions. *Nuclear Physics A* (2005), vol. 757(1-2):pp. 102–183
- [Str96] S. Stringari: Collective Excitations of a Trapped Bose-Condensed Gas. *Physical Review Letters* (1996), vol. 77(12):p. 2360
- [Tho94] H. Thomas, G. E. Morfill, V. Demmel, J. Goree, B. Feuerbacher, and D. Möhlmann: Plasma Crystal: Coulomb Crystallization in a Dusty Plasma. *Physical Review Letters* (1994), vol. 73(5):p. 652
- [Tho04] M. H. Thoma: Strongly coupled plasmas in high-energy physics. *Plasma Science, IEEE Transactions on* (2004), vol. 32(2):pp. 738–741
- [Tho05] M. H. Thoma: The quark–gluon plasma liquid. *Journal of Physics G: Nuclear and Particle Physics* (2005), vol. 31(1):pp. L7–L12
- [Tho09] M. H. Thoma: What can we learn from electromagnetic plasmas about the quark–gluon plasma? *Journal of Physics A: Mathematical and Theoretical* (2009), vol. 42(21):p. 214004
- [Tot01] H. Totsuji, C. Totsuji, and K. Tsuruta: Structure of finite two-dimensional Yukawa lattices: Dust crystals. *Physical Review E* (2001), vol. 64(6):p. 066402

- [Tot05] H. Totsuji, T. Ogawa, C. Totsuji, and K. Tsuruta: Structure of spherical Yukawa clusters: A model for dust particles in dusty plasmas in an isotropic environment. *Physical Review E* (2005), vol. 72(3):pp. 036406–6
- [Tot06a] H. Totsuji: Equilibrium properties of two-dimensional Yukawa plasmas. *Journal of Physics A: Mathematical and General* (2006), vol. 39(17):pp. 4493–4499
- [Tot06b] H. Totsuji: Thermodynamic instability and critical fluctuations in dusty plasmas modelled as Yukawa OCP. *Journal of Physics A: Mathematical and General* (2006), vol. 39(17):pp. 4565–4569
- [Tsu93] K. Tsuruta and S. Ichimaru: Binding energy, microstructure, and shell model of Coulomb clusters. *Physical Review A* (1993), vol. 48(2):p. 1339
- [vV01] H. W. T. van Vlijmen and M. Karplus: Normal mode analysis of large systems with icosahedral symmetry: Application to (Dialanine)₆₀ in full and reduced basis set implementations. *The Journal of Chemical Physics* (2001), vol. 115(2):pp. 691–698
- [Wal91] D. J. Wales: Instantaneous normal mode analysis and coexistence phenomena in small clusters. *Journal of the Chemical Society, Faraday Transactions* (1991), vol. 87(15):pp. 2399–2405
- [Wal97] D. J. Wales and J. P. K. Doye: Global Optimization by Basin-Hopping and the Lowest Energy Structures of Lennard-Jones Clusters Containing up to 110 Atoms. *Journal of Physical Chemistry A* (1997), vol. 101(28):pp. 5111–5116
- [Why52] L. L. Whyte: Unique Arrangements of Points on a Sphere. *The American Mathematical Monthly* (1952), vol. 59(9):pp. 606–611
- [Win87] D. J. Wineland, J. C. Bergquist, W. M. Itano, J. J. Bollinger, and C. H. Manney: Atomic-Ion Coulomb Clusters in an Ion Trap. *Physical Review Letters* (1987), vol. 59(26):p. 2935
- [Wol65] R. Wolfe, J. H. Wernick, and S. E. Haszko: Thermoelectric properties of FeSi. *Physics Letters* (1965), vol. 19(6):pp. 449–450
- [Wri09] J. Wrighton, J. Dufty, C. Henning, and M. Bonitz: Linear response for confined particles. *Journal of Physics A: Mathematical and Theoretical* (2009), vol. 42(21):p. 214052

List of the Author's Publications

Complete List of the Author's Peer-Reviewed Journal Publications

1. C. Henning, H. Baumgartner, A. Piel, P. Ludwig, V. Golubnychiy, M. Bonitz, and D. Block,
Ground state of a confined Yukawa plasma,
Physical Review E **74**, 056403 (2006)
2. D. Block, M. Kroll, O. Arp, A. Piel, S. Käding, Y. Ivanov, A. Melzer, C. Henning, H. Baumgartner, P. Ludwig, and M. Bonitz,
Structural and dynamical properties of Yukawa balls,
Plasma Physics and Controlled Fusion **49**, B109-B116 (2007)
3. C. Henning, P. Ludwig, A. Filinov, A. Piel, and M. Bonitz,
Ground state of a confined Yukawa plasma including correlation effects,
Physical Review E **76**, 036404 (2007)
4. H. Baumgartner, H. Kählert, V. Golubnychiy, C. Henning, S. Käding, A. Melzer, and M. Bonitz,
Shell structure of Yukawa balls,
Contributions to Plasma Physics **47**, 281-290 (2007)
5. M. Bonitz, P. Ludwig, H. Baumgartner, C. Henning, A. Filinov, D. Block, O. Arp, A. Piel, S. Käding, Y. Ivanov, A. Melzer, H. Fehske, and V. Filinov,
Classical and quantum Coulomb crystals,
Physics of Plasmas **15**, 055704 (2008)
6. C. Henning, K. Fujioka, P. Ludwig, A. Piel, A. Melzer, and M. Bonitz,
Existence and vanishing of the breathing mode in strongly correlated finite

- systems*,
Physical Review Letters **101**, 045002 (2008)
7. A. Piel, O. Arp, D. Block, I. Pilch, T. Trottenberg, S. Käding, A. Melzer, H. Baumgartner, C. Henning, and M. Bonitz,
Complex plasmas: forces and dynamical behaviour,
Plasma Physics and Controlled Fusion **50**, 124003 (2008)
 8. C. Henning, H. Kählert, P. Ludwig, A. Melzer, and M. Bonitz,
Spectral properties of spherically confined dusty plasma crystals,
Journal of Physics A: Mathematical and Theoretical **42**, 214023 (2009)
 9. J. Wrighton, J.W. Dufty, C. Henning, and M. Bonitz,
Linear response for confined particles,
Journal of Physics A: Mathematical and Theoretical **42**, 214052 (2009)
 10. S. Bauch, K. Balzer, C. Henning, and M. Bonitz,
Quantum breathing mode of trapped bosons and fermions at arbitrary coupling,
submitted for publication, ArXiv: 0903.1993 (2009)

Contributions to Books

- C. Henning and M. Bonitz,
Statistical theory of spherically confined dust crystals,
In: **Introduction to complex plasmas**, Eds. Michael Bonitz, Norman Horing,
Jürgen Meichsner, and Patrick Ludwig
to be published in 2009 in Springer Series “Atomic, Optical and Plasma Physics”

Selected Contributions to International Conferences

- C. Henning, V. Golubnychiy, H. Baumgartner, P. Ludwig, M. Bonitz, O. Arp,
D. Block, A. Piel, A. Melzer, W.D. Kraeft,
Spherical crystals in dusty plasmas - Experiment, simulation and theory,
Talk at conference **Physics of Non-ideal Plasmas**, Darmstadt, September
4-8, 2006

-
- C. Henning, M. Bonitz, A. Piel, P. Ludwig, H. Baumgartner, and V. Golubnichiy,
Density profile of strongly correlated spherical Yukawa plasmas,
Talk at workshop **Diagnostics and Simulation of Dusty Plasmas**, Kiel,
September 13-15, 2006
 - C. Henning, K. Fujioka, P. Ludwig, and M. Bonitz,
Density profile and breathing mode of strongly correlated spherical Yukawa plasmas,
Talk at **49th Annual Meeting of the Division of Plasma Physics**, Orlando,
Florida, November 12-16, 2007
 - C. Henning,
Statistical theory of spatially confined Yukawa plasmas,
Lecture at **Summer Institute “Complex Plasmas”**, Hoboken, NJ, July 30
- August 8, 2008

List of the Author's Publications

Danksagung

An dieser Stelle möchte ich mich bei allen Personen bedanken, die mich in meiner wissenschaftlichen Tätigkeit und bei der Erstellung dieser Doktorarbeit unterstützt haben.

Ganz besonderer Dank gebührt in diesem Zusammenhang Prof. Dr. Michael Bonitz, der die Anfertigung der vorliegenden Arbeit überhaupt erst ermöglicht hat und mir dabei die letzten Jahre stets mit Rat und Tat und mit viel Engagement zu Seite stand.

Ebenso möchte ich Prof. Dr. Alexander Piel und Prof. Dr. James Dufty für ihre engagierten Diskussionen bedanken, die mir nicht unwesentlich geholfen haben, ein besseres Verständnis von in dieser Arbeit vorgestellten Themen zu erhalten.

Mein besonderer Dank gilt auch allen Mitgliedern und Gästen der Arbeitsgruppe, haben sie doch ein sehr angenehmes und besonders kreatives Arbeitsumfeld geschaffen, ohne das ein produktives wissenschaftliches Arbeiten für mich gar nicht möglich gewesen wäre. Vor allem danke ich Karsten Balzer, Sebastian Bauch, Jens Böning, Torben Ott, Hanno Kählert, Kenji Fujioka und insbesondere Patrick Ludwig.

Schließlich möchte ich mich auch von ganzem Herzen bei meiner Familie bedanken – vor allem bei meiner lieben Frau Jenny, die mich in meiner Promotionszeit so sehr unterstützt hat, und bei meinen beiden Kindern Yannick und Emma, die durch ihr Lächeln Probleme aller Art haben vergessen lassen.

Danke!

Selbständigkeitserklärung

Diese Dissertationsschrift wurde von mir in Form und Inhalt unter Anleitung von Prof. Dr. Michael Bonitz und nur unter Zuhilfenahme der angegebenen Hilfsmittel angefertigt. Diese Arbeit hat weder in gleicher, noch in ähnlicher Form an anderer Stelle im Rahmen eines Prüfungsverfahrens vorgelegen.

Kiel,
(Ort)

(Datum)

(Unterschrift)



Curriculum Vitae

Persönliche Daten

Christian Henning

geb. am 02.08.1979 in Potsdam
deutsche Staatsangehörigkeit
verheiratet, 2 Kinder



Studium

- 02/2006 – 07/2009 Promotionsstudium
am Institut für Theoretische Physik und Astrophysik
der Christian-Albrechts-Universität zu Kiel
- 10/2000–02/2006 Studium der Physik und Mathematik an der
Christian-Albrechts-Universität zu Kiel
- Februar 2006: Physikdiplom
 - Januar 2006: Abgabe der Diplomarbeit
(*Bose-Einstein-Kondensation im Funktionalintegralzugang*)
 - Oktober 2002: Physik-Vordiplom

Schule und Zivildienst

- 08/1999–06/2000 Zivildienst (Altenpflegeheim Luisenhaus in Potsdam)
- 08/1992–06/1999 Wolkenberg-Gymnasium, Michendorf
- Juni 1999: Allgemeine Hochschulreife